ARS JOURNAL

A PUBLICATION OF THE AMERICAN ROCKET SOCIETY

FORMERLY JET PROPULSION

July 1959 Volume 29 Number 7

Hands of the Giants

crack an egg or shape a missile

100,000,000 lbs. of pressure—so delicately controlled that it can be made to crack the shell of an egg. Use the fabulous forces of present day forging skills to crack the barriers of space—weight, strength, high temperatures. Forge the future, today.

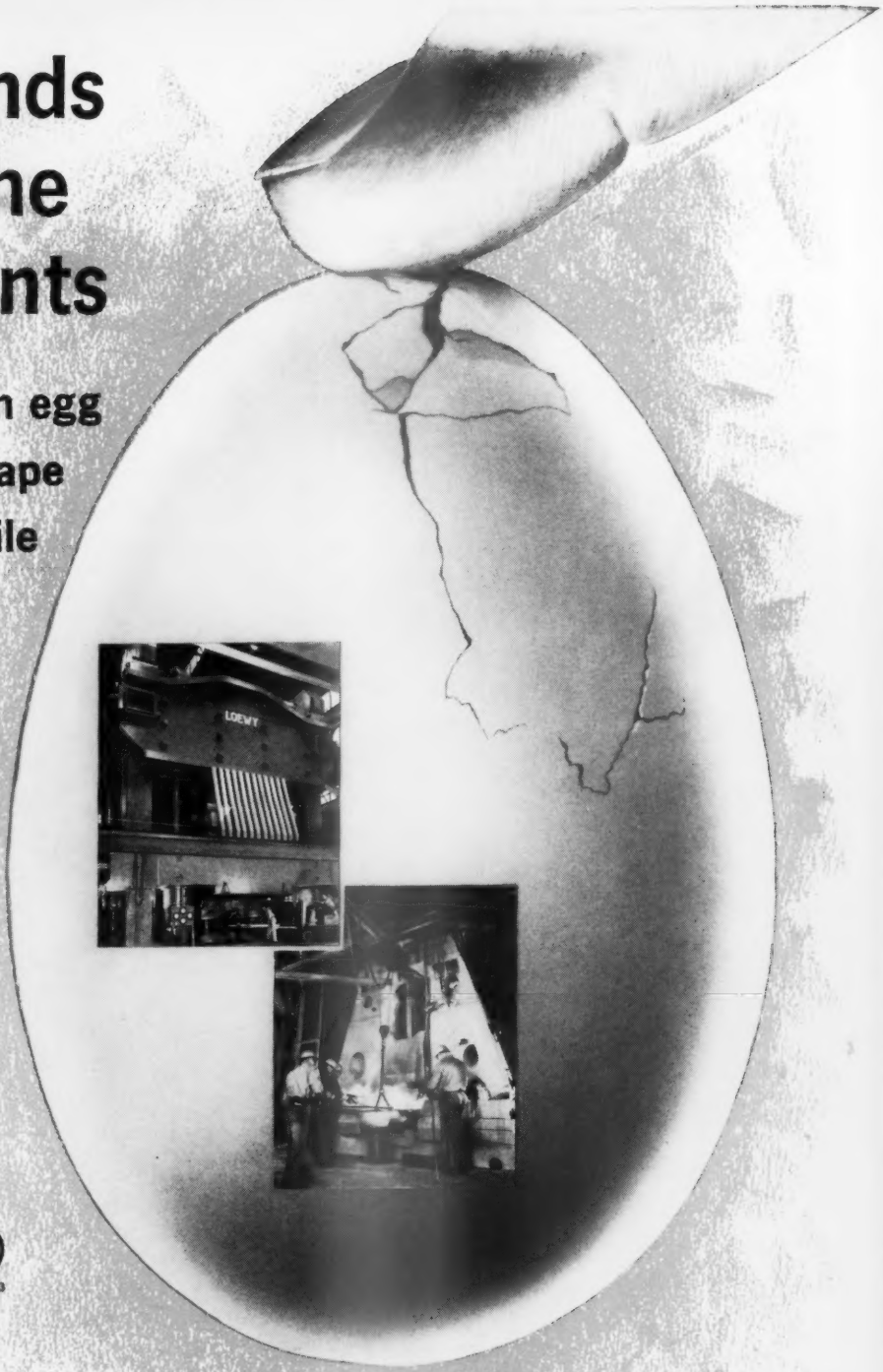

EST. 1883

WYMAN-GORDON

FORGING

ALUMINUM MAGNESIUM STEEL TITANIUM BERYLLIUM MOLYBDENUM COLUMBIUM
AND OTHER UNCOMMON MATERIALS

WORCESTER, MASSACHUSETTS

HARVEY, ILLINOIS
DETROIT, MICHIGAN
GRAFTON, MASSACHUSETTS
FORT WORTH, TEXAS
FRANKLIN PARK, ILLINOIS
LOS ANGELES, CALIFORNIA

ARS JOURNAL

A PUBLICATION OF THE AMERICAN ROCKET SOCIETY

FORMERLY JET PROPULSION

American Rocket Society

500 Fifth Avenue, New York 36, N. Y.

Founded 1930

Scope of ARS JOURNAL

This Journal is devoted to the advancement of astronautics through the dissemination of original papers disclosing new scientific knowledge and basic applications of such knowledge. The sciences of astronautics are understood here to embrace selected aspects of jet and rocket propulsion, space flight mechanics, high-speed aerodynamics, flight guidance, space communications, atmospheric and outer space physics, materials and structures, human engineering, overall system analysis, and possibly certain other scientific areas. The selection of papers to be printed will be governed by the pertinence of the topic to the field of astronautics, by the current or probable future significance of the research and by the importance of distributing the information to the members of the Society and to the profession at large.

Information for Authors

Manuscripts must be as brief as the proper presentation of the ideas will allow. Exclusion of dispensable material and conciseness of expression will influence the Editors' acceptance of a manuscript. In terms of standard-size double-spaced typed pages, a typical maximum length is 22 pages of text (including equations), 1 page of references, 1 page of abstract and 12 illustrations. Fewer illustrations permit more text, and vice-versa. Greater length will be acceptable only in exceptional cases.

Short manuscripts, not more than one-quarter of the maximum length stated for full articles, may qualify for publication as Technical Notes or Technical Comments. They may be devoted to new developments requiring prompt disclosure or to comments on previously published papers. Such manuscripts are usually published within two months of the date of receipt.

Sponsored manuscripts are published occasionally as an ARS service to the industry. A manuscript that does not qualify for publication, according to the above-stated requirements as to subject, scope or length, but which nevertheless deserves widespread distribution among jet propulsion engineers, may be printed as an extra part of the Journal or as a special supplement, if the author or his sponsor will reimburse the Society for actual publication costs. Estimates are available on request. Acknowledgment of such financial sponsorship appears as a footnote on the first page of the article. Publication is prompt since such papers are not in the ordinary backlog.

Manuscripts must be double spaced on one side of paper only with wide margins to allow for instructions to printer. Include a 100 to 200 word abstract. State the authors' positions and affiliations in a footnote on the first page. Equations and symbols may be handwritten or typewritten; clarity for the printer is essential. Greek letters and unusual symbols should be identified in the margin. If handwritten, distinguish between capital and lower case letters, and indicate subscripts and superscripts. References are to be grouped at the end of the manuscript and are to be given as follows: For journal articles: authors first, then title, journal, volume, year, page numbers for books: authors first, then title, publisher, city, edition and page or chapter numbers. Line drawings must be clear and sharp to make clear engravings. Use black ink on white paper or tracing cloth. Lettering should be large enough to be legible after reduction. Photographs should be glossy prints, not matte or semi-matte. Each illustration must have a legend; legends should be listed in order on a separate sheet.

Manuscripts must be accompanied by written assurance as to security clearance in the event the subject matter lies in a classified area or if the paper originates under government sponsorship. Full responsibility rests with the author.

Submit manuscripts in duplicate (original plus first carbon, with two sets of illustrations) to the Editor, Martin Summerfield, Professor of Aeronautical Engineering, Princeton University, Princeton, N. J. Preprints of papers presented at ARS national meetings are automatically considered for publication.

ARS JOURNAL is published monthly by the American Rocket Society, Inc. and the American Interplanetary Society at 20th & Northampton Sts., Easton, Pa., U. S. A. Editorial offices: 500 Fifth Ave., New York 36, N. Y. Price: $12.50 per year, $2.00 per single copy. Second-class mail privileges authorized at Easton, Pa. This Publication is authorized to be mailed at the special rates of postage prescribed by Section 132.122. Notice of change of address should be sent to the Secretary, ARS, at least 30 days prior to publication. Opinions expressed herein are the authors and do not necessarily reflect the views of the Editors or of the Society.

The Lockheed-developed U.S. Navy POLARIS:

Missiles launched from ocean depths

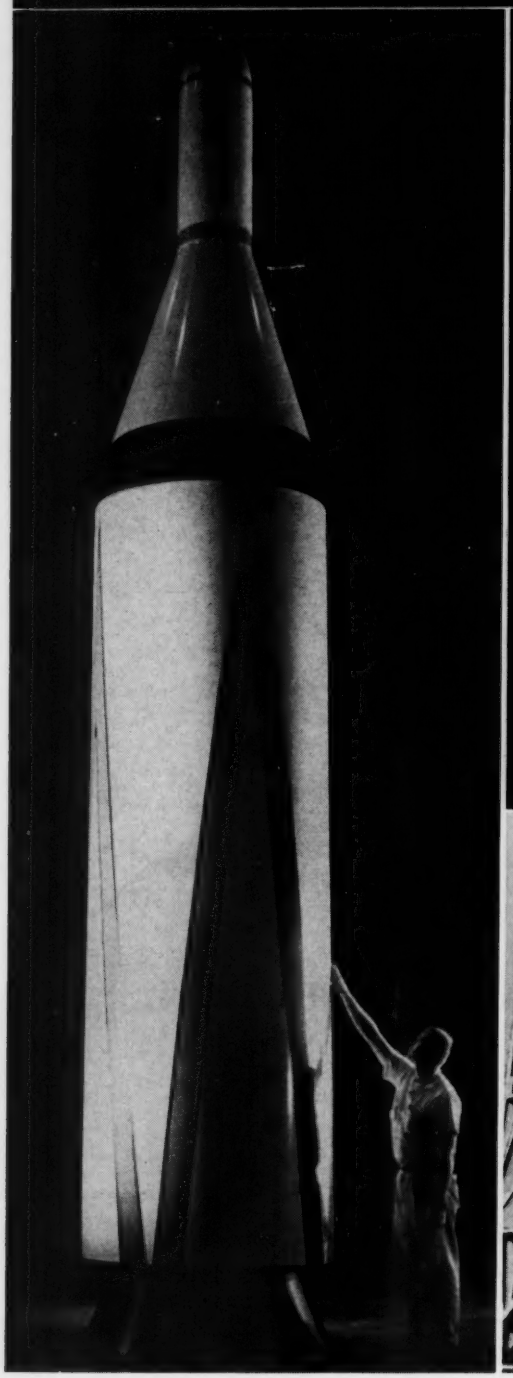

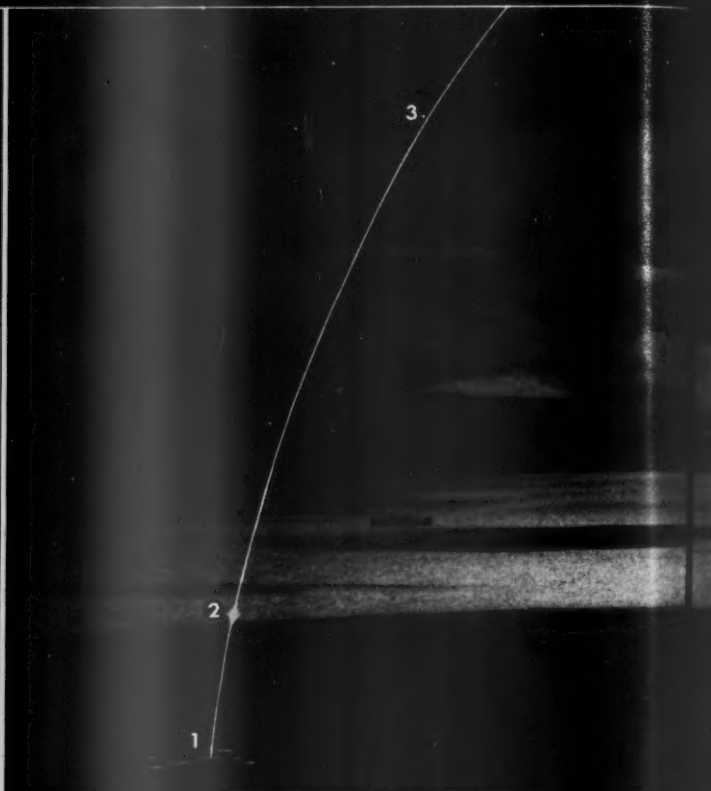

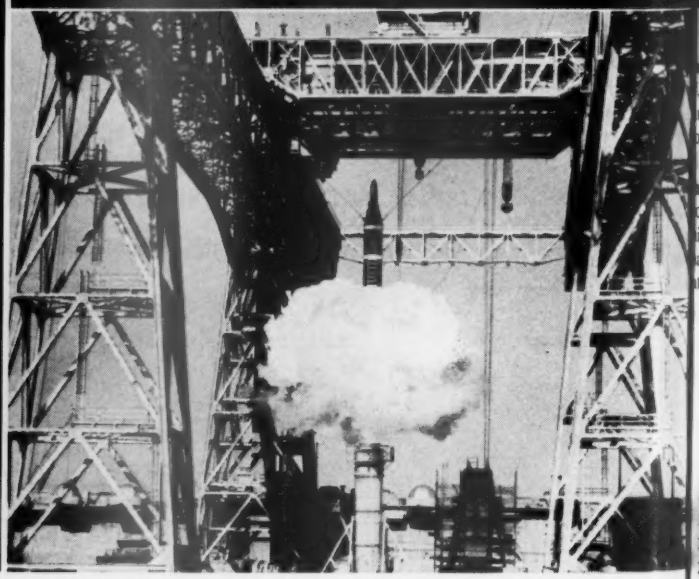

Above: *Propulsion system firings* light up night sky at Lockheed Missiles and Space Division's 4000-acre test base in the Santa Cruz mountains, Calif. A nearby vertical test stand permits simulated flights of complete POLARIS missiles, to test their propulsion and guidance systems.

Left: *Nuclear powered U. S. Navy sub* (1) launches solid-propellant POLARIS missile which erupts from ocean depths (2)—then rockets its way on a ballistic missile trajectory high above the earth's atmosphere (3) into outer space. Re-entering the atmosphere (4) the re-entry body of the POLARIS plunges earthward to destroy its target (5).

Launching an IRBM from submerged submarines involves technological developments that are unique in ballistic missile history.

As POLARIS Missile System manager and prime contractor, Lockheed's Missiles and Space Division is responsible for coordinating all phases of its design, development, and production.

The POLARIS, a solid-propellant missile, will be operational in 1960—ahead of schedule. The operational missiles will be delivered to U. S. Navy submarines in Lockheed ready-service transporters under controlled humidity and temperature conditions. And Lockheed's ACRE—Automatic Checkout and Readiness Equipment—will maintain the constant ready-to-fire capability of POLARIS missiles, right up to the moment of launch.

With an ultimate range of 1500 nautical miles, the POLARIS will become one of the most formidable deterrent weapons ever devised. For any significant military target on earth will be within range of its nuclear warheads.

ft: *"Operation Sky-Catch" tests,* conducted jointly by .S. Navy, Westinghouse and Lockheed, reveal effects of unch stresses. To prevent damage to POLARIS test missile mponents, huge overhead assembly catches it in mid-air.

r left: *Carrying awesome destructive power,* Navy's OLARIS is markedly smaller than other U. S. ballistic issiles of same range. To enable one submarine to carry any missiles, Lockheed scientists achieved miniaturi- tion breakthroughs on all major systems of POLARIS.

LOCKHEED

JET TRANSPORTS • JET FIGHTERS • JET TRAINERS • COMMERCIAL & MILITARY PROP-JET TRANSPORTS • ROCKETRY
BALLISTIC MISSILE RESEARCH & DEVELOPMENT • WEAPON SYSTEM MANAGEMENT • ANTI-SUBMARINE PATROL AIRCRAFT
NUCLEAR-POWERED FLIGHT • ADVANCED ELECTRONICS • AIRBORNE EARLY-WARNING AIRCRAFT • AIRPORT MANAGEMENT
NUCLEAR REACTOR DESIGN & DEVELOPMENT • GROUND SUPPORT EQUIPMENT • WORLD-WIDE AIRCRAFT MAINTENANCE

Recent Advances in Solid Propellant Grain Design

JEAN A. VANDENKERCKHOVE[1]

Université Libre de Bruxelles
Bruxelles, Belgium

The author has been Assistant at the Institute of Aeronautics of the Université Libre de Bruxelles since 1954. He was attaché to Professor von Kármán in 1955 and is currently working with Professor Jaumotte, Head of the Institute and one of the Belgian representatives at the Combustion and Propulsion Panel of AGARD (NATO). He received a Mechanical and Electrical Engineer degree from the Université Libre de Bruxelles in 1952 and an M.S. degree from the California Institute of Technology in 1954. He has written several papers, especially in the area of solid propellant rockets, and is co-author of the book "Rocket Propulsion," which, after a first French edition in 1957, is to be published in English and in German this year.

A WIDE variety of grain designs has been actually used or can be considered (1).[2] However all possibilities more or less fall into one of the three following categories.[3]

End-Burning Grains

With end-burning grains, also called restricted or cigarette-burning grains, the combustion is limited to the transverse cross section of the chamber.

It is possible, with such rockets, to achieve near constant thrusts during very long burning times, up to 10 min and more, since the burning area remains constant, and the available propellant thickness, which is equal to the chamber length, can become quite important. However, despite their optimum loading density, such end-burning rockets are mostly low performance, low thrust motors. Indeed, for long durations, it is difficult to protect the chamber hardware from heating, and the walls must then become fairly heavy to resist pressure. Moreover, inhibiting poses a difficult problem, and the center of gravity shifts during combustion. Finally, it is often impossible, with available burning rates, to develop large thrusts with reasonably limited cross sections.

Side-Burning Grains

With side-burning grains, the combustion takes place on a straight cylinder formed by the lateral surfaces of the grain, and the end surfaces are often protected from burning, or at least they do not represent a significant fraction of the burning area.

In view of their small cross sections, light weights and wide range of thrust laws obtainable, these side-burning grains are used in most cases, even for relatively long burning times of the order of 1 min.

Moreover, the chamber walls can often be protected from heating by the propellant itself, which can be free-standing or case-bonded. However, suitable passages or port areas must be provided for the gas flow within the chamber, and the loading density is accordingly reduced. In fact, the latter decreases together with burning time. From the above mentioned geometrical property, it is seen that the grain design can be studied in a transverse cross section. Fig. 1 represents several possible cross sections; it illustrates the wide possibilities offered by this category.

A side-burning grain is called unrestricted when the combustion takes place on almost all lateral surfaces (Fig. 1, cases A, B, C, L, M, N and O). The use of unrestricted grains results in severe wall heating and relatively large losses due to final grain fragmentation. Modern designers generally try to protect the walls by the propellant itself (Fig. 1, cases D, E, F, G, H, I, J and K), in which case wall heating can be kept low, thus making for very light chambers.

Side-burning grains are often called cylindrical grains; however such charges need not necessarily be cylindrical on their inhibited surfaces.

Noncylindrical Grains

This last category includes the grains which cannot enter one of the two previously described classes. It is characterized by the fact that the generatrices of the burning area are not parallel straight lines any more. Fig. 2 illustrates three designs representative of this category, the so-called slotted, cylindroconical and cruciform grains. The computation of the characteristics of such charges is often difficult, because it cannot be reduced to a two-dimensional problem. However, chamber slenderness is often quite high, and it is then possible to simplify the problem by considering, as a first approximation, that the grain is composed of several portions of straight side-burning surfaces (slightly tapered port), or that the grain is a straight side-burning surface on which small modifications are added (influence of end surfaces or other peculiarities, such as small holes drilled for eliminating irregular burning).

It must be noted that the grain characteristics sometimes heavily depend on the inhibiting pattern. For instance, the cruciform grain with no inhibition at all, is strongly regressive, whereas it is progressive if all arms are completely inhibited. It has neutral characteristics only when 50 per cent of the supporting surfaces are restricted, in which case it is rigorously a side-burning grain only at the beginning of the combustion, since noncylindrical areas develop afterward near the edges of the inhibitor strips. (The arrangement of inhibitor strips shown in Fig. 2 has been selected to avoid irregular burning.)

On the other hand, the amount of final losses or slivers also depends heavily upon grain geometry. Near the end of the

Received May 19, 1959.

[1] Associate Member ARS.

[2] Numbers in parentheses indicate References at end of paper.

[3] Adapted by permission from material in "Rocket Propulsion" by M. Barrère, A. Jaumotte, B. Fraeys de Veubeke and J. Vandenkerckhove, distributed in the U. S. by Van Nostrand Co., and published by Elsevier, Amsterdam, 1959.

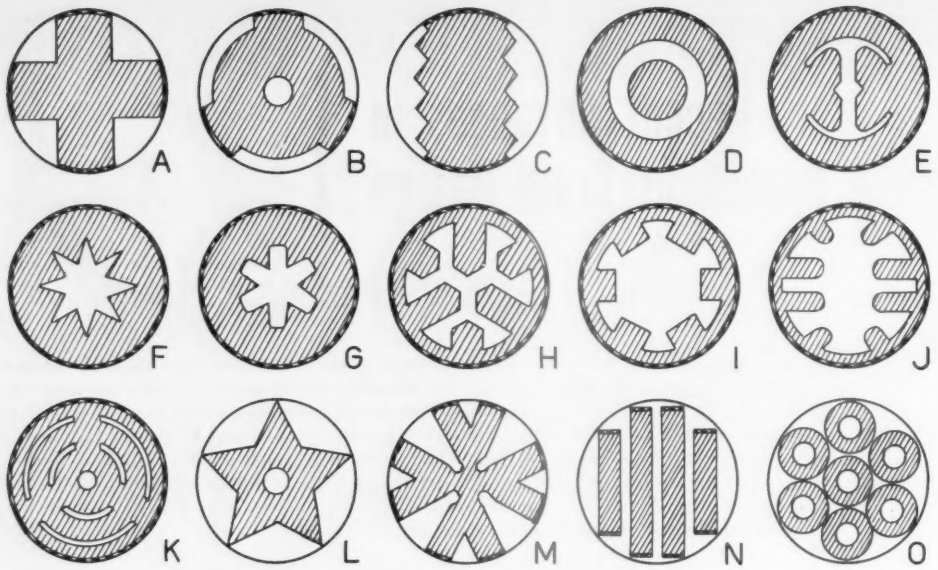

Fig. 1 Wide variety of side-burning grain cross sections

combustion, the burning area is often strongly regressive. Indeed, when the major part of the burning surface disappears, near burnout, a fraction of the propellant remains attached to the walls or to the inhibitor, and continues to burn at low pressure without producing an appreciable thrust. That fraction, which should be kept to 5 per cent or less, must be considered as a loss whose importance can be computed by geometry ("theoretical unburnt residue"). This phenomenon is known as the tail-off. Since it is difficult to tell how much of the slivers will actually burn, variability is thus added to the thrust law.

On the other hand, with some designs, the combustion takes place on both sides of the propellant thickness (Fig. 1, cases A, B, C, K, L, M, N and O), and final breakup takes place in an erratic manner. A loss of about 5 per cent of the web thickness is often assumed to account for final fragmentation. The actual value, however, depends upon grain geometry, the higher the grain compactness, the lower the loss. The free slivers are then discharged through the nozzle. The characteristics of many simple grain designs are discussed with some detail in the literature (2 through 8).

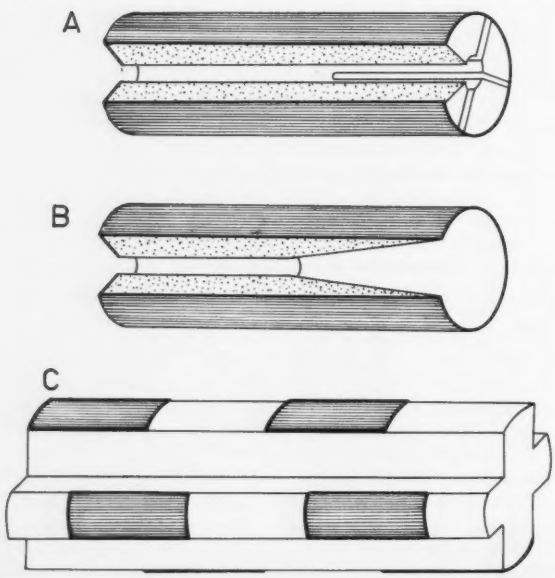

Fig. 2 A: slotted grain, B: cylindroconical grain, C: cruciform grain with its classical arrangement of inhibitor strips

Internal Ballistics

The proper grain design must give the requested thrust program $F(t)$ which can be neutral, progressive, regressive or assume any other pattern, a dual thrust law, for instance.

Due to the slight dependence of thrust coefficient on expansion ratio, the thrust is roughly proportional to chamber pressure which, certain second order effects being neglected, is given by the well-known relation

$$p_c = (\rho_p a K c^*)^{1/(1-n)} \qquad [1]$$

with

$$K = A_b/A_t$$

if the burning rate is expressed by

$$r = dy/dt = a p_c^n \qquad [2]$$

where

- ρ_p = specific mass of the propellant
- c^* = its characteristic velocity
- a = constant which depends only on grain temperature
- n = constant called the combustion index which is always smaller than 1
- K = ratio of burning area A_b to nozzle throat area A_t

The burning rate r is, indeed, the derivative with respect to time of the burnt distance y which varies from 0 to w, w being the web thickness.

In grain design, it is desirable to use the burnt distance y as the independent variable. This can be easily done by integration of Equation [2] in which the pressure is known as a function of time $p_c(t)$. We thus obtain, successively, the

functions $y(t)$, $p_c(y)$, and finally, through Equation [1], $K(y)$. The problem can thus be reduced to a geometrical one. For instance, a progressive thrust law is obtained when A_b steadily increases with y (9).

Similarly, a dual thrust law in which the high thrust level is developed during a short booster phase and is followed by a long sustainer period at moderate thrust, can be obtained with a single grain which, at the beginning, provides a large burning area, which after a while, suddenly drops to a much lower value (see the wagon-wheel design description in section on design charts).

Equation [1] can be viewed as the transfer function between grain geometry and chamber pressure, the term $1/(1 - n)$ which only depends on the propellant nature, acting as the amplification factor.

It is seen that for large values of the combustion index (n = 0.7 for instance) small variations in burning area result in very important thrust changes, a property which could, conceivably, be used to advantage, although in most cases small values of n ($n \leq 0.4$) are to be favored for the purpose of reducing dispersion.

This brings us to study briefly the problem of propellant selection in relation to grain design. For this purpose we shall assume that the chamber diameter is known (see section on overall grain dimensions) and that the thrust law is approximately neutral. The selection of propellant, chamber pressure and grain design is more or less arbitrary. It depends primarily upon the web thickness w needed to obtain the design burning time t_b through the relation $\bar{r}\, t_b = w$, in which $\bar{r}$ is the mean burning rate.

With side-burning grains which are used in most cases, design studies indicate that it is difficult to get web thicknesses much over one-half the chamber radius (Fig. 1, cases F and G). However, small web thicknesses can be easily obtained in a wide variety of shapes (Fig. 1, cases H, I, J, K, M, N and O), but a decrease in web thickness generally results in increased production complexity and a higher sliver fraction, especially when the combustion takes place on both sides of the propellant thickness. It thus appears that, whatever the burning time, it is favorable to select a design which protects the walls and whose web is, very roughly, equal to one-half the chamber radius, the burning rate being chosen so as to correspond to optimum pressure for which the chamber weight can be minimized. Two cases will be considered.

Long Burning Times

When the preceding "rule of thumb" cannot be readily satisfied with a suitable propellant, the web thickness can be slightly increased. However it seems difficult to exceed $w = 0.7\ R_c$.

The chamber pressure can also be somewhat lowered at a slight cost in specific impulse. If this is not sufficient, the burning rate can, in some cases, be reduced without much lowering the specific impulse, but often a less energetic formulation must be used.

In extreme cases, the chamber radius must be increased, or an end-burning geometry must be chosen. In practice, however, burning times in excess of 30 sec can be obtained with side-burning grains of reasonably low diameter.

Short Burning Times

Obtaining short burning times is much simpler, since the web can be reduced easily at the cost of increased production complexity and higher sliver fraction.

It must be emphasized, however, that throughout the preceding discussion, the terms "long" or "short" burning times do not have an absolute meaning, since the scale effect must be accounted for. Indeed, it is much easier to obtain a long burning time with a large motor than with a small one. Therefore, high burning rates must be favored either when the burning time is short or when the rocket is large.

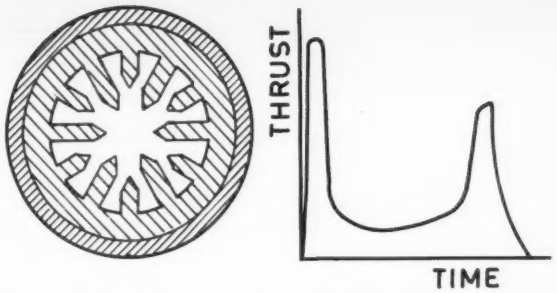

Fig. 3 Grain design using two propellants and its thrust law. During the first phase, a wagon-wheel design provides the initial boost; it is followed by a sustainer period at the end of which a layer of fast burning propellant is reached and provides a final impulse

If a complicated thrust law is to be obtained, as with a dual-thrust motor, it is often difficult to vary, with a single grain, the burning surface within sufficiently wide limits, and two propellants having different burning rates can be used (10, 11, 12). Such a case is represented on Fig. 3 adapted from (10).

Before leaving the subject of internal ballistics, two important phenomena must be mentioned.

The first one is the pressure drop along the grain length which, for a constant port area, results from the mass addition and the corresponding flow acceleration. The maximum pressure is reached at the chamber front end, and its value can be approximately computed by Equation [1] in which ratio K is replaced by an effective value

$$K_{eff} = K[1 + (\Gamma^2/2)J^2]$$

with

$$J = A_t/A_p$$

where

Γ = function of the specific heat ratio alone (for $\gamma = 1.25$, we have $\Gamma = 0.658$)
A_p = port area at the moment under consideration

In high performance designs, the loading density is quite high together with ratio J ($J \geq 0.65$).

A sizable pressure peak thus takes place right at the beginning of the burning time when J still has its maximum value.

This phenomenon can be compensated by reducing slightly the initial burning area so as to keep K_{eff} constant during combustion.

The second phenomenon consists in an increase in burning rate under influence of the flow velocity in the port. It is called erosive burning.

These two phenomena result in a variation in burning rate along the grain length which increases tail-off, and, in severe cases, may lead to burn-through due to premature contact of the flame front with a portion of the chamber walls.

By tapering the port area so as to increase the passage area in proportion to the mass addition in each section, the mean flow velocity and the pressure can be kept constant, together with the burning rate, along most of the grain length (see Fig. 4).

The loading density can thus be improved significantly with short burning times, and a constant web thickness can be used.

Similarity Rules

In designing a solid propellant rocket, the thrust law (thrust vs. time) is generally imposed, but the choice of motor dimen-

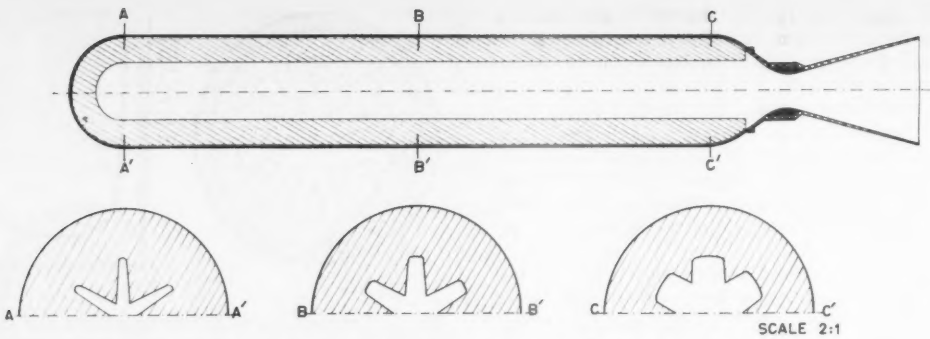

Fig. 4 Longitudinal section of a case-bonded rocket with tapered port

sions, chamber pressure and propellant nature is left, within limits, to the designer.

In certain cases, however, the motor length, its diameter or even the chamber wall thickness can be imposed by ballistical or structural considerations.

The choice of one of the powerplant characteristics, its length for instance, influences almost all of the other parameters.

The similarity rules of solid propellant motors provide the means of easily arriving at a first approximation of the characteristics of a new design by extrapolating the dimensions of existing powerplants (13).

Let us consider a family of geometrically similar solid propellant rockets (same propellant and same grain design). Each member of the family is characterized by a length l (the chamber diameter for instance), and it can be readily shown that:

Burning time t_b is proportional to l.

Thrust is proportional to l^2.

Total impulse I is proportional to l^3.

Chamber pressure p_c (or its variation as a function of a dimensionless time scale) is independent of l.

Loading density of the chamber and the ratio J of the throat area to port area, which characterize internal ballistics, are independent of l.

These similarity rules often allow for the reduction of the number of full-scale tests, since much data can be obtained with scaled-down models.

Overall Grain Dimensions

In most cases, the overall grain dimensions, i.e., diameter and length, are approximately equal to the overall chamber dimensions, allowance being made for the inhibitors, liners, supporting elements and constructional features, such as the end closures.

The grain design is thus directly affected by the motor dimensions. When the latter are imposed, the choice of a suitable grain configuration can be carried out almost straightforwardly.

However, for system analysis where optimum design has to be determined, it has been pointed out by Thackwell among others, that the motor dimensions should be kept as flexible as possible (14).

Most of the published works have taken advantage of this concept, either by direct scaling of known powerplants by means of the above mentioned similarity rules, or in a somewhat less restrictive manner, by assuming a priori some kind of geometrical condition and by allowing the other parameters, the chamber pressure or the grain slenderness, to vary within limits (14 through 17).

A widely used condition has been that the grain web thickness must always be kept equal to one-half the chamber radius. The loading density of the chamber can also be chosen a priori.

Such a view, although it has provided very useful results, is somewhat restrictive, because it requires the preliminary choice of the propellant kinetic characteristics (burning rate vs. pressure). From a theoretical point of view, such an approach does not provide a truly optimum design, since the chamber dimensions are determined a posteriori from the grain design choice.

A much more general approach is obtained by minimizing the total hardware weight while limiting the assumptions made on grain design and propellant performance to a minimum (18, 19).

In fact, this method requires only the choice of the propellant energetic properties (its characteristic velocity c^*) and the assumption that a side-burning grain is used (possibly with a tapered port area).

The propellant volume required for obtaining the specified total impulse can thus be computed readily. It decreases slightly when chamber pressure increases due to the favorable influence of expansion ratio on thrust coefficient.

Similarly, for a given thrust level, the nozzle throat area, varies approximately as the reciprocal of chamber pressure. It must remain proportional to the initial port area, since the value of the parameter $J = A_t/A_p$, which must always be smaller or at most equal to unity, can be chosen a priori, taking into account the magnitude of the difficulties that could be encountered during the development. The ratio J is representative of the empty space in the chamber. In the case of a tapered port area, its mean value along the grain length must be used.

For each pressure, the propellant volume and grain port area are known, and the inert hardware weight can be given as a function of chamber radius alone. Thus an optimum chamber radius exists for each pressure.

When chamber pressure increases, the minimum dead weight steadily increases, while the propellant weight decreases as shown by Fig. 5.

An optimum pressure therefore exists for which the total rocket motor weight passes through a minimum. It can be shown that this true optimum does not correspond to the maximum loading density or to the maximum value of the ratio Λ of the propellant weight to total motor weight.

This method provides true optimum dimensions which can often be adhered to. In some cases, however, this may not be actually possible, and it then provides the tool for evaluating the penalty resulting from the specifications. For instance, an overlong burning time at moderate thrust may lead to excessive chamber diameter, whereas a large impulse produced in a very short time may result in a poor loading density.

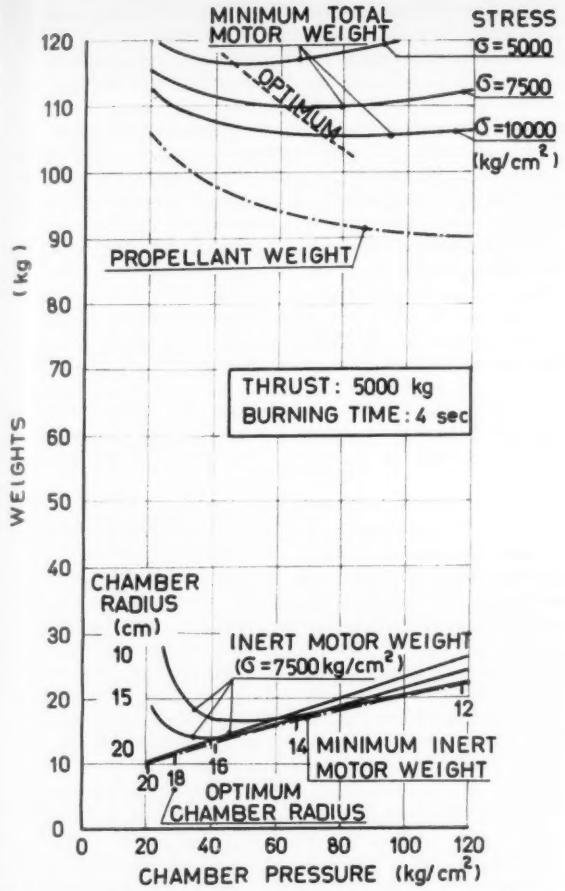

Fig. 5 Inert motor weight, propellant weight and minimum total motor weight as functions of chamber pressure. The locus of the minimum inert weight is the envelope of the curves of the inert weights obtained by taking arbitrarily different chamber radii. The motor is due to give a 5000 kg thrust during 4 sec. Its ratio J is taken equal to 0.5

Fortunately, it is seen that, in most cases, the optimum is not very pronounced, especially when construction is light and burning time is long.

Finally, it must be emphasized that the preceding method maximizes the ratio of total impulse to total motor weight. In many cases, however, the burnout velocity of the missile is to be optimized, and the method must be slightly modified, taking into account the fact that the dead weight must still be minimized.

Fundamentals of Grain Design

A solid propellant grain burns in such a manner that any point on its surface moves perpendicularly to the tangent plane at that point. Therefore, in a cross section, a cusp on the perimeter, convex toward the gas phase, remains a cusp as burning progresses, while a cusp concave toward the gas phase becomes an arc of a circle, with its center at the original cusp. As combustion proceeds, new convex cusps can be formed, as the result of the interaction between two smooth curves (see Fig. 6, case A); less frequently, convex cusps also disappear.

In most cases, as pointed out earlier, the grain characteristics can be studied in a cross section perpendicular to the grain axis. In such a two-dimensional study, the most interesting parameters are:

The length S of the burning perimeter, which is a function of the burnt distance y. (For a side-burning design, we have $SL = A_b$, L being the grain length.)

The port area A_p from which the ratio J can be readily deduced.

The geometrical amount of slivers, which can be defined as the final grain cross-section area A_f when the burning area begins to drop sharply, near burnout.

Epstein has established two useful properties (20):

1 The length $S_{(y)}$ of a portion of perimeter AB, *free of convex cusps*, can be expressed as a function of its initial length $S_{(y=0)}$, of the burnt distance y, and of the angles φ_A and φ_B made by the end tangents with a direction of reference (see Fig. 6 case A), by the relationship

$$S_{(y)} = S_{(y=0)} + y(\varphi_A - \varphi_B)$$

If the perimeter is a closed curved, we thus have

$$\varphi_B = \varphi_A + 2\pi$$

and the rate of increase in length of a closed perimeter free of convex cusps does not depend on its length or form.

As an illustration of the usefulness of this property, it can readily be shown that, during combustion, the increase in burning perimeter of the multiperforated grain, represented by case K of Fig. 1, is equal to $14\pi w$, w being the web thickness.

It appears, therefore, that an internal burning grain without cusps is progressive, the larger the number of perforations, the more pronounced the progressivity. Likewise, an uninhibited and cusp-free outer surface has a regressive influence; hence a tubular grain is neutral.

2 The length $S_{(y)}$ of a portion of perimeter AB containing one convex cusp, can be expressed as a function of the

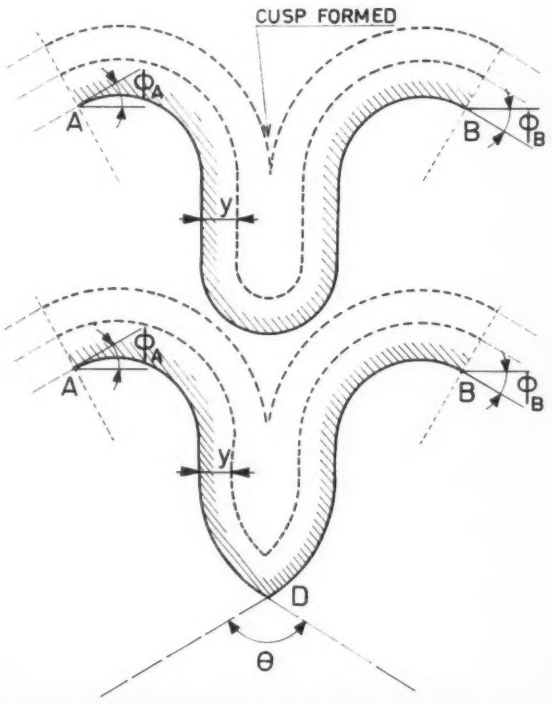

Fig. 6 Evolution of a portion of burning perimeter as combustion proceeds

parameters $S_{(y=0)}$, y, φ_A, φ_B and of the cusp apex angle θ (see Fig. 6, case B), by the relationship

$$S_{(y)} = S_{(y=0)} + y(\varphi_A - \varphi_B) + \int_0^y 2\left(\frac{\pi}{2} - \frac{\theta}{2} - \cot\frac{\theta}{2}\right) dy$$

As pointed out by Epstein, it is thus possible to compute a suitable design from the a priori choice of a few parameters (number of axis of symmetry of the perimeter).

For instance, neutral characteristics can be obtained with an internal burning design having n identical convex cusps or star points (Fig. 1, cases F and G), if, during combustion, θ can be kept constant and equal to the value $\bar{\theta}$ given by

$$\frac{\pi}{2} + \frac{\pi}{n} = \frac{\bar{\theta}}{2} + \cot\frac{\bar{\theta}}{2}$$

This relationship yields:

n	$\bar{\theta}/2$ (deg)
4	28.21
5	31.12
6	33.53
7	35.55
8	37.30
9	38.83
10	40.20
12	42.52

Design Charts

In practice, the grain designer has at his disposal a series of charts on which the characteristics of numerous relatively simple designs are represented in a wide range of values of the different parameters. Very often, one of these basic geometries, generally built with segments of straight lines and with radial arcs, is well suited and can be readily selected, with possibly minor changes.

The computation of such charts is a necessary, straightforward but tedious geometrical job, the description of which is outside the scope of this review. Almost every group working on solid propellants has developed its own satisfactory method around the same basic equations. Some methods, however, are believed to be more convenient than others for the purpose of providing the maximum amount of information in the minimum number of charts covering the widest range of the design parameters. A dimensionless presentation is, of course, to be favored for this purpose.

With such charts, the grain designer can investigate rapidly and systematically the complete range of possible shapes, and is thus in a position to optimize the design.

The most important case of internal burning, single-perforated grains (internal burning star and wagon-wheel configurations) has been extensively studied in (5 and 21 through 25).

As an illustration, Fig. 7 represents the charts giving the characteristics S/l, A_p/l^2 and A_f/l^2 of the eight-pointed internal burning star, as functions of the reduced burnt distance $(f + y)/l$.

Radius l of the basic perforation without fillet has been chosen as unity, and the other geometrical parameters n, ε, f, θ and w are defined on Fig. 7.

Depending upon the value of angle θ, the combustion can be progressive, neutral or regressive during the first phase, during which the straight star points have not yet disappeared.

During the second phase, the star points have disappeared, and after a while the grain becomes always progressive.

As an example of the information provided by the charts, Fig. 8 represents the characteristics of one particular eight-pointed wagon-wheel design which gives a dual-thrust law. The geometrical parameters are defined on the left of the figure.

It must be noted that the second phases of the wagon-wheel and internal burning star are identical, and that the second phase progressivity can be compensated by allowing the grain ends to burn unrestricted, and by tapering the grain length

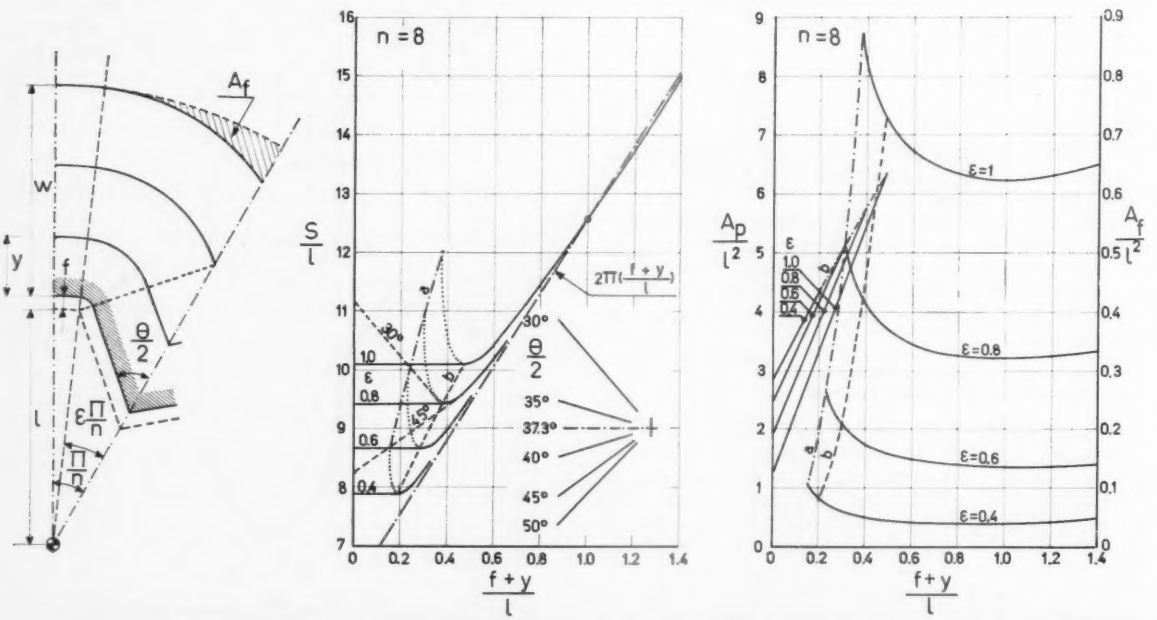

Fig. 7 Geometrical definitions of the internal burning star design and charts representing the characteristics of the eight-pointed star in a dimensionless form. Burning perimeter during the first and second phases, port area during the first phase and sliver area during the second phase, as functions of the dimensionless burnt distance. From (24)

at the outer diameters (Fig. 4). Both methods result in a decreasing grain length, as combustion proceeds.

It must be emphasized that, in addition to suitable geometrical characteristics, the choice of a design must also take into account several other important factors:

1 In many applications, the reproducibility of the thrust law is of prime importance, and the tail-off period must be reduced to a minimum. This could be achieved with an internal burning star by filling with an inert material the dark zone representing A_f on the left of Fig. 7. Other more elaborate designs can conceivably be developed, for instance by means of grains made with two propellants having slightly different burning rates.

In the case of ballistic missiles, however, thrust termination methods must be resorted to.

2 Some designs are more subject than others to irregular or resonance burning as discussed for instance by Green (26).

3 Finally, the actual realization of cores or mandrels representing the chamber free-volume is sometimes difficult and limits the choice of grain shapes.

Mechanical Behavior of Grains

In many cases, due to the mechanical and thermal stresses, the grain resistance is critical and can be improved through proper design. The physical properties of the propellant must thus be carefully taken into account in the choice of the grain geometry.

As a rule, hard propellants are used for unrestricted and free-standing grains which are locally supported. In these cases, the allowable grain deformation under acceleration and internal pressure difference has to remain sufficiently small. For instance, Wimpress has shown that in the simple case of a tubular unrestricted grain, the maximum possible value of ratio J increases together with the modulus of elasticity of the propellant (3).

On the other hand, soft propellants are needed for case-bonded grains for which a good elongation is imperative in order to accommodate the chamber expansion. The strains are then imposed, and the stresses must be kept within the possibilities of the propellant which depend, among other factors, on temperature and rate of the strain.

The discussion of the rheological properties of the propellants is outside the scope of this survey, and we shall only summarize here the few fundamental papers which have been published on this subject and which are of direct interest for grain design.

It must be noted, however, that these published works are more or less oversimplified, since they assume a perfectly elastic behavior whereas the propellant can exhibit viscoelastic properties. Even so they are limited by necessity, to simple two-dimensional models. However, these works provide the grain designer with very useful qualitative and even quantitative indications for stress analysis.

Thermal Stresses

An important environmental effect on a rocket is the thermal stress produced in the propellant by the thermal cycling during storage. This problem has been excellently studied by Geckler and his collaborators, in the case of an infinitely long tubular grain (27, 28, 29).

These authors have shown that the most severe stresses occur with case-bonded grains after a sufficiently long time, when thermal equilibrium is achieved. In this particular case, the outer tangential strain of the propellant must be equal to the differential expansion between the case and the propellant. Therefore, the pressure applied by the chamber on the propellant can be computed, and the stresses can be expressed by means of Lamé's equations. The maximum tensile stress is seen to be the tangential stress σ_θ at the inner radius after a cooling period. It can be expressed in a dimensionless form by the relationship

$$\frac{(1-\nu)\sigma_\theta}{E\alpha_p(T_e - T_0)} = \frac{(\alpha_c/\alpha_p) - 1}{1 - \dfrac{1 - (R_i/R_e)^2}{2(1-\nu)}}$$

where

ν = Poisson's ratio
E = modulus of elasticity of the propellant
α_p = coefficient of linear thermal expansion of the propellant
α_c = coefficient of linear thermal expansion of the chamber
T_0 = stress-free temperature
T_e = final temperature
R_i = inner radius of the grain
R_e = outer radius of the grain

Fig. 9 represents the variation of

$$\frac{(1-\nu)\sigma_\theta}{E\alpha_p(T_e - T_0)}$$

as a function of α_c/α_p for different values of R_i/R_e in the case $\nu = 0.4$.

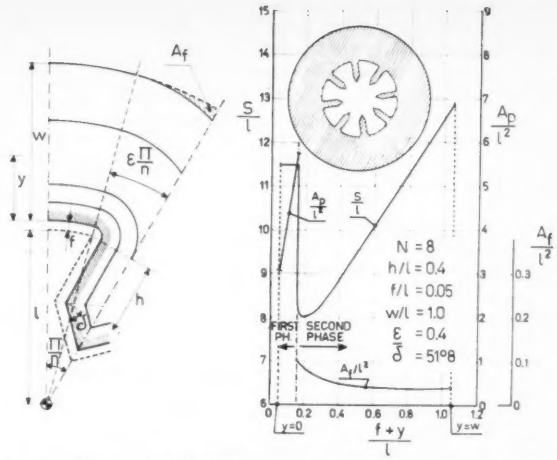

Fig. 8 Geometrical definitions of the wagon-wheel design an characteristics of one particular design of this family

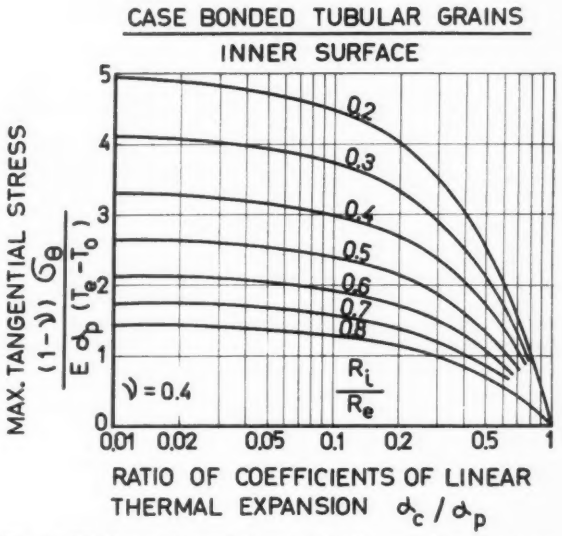

Fig. 9 Maximum thermal stress at the inner radius of a case-bonded tubular grain for several values of the ratio R_i/R_e (Poisson's ratio $\nu = 0.4$)

For our purpose, the important conclusion is that the maximum tensile stress increases together with the ratio R_e/R_i which is representative of the web thickness.

The same conclusion holds true with free-standing grains, but the stresses are then considerably less severe, and their maximum occurs early during the heating period.

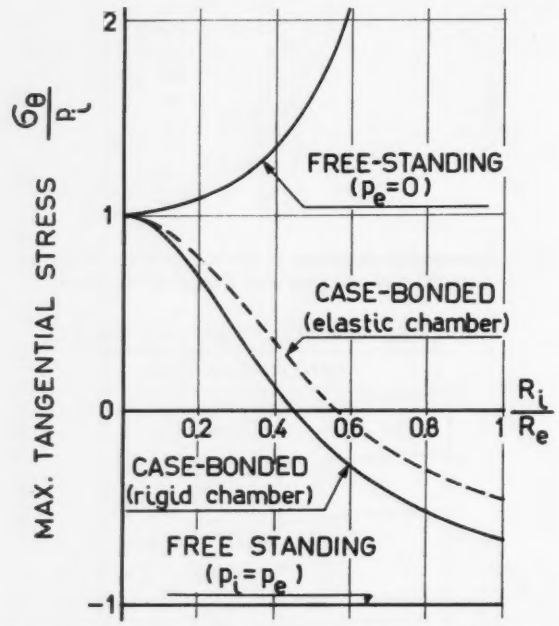

Fig. 10 Maximum tangential stress at the inner radius as a function of the ratio R_i/R_e. The curves corresponding to case-bonded grains have been computed with $\nu = 0.4$

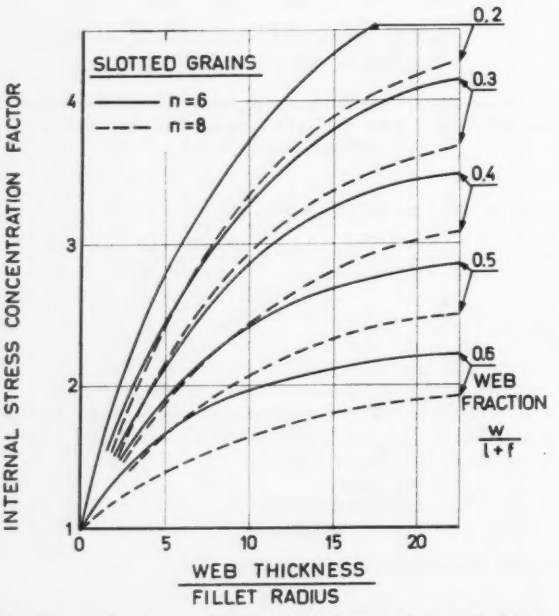

Fig. 11 Design curves showing the influence of the web thickness and fillet radius on the stress concentration factor at the inner surface, for six- and eight-slotted configurations. Adapted from (30)

Mechanical Stresses

During combustion, stresses are also induced, even if the pressure difference between the front and nozzle ends and the axial acceleration are neglected.

Lamé's equations can again be used for computing the maximum tensile stress, which is the tangential stress at the inner radius, except in the simple hydrostatic case of a free-standing grain whose inner and outer surfaces are subjected to the same pressure ($p_e = p_i$) (2).

For an internal burning free-standing grain whose outer annulus between the propellant and the wall is not pressurized by the combustion gases ($p_e = 0$), the maximum tangential stress varies from p_i to infinity when the web increases.

Such a high stressing cannot be tolerated, and it is thus current practice to allow for gas passage into the outer annulus in order to provide external support for the grain and prevent its failure.

A more interesting fact, for our purpose, is that for case-bonded grains, tensile stresses only occur when the web thickness becomes larger than approximately one-half the chamber radius. Above that value, the maximum tensile stress increases fairly rapidly, and elasticity of the chamber walls tends to increase its value. Fig. 10 represents the dimensionless maximum tangential stress σ_θ/p_i as a function of the ratio R_i/R_e in the cases discussed above (p_i is the effective pressure in the perforation).

Stress Concentrations

The preceding discussion has been limited to hollow, circular cylinders. Actual grains, however, exhibit much more complex shapes, which are associated with stress concentrations.

For instance, the internal burning grains with their complex perforations are subject to the inherent weakness that stress concentrations occurring around the small angles of the star points tend to aggravate any susceptibility of the propellant to mechanical failure. The actual stress can easily exceed two or three times that which occurs in a simple thick walled cylinder. The grain must then be designed with a configuration that maintains the stress concentration at a minimum possible level. Using photoelastic methods, Ordahl and Williams have investigated the quantitative relationships between the various parameters of the grain geometry and the elastic stress distribution (30). Figure 11 represents some of their results.

On this figure, the stress concentration factor K is defined as

$$K = \frac{\sigma_\theta - \sigma_R}{\sigma_\theta^0 - \sigma_R^0}$$

where σ_θ and σ_R are the actual tangential and radial stresses, and σ_θ^0 and σ_R^0 are the stresses which would occur in the equivalent tubular grain. Within the range of validity of the experimental method, these authors have shown that:

1 The stress concentration increases as the ratio of the web thickness to fillet radius increases. (It is thus imperative to use sufficiently large fillets.)

2 The stress concentration decreases as the web fraction increases.

3 For a given web thickness and fillet radius, the stress concentration decreases as the number of star points is increased.

4 The stress concentration decreases as the star point angle increases.

5 The stress concentration decreases as the width of the slot increases

Reference (30) only considers steady-state stresses due to pressure or differential thermal expansion of case-bonded grains. In a recent paper, Williams has extended his investigation to the case of transient thermal stresses for which two concentrations must be considered: A geometric concen-

tration factor K_g representing the difference in planar rigidity of the star from a thick walled cylinder of the same web fraction, and a temperature factor K_t due to the concentration of heat flux at the star points (31).

The actual concentration factor K is the product $K_g K_t$. The geometric concentration factor K_g is found to be very similar to the one measured with pressure loading, while the temperature factor K_t is always smaller than unity.

This favorable influence is more pronounced for small web fractions and small fillet radii. It decreases slightly when the number of star points increases, and appears to be the result of the relaxation (negative concentration) of heat flux away from the star points toward the regions of higher thermal inertia.

References

1 Vogel, J. M., "A Quasi-Morphological Approach to the Geometry of Charges for Solid Propellant Rockets," JET PROPULSION, vol. 26, no. 2, Feb. 1956, pp. 102–105.

2 Barrere, M., Jaumotte, A., de Veubeke, B. and Vandenkerckhove, J., "Rocket Propulsion," Elsevier Publishing Co., Amsterdam, 1959, distributed in United States by the Van Nostrand Co.

3 Wimpress, R. N., "International Ballistics of Solid-Fuel Rockets," McGraw-Hill, Inc., New York, 1950.

4 Sutton, G. P., "Rocket Propulsion Elements," 2nd ed., John Wiley and Sons, New York, 1956.

5 Bartley, C. E. and Mills, M. M., "Solid Propellant Rockets in Jet Propulsion Engines," vol. XII of "High Speed Aerodynamics and Jet Propulsion," Princeton University Press, 1959.

6 Verdier, H., "Introduction a l'étude des propulseurs à poudre ou à monergol solide," cours professé à l'Ecole Nationale Supérieure de l'Aeronautique, Paris.

7 Shafer, J. I., "Solid Rocket Propulsion," in "Space Technology," John Wiley and Sons, New York, 1959.

8 Warren, F. A., "Rocket Propellants," Reinhold Publishing Corp., New York, 1958.

9 Price, E. W., "Charge Geometry and Ballistic Parameters for Solid Propellant Rocket Motors," JET PROPULSION, vol. 24, no. 1, Jan. 1954, pp. 16–21.

10 Ritchey, H. W., "Thrust Programming of Solid Propellant Boosters by Choice of Propellant Configuration and Composition," JET PROPULSION, vol. 25, no. 10, Oct. 1955.

11 Newman, R. S., "The Dual-Thrust Solid Propellant Rocket Engine," ASTRONAUTICS, vol. 3, no. 3, March 1958.

12 Miles, G. H., "Comparison of Dual-Thrust Motors with Separate Booster and Sustainer Motors as Solid-Propellant Propulsive Systems for Guided Missiles," presented at the ASME-ARS Conference, Dallas, March 1958, ARS preprint 577-58.

13 Ritchey, H. W., "Solid Propellants and the Conquest of Space," ASTRONAUTICS, vol. 3, no. 1, Jan. 1958.

14 Thackwell, H. L., "The Use of Weapon System Engineering Concepts in the Design of Solid Propellant Rocket Power Plants," ARS preprint 232-55.

15 Gallagher, J. L. and Phillips, T. E., "Solid Propellant Engine Selection Studies for Ballistic Missiles," presented at the ASME-ARS Conference, Dallas, March 1958, ARS preprint 579-58.

16 Barrere, M., Moutet, A. and Delacarte, J., "Contribution a l'étude de la combustion des poudres composites," Memorial des Poudres, to be published.

17 Boedewadt, V. T., "Gunstigste Formen Fester Treibstoffe," *Raketentechnik und Raumfahrtforschung*, vol. 3, no. 1, Jan.-March, 1959.

18 Vandenkerckhove, J., "Note on the Optimum Design of Solid Propellant Powerplants for Weapon Systems Engineering," IXth IAF Congress, Springer-Verlag, Vienna, 1959.

19 Vandenkerckhove, J., "Optimum Design of Solid Propellant Rockets," USAF-ARDC, contract S. 61(052)58-13, Part II, Publication de L'Institut d'Aeronautique, Université Libre de Bruxelles.

20 Epstein, L. I., "The Design of Cylindrical Propellant Grains," JET PROPULSION, vol. 26, no. 9, Sept. 1956, pp. 757–759.

21 Piasecki, L. and Robillard, G., "Generalized Design Equations for an Internal-Burning Star-Configuration Solid-Propellant Charge and Method of Calculating Pressure-Time and Thrust-Time Relationships," Jet Propulsion Laboratory, Memo 20-135, Sept. 18, 1956.

22 Stone, M. W., "A Practical Mathematical Approach to Grain Design," JET PROPULSION, vol. 28, no. 4, April 1958, pp. 236–244.

23 Kasley, B., "Grain Design Handbook," Redstone Arsenal Rep. no. 3.Y.12, June 8, 1956.

24 Vandenkerckhove, J., "Internal Burning Star and Wagon-Wheel Designs for Solid Propellant Grains," USAF-ARDC, contract S. 61 (052)-58-13, Part I, Publication de l'Institut d'Aéronautique de l'Université Libre de Bruxelles.

25 Vandenkerckhove, J., "Comment on 'A Practical Mathematical Approach to Grain Design'," JET PROPULSION, vol. 28, no. 11, Nov. 1958, pp. 766–768.

26 Green, L., Jr., "Some Effects of Charge Configuration in Solid Propellant Combustion," JET PROPULSION, vol. 28, no. 7, July 1958, pp. 483–485.

27 Geckler, R. D. and David, R. S., "Modern Developments in Solid Propellant Rocket Engineering," *Aeron. Engng. Rev.*, vol. 16, no. 8, Aug. 1957.

28 Geckler, R. D., "Thermal Stresses in Solid Propellant Grains," JET PROPULSION, vol. 26, no. 2, Feb. 1956, pp. 93–97.

29 Zwick, S. A., "Thermal Stresses in an Infinite, Hollow Case-Bonded Cylinder," JET PROPULSION, vol. 27, no. 8, Aug. 1957, pp. 872–876.

30 Ordahl, D. D. and Williams, M. L., "Preliminary Photoelastic Design Data for Stresses in Rocket Grains," JET PROPULSION, vol. 27, no. 6, June 1957, pp. 657–662.

31 Williams, M. L., "Some Thermal Stress Design Data for Rocket Grains," ARS JOURNAL, vol. 29, no. 4, April 1959, pp. 260–267.

Explorer Rocket Research Program

G. ROBILLARD[1]

California Institute of Technology
Pasadena, Calif.

Nine Jupiter-C missiles have been launched at Cape Canaveral since September 1956, the first three testing the propulsion system, airframe, guidance components and re-entry conditions of the nose cone, the remaining six were used as carriers of the Explorer satellites I through VI. This was a joint program of Jet Propulsion Laboratory and Army Ballistic Missile Agency with considerable assistance from the University of Iowa, Air Force Cambridge Research Center, the Vanguard tracking teams and many others. The Jupiter-C is a four-stage vehicle burning solid propellant. The first stage is a modified Redstone missile, developing a thrust of 83,000 lb. The second stage is powered by an annular ring of 11 solid propellant motors, patterned after the Sergeant missile. The third stage consists of three motors, identical to the second, fitted inside the ring of second-stage motors. The fourth stage is a single motor, identical to the motors of the other high speed stages. The satellite payloads of the Explorer series were contained in a shell 80-in. long by 6 in. in diameter, which, together with its package of instruments for Explorer I, weighed 30.8 lb. The experiments were designed especially to study and measure cosmic radiation in great detail. Explorer IV, the latest one to attain a successful orbit, achieved a perigee altitude of 160 miles and an apogee altitude of 1390 miles.

SINCE September of 1956, nine Jupiter-C missiles have been launched from the firing pad at Cape Canaveral. The first Jupiter-C firing tested the propulsion system, airframe and guidance components of the missile, and the second and third firings tested a model of the Jupiter nose cone under realistic re-entry conditions. The remaining six Jupiter-C missiles were used as the launching vehicles for Explorer satellites I through VI (Fig. 1). Of the six satellite firings, Explorers I, III and IV achieved satisfactory orbits.

The Jupiter-C missile was designed and developed as a joint program under the technical direction of the Jet Propulsion Laboratory and the Army Ballistic Missile Agency. The Jet Propulsion Laboratory developed the three high speed stages, and the Army Ballistic Missile Agency handled the development, construction and operation of the first stage booster rocket and the guidance system. Many other organizations have contributed to the success of the Explorer satellite program, most notably the State University of Iowa, the Air Force Cambridge Research Center, and the satellite tracking teams of the Vanguard organization.

Design of the Jupiter-C

The Jupiter-C missile is a four-stage vehicle. The first stage consists of a modified Redstone rocket. The three high speed stages are comprised of clusters of solid propellant rockets placed in a spinning tub which is mounted in the nose of the first stage.

The standard Redstone missile delivers a thrust of 75,000 lb and employs alcohol as the fuel and liquid oxygen as the oxidizer. For the Explorer missions, the propellant tanks were enlarged in order to permit an increase in burning time to 155 sec, and the alcohol was replaced by another fuel, called hydyne. This latter change resulted in an increase in thrust of about 8000 lb, giving a total thrust of 83,000 lb. The fuel change was effected without major modification of the engine.

The last three stages of the missile are spun in order to minimize dispersion of the payload due to any thrust misalignment of the unguided solid propellant rocket clusters. The tub is spun by two battery-powered electric motors mounted in the top of the instrument compartment, which is emplaced between the tanks of the first-stage rocket and the spinning tub and contains the guidance and control equipment for the missile. This compartment also holds a spatial attitude control system for horizontal alignment of the high speed stages before the ignition of the second stage

The second stage of the Jupiter-C is composed of an annular ring of 11 solid propellant motors (Fig. 2), each of which is a 6-in. OD scale model of an early version of the powerplant of the Sergeant missile. All of the solid propellant motors of the three high speed stages are identical in configuration. This motor was chosen for this task because it was a reasonably high performance rocket and was known to be extremely reliable, having undergone over 300 static tests. The 11-motor ring of the second stage is mounted in bulkheads inside the spinning tub and is held accurately in position by launching lugs. Extremely accurate positioning and balance of the three upper stages and the payload are required in order to prevent vibration caused by the spinning tub and to minimize dispersion of the stages in launching and firing. Because of the centrifugal forces on the spinning second-stage motors, it was considered necessary to test these motors under simulated flight conditions on the ground. The radial load amounts to 180 g at the full spin rate of 700 rpm. Pairs of motors were spun and fired in a static-test jig. The motors operated well, but it was necessary to make a small change in the nozzle design in order to prevent the cantilevered nozzles from deflecting outward under the spin loads.

The third stage (Fig. 3) consists of three motors, identical to those in the second stage, which are connected by bulkheads in a fashion similar to that used for the second-stage installation. The three-motor cluster fits inside of the ring of motors comprising the second stage and is held in place by launching lugs.

A conical structure attached to the top of the third stage contains the timer and batteries for firing the third and fourth stages and serves to support the single fourth-stage motor.

Presented at the ARS 13th Annual Meeting, New York, N. Y., Nov. 17–21, 1958.

[1] Division Chief, Solid Propellants Division.

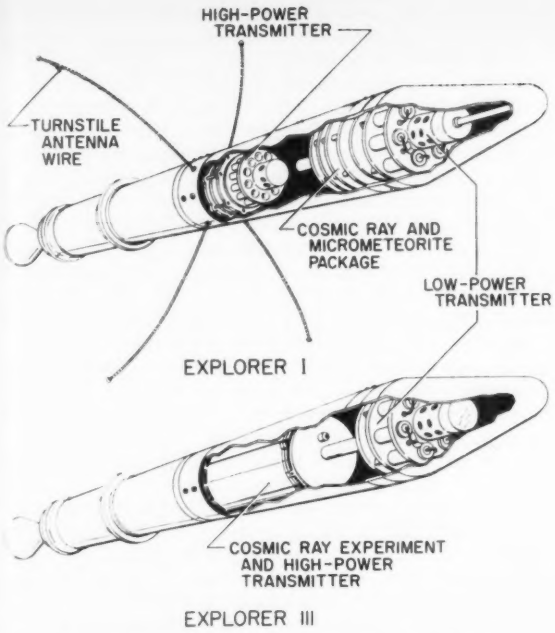

Fig. 1 Cutaway views: Explorer I and Explorer III

This motor is identical in configuration to those of the other high speed stages, except in the manner in which it is supported and in its nozzle exit diameter which is somewhat smaller to allow adequate launching clearance.

By the time permission was obtained to fire Explorer I, sufficient tests had been made of a propellant having improved performance over that used in Sergeant to permit its use in the fourth-stage motor. The fourth-stage rocket places the lowest requirement on the physical properties of propellant, in that the rocket is spun on its own axis; hence the radial loads are a minimum. Previous to the firing of Explorers IV and V, this propellant was qualified by extensive static spin-testing for use in the third stage, and an even more energetic propellant had qualified for use in the fourth stage. These propellant changes, together with a decrease in the weight of some of the inert parts by design refinements, account for the increased payload weights of the latter satellites. Some potential for increased payload using this missile configuration still exists, but the return in terms of payload weight is rapidly diminishing with respect to the amount of development effort required.

The satellite payload (Fig. 1) is rigidly attached to the head end of the fourth-stage rocket motor through an insulating ring which forms the antenna gap for one of the two payload transmitters. The second transmitter operates across a similar gap between the cylindrical portion of the payload and its nose cone.

The entire high speed assembly, including the payload, is very carefully aligned and balanced in its tub before the assembly is mounted on the Redstone booster.

The design of the Jupiter-C was carried out to afford a vehicle which would provide maximum reliability with minimum development effort. For this reason, proved components were used wherever possible, and in order to assure reliability, redundant systems were used in many places to prevent system failure caused by malfunction. The ignition system for the high speed stages is one example of such redundancy. The problem of reliable ignition at high altitude was resolved in three ways:

1 An igniter was designed which would fire the motors reliably in a laboratory vacuum.

2 The rocket motors were sealed so that they would hold atmospheric pressure.

3 The igniter was sealed in an inner container capable of holding atmospheric pressure if the motor seal should leak.

Firing Sequence

Prior to takeoff, the tub is spun up to 550 rpm and held at this speed. About 70 sec after takeoff, a governor controlled by the missile programmer increases the rotational speed gradually up to 750 rpm at a time about 20 sec before first-stage burnout. This procedure eliminates resonance between the spin frequency and the natural bending frequencies of the missile. These bending frequencies increase as the propellants of the first stage are consumed; thus the spin rate is increased gradually, so that the spin frequency always remains between those of two of the natural modes of vibration of the missile.

The missile takes off vertically under its thrust of 83,000 lb. During the 155-sec burning time of the first stage, the vehicle is tilted into a trajectory which is approximately 40

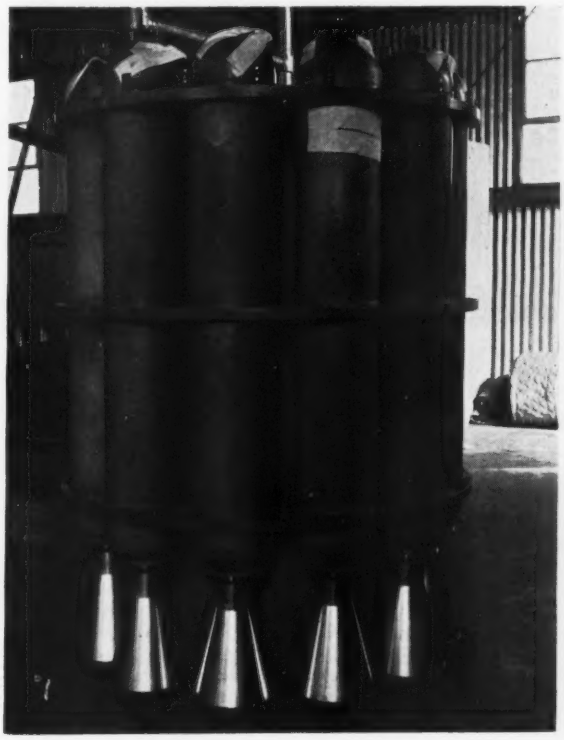

Fig. 2 Second-stage cluster of solid propellant motors

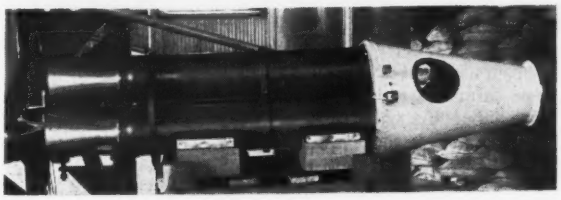

Fig. 3 Third-stage motor cluster

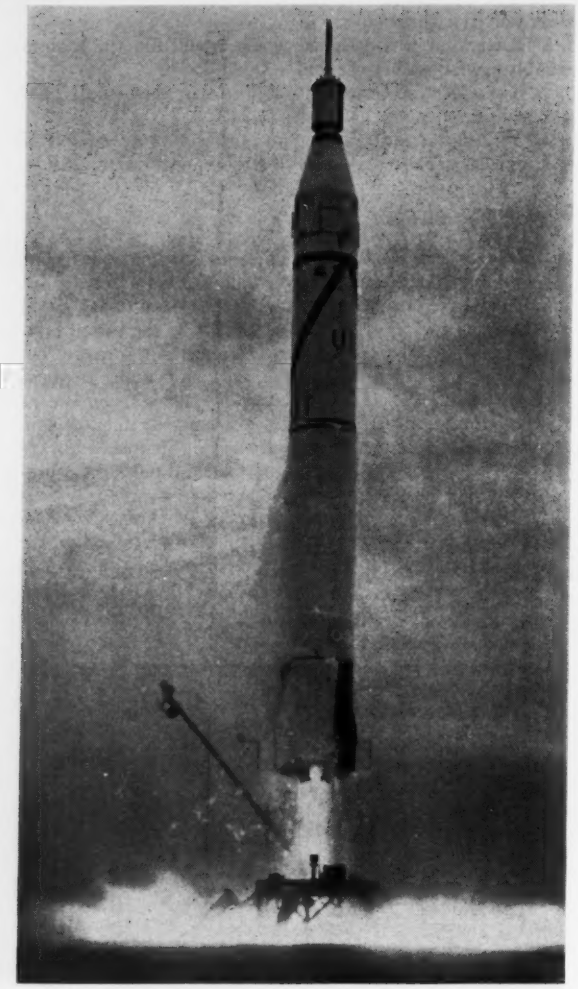

Fig. 4 Explorer launching

deg inclined to the horizon at burnout. A depletion cutoff technique is used to maximize the impulse delivered by the Redstone motor. Contacts are placed in the discharge lines from the fuel and oxygen pumps; whichever of these contacts first senses a pressure drop triggers a relay which closes both propellant main valves to the combustion chamber. Five sec after burnout, a timer activates the six explosive bolts which secure the guidance compartment to the tank section of the first-stage motor. Coil springs wrapped around these bolts exert a gentle push on the guidance compartment and separate it cleanly from the booster. The failure of Explorer V to achieve orbit is attributed to a malfunction at this point in the launching sequence. In this one instance, the Redstone booster was still exerting some thrust after separation; hence the separated booster section was able to overtake and ram the guidance compartment. This impact caused the gyros in the guidance compartment to tumble; consequently, the reference planes were misoriented during the ensuing portions of the launching sequence.

From the point of separation, the two portions of the missile coast through a vacuum trajectory until the apex is attained after about 404 sec after takeoff. During the free-coasting period between separation and apex, the spatial attitude control system in the guidance compartment aligns the high speed stages into an exactly parallel position with respect to the local horizon. This reorientation uses the gyros of the guidance compartment as reference and is accomplished by means of small compressed air nozzles located at the base of the guidance compartment.

Because of the relatively crude cutoff technique based on propellant depletion used in the first stage, it is impossible to predict the exact time when apex will be attained. Only by igniting the high speed stages at the moment of apex and by accurate alignment of the stages in the horizontal direction can orbital flight be assured. Three independent methods are employed to determine the time of apex. First, a radar tracking plot is used to determine the time at which apex will be reached; second, an accelerometer in the missile relays by telemetry the buildup of velocity in the first stage; and third, standard Doppler tracking furnishes the same information. The data obtained from these sources are fed into a small computer that provides an average estimate of apex time, but allows for the respective quality of the three types of data. This value is then used to set a timing device which sends a radio signal to the missile to fire the second stage. The computation is accomplished in the 4-min interval between separation and apex.

Each of the three high speed stages has a burning time of about 6 sec, and 2 sec of coasting time are allowed between the firing of successive stages to permit complete thrust decay. The second-stage firing signal is received by the command transmitter in the instrument compartment, and the stage is fired by an electrical signal from batteries in the guidance compartment. The pressure rise in the second-stage motors signals the start of a timer housed in the conical support for the fourth stage, which, 8 sec later, fires the third stage and, 8 sec after that, the fourth stage. As each stage fires, it breaks shear pins holding it to the preceding assembly and leaves that stage behind to fall back to Earth.

The failure of Explorer II to achieve an orbit has been traced to a structural failure in the igniter support for the fourth stage. The light plastic cone which supported the igniter from the nozzle end of the rocket motor apparently failed under the combined spin, inertial and vibration loads, thereby allowing the igniter to slip out through the nozzle into the conical structure supporting the fourth stage. Strengthening the igniter support prevented this malfunction in subsequent rounds.

The payload of Explorer VI contained a fifth small solid propellant rocket motor stage oriented in such a manner that its nozzle exhausted through the nose cone of the payload. This motor was designed to be fired by a timer at apogee after the first half-revolution of the satellite around the Earth. At this time the motor would have been oriented in such a way that it could impart additional velocity to the payload along its path, thereby raising the perigee height well above its initial value. This "kick-in-the-apogee" technique is an economical way of achieving a high orbit, because it eliminates the necessity of raising all of the missile hardware to a high altitude.

Payloads and Orbits

The entire orbiting assembly in Explorer I, that is, the empty rocket motor shell from the fourth stage plus the instrument compartment, weighs 30.8 lb. The instrument compartment alone weighs 18.0 lb. The total assembly is 80-in. long and 6 in. in diameter. This satellite achieved an initial orbit having a perigee altitude of 225 miles and an apogee altitude of 1594 miles, corresponding to a period of revolution of 114.78 min. Tracking data showed that the satellite was injected into orbit at an angle only about 0.8 deg from the horizontal, although a suitable orbit would have been achieved even if this error were as great as 4 deg.

The shell of the instrument compartment was constructed of 410 stainless steel, 0.025-in. thick. The outside surface was sandblasted and then coated in stripes with aluminum oxide (Rokide A). The region of the stagnation point of the

nose cone was completely covered to guard against aerodynamic heating during launch. The payload surface was treated in this manner so that the heat absorbed by radiation from the sun and by reflected radiation from the Earth plus the heat generated internal to the payload would balance the heat radiated by the payload to space. By this means, it was possible to maintain the electronic components within a temperature range in which they could function properly. Because this technique could not be expected to maintain a constant temperature of the satellite skin as the satellite moved into and out of the Earth's shadow, the sensitive components were thermally insulated from the skin to smooth out the temperature fluctuations. The success of this technique is indicated by the fact that the maximum and minimum temperatures recorded within the instrument compartment were 104 and 43 F, respectively.

Explorer I carried two minimal weight transistorized radio transmitters. The low power transmitter radiated 10 mw of energy, whereas the second transmitter radiated 60 mw. Because of its higher power requirement, the 60-mw unit transmitted for only about 2 weeks; however, the low power transmitter was tracked for several months after launching.

The primary mission of the transmitters was to provide a signal for tracking the satellite. The high power transmitter could be received by sensitive amateur receivers, but the low power transmitter could be tracked only by the more sophisticated narrow-band microlock and minitrack receivers. In addition to providing a tracking signal, the transmitters were used to telemeter scientific data from the satellite; these data included measurements of temperature, micrometeorite impacts and cosmic-ray intensity.

Temperatures were measured at four points: One directly under the stagnation point of the nose cone, two others at two locations on the outer skin, and another directly within the electronic package itself.

Micrometeorite impacts were counted by two devices. A sensitive microphone attached to the inside of the payload shell, by means of an amplifier and a scale-of-two circuit, caused a frequency shift of a subcarrier oscillator each time an impact occurred anywhere on the satellite. In addition to the microphone, a micrometeorite erosion gage consisting of 11 grids of fine brittle wire was mounted just forward of the nozzle of the last stage rocket motor. These grids were wired in parallel; each time a grid was broken by micrometeorite impact the resistance of the circuit changed, and the change was reflected in the frequency of a subcarrier oscillator.

The intensity of cosmic radiation was detected by a Geiger-Müeller tube. This instrument was able to count only the number of impingements within its sensitivity range and was unable to differentiate between particles of various energy levels. Inasmuch as the cosmic-ray intensity had been predicted to be of the order of 30 to 40 counts per sec, the range of the instrumentation was set to bracket this range. The field of cosmic radiation encountered at altitudes greater than 600 miles, however, was so intense as to saturate the instrument completely. The only conclusion which could be reached was that the intensity was at least 1000 times greater than expected.

With Explorer I, telemetering data could be gathered only when the satellite was over one of the ground receiving stations. These stations were located in Florida, Nigeria, Singapore and California, and at a number of places along the 65 deg west meridian. Because of the relatively small number of receiving stations, much of the orbit was not observed, and for this reason much of the telemetered data was lost. In order to eliminate this difficulty, Explorer III carried a miniaturized tape recorder which stored the information acquired throughout one complete orbit and reported it on command when the satellite passed over a suitably equipped receiving station. Playback was accomplished at high speed, so that approximately 2 hr of data could be transmitted in 5 sec. Between interrogations, the high power transmitter was turned off to conserve power. Only the cosmic-ray information was transmitted in this fashion; the other experiments, similar to those in Explorer I, were telemetered continuously by the low power transmitter.

Explorer III attained an orbit having a perigee altitude of 120 miles and an apogee altitude of 1740 miles, with a period of 115.8 min. The orbit was inclined about 33½ deg to the equator. The greater ellipticity of this orbit was caused by a significant elevation error at injection. In retrospect, this represents a particularly favorable malfunction, since the high apogee orbit has made it possible to obtain exceedingly interesting data from the cosmic-ray experiment.

The instrumentation in Explorer IV was designed specifically to study the cosmic radiation in greater detail. Improvements in the performance of the high speed stages for this firing permitted the payload weight to be increased by 7 lb. By eliminating all of the other experiments, including the tape recorder, it was possible to package four instruments for measuring cosmic-ray data in this satellite. Two scintillation counters were carried in addition to two Geiger-Müeller tubes similar to those carried in the earlier satellites. One of the Geiger tubes is shielded with lead to eliminate data below fixed energy levels. The other tube is set to respond to any particle which penetrates the shell of the satellite and the casing of the Geiger tube. One of the scintillation counters records a pulse each time a particle passes through it. The other can measure the energy level of the particles which it encounters. Both scintillation counters are shielded by lead, except for one window in each where the shielding has been made as light as possible and a hole has been cut in the shell of the satellite.

Explorer IV was fired on a much more northerly orbit than its predecessors. It achieved a perigee altitude of 160 miles and an apogee altitude of 1390 miles; the period of the satellite was 110.3 min. Its orbit inclined 50.4 deg to the equator. By this means, it was able to investigate a far greater volume of space with respect both to latitude and to altitude than were the earlier vehicles.

Scientific Data

The justification for a project of this magnitude, of course, is the scientific data which are obtained. The Explorer project has, in fact, acquired a great deal of very interesting data; so much so that it may be several years before this extensive accumulation is completely analyzed. However, sufficient preliminary information is now available to sketch a rough picture of space in the vicinity of the Earth.

Although the temperature measurements taken inside the satellite were not intended to measure any fundamental quality of the space environment, they served to prove the success of the scheme which had been employed to control the satellite's temperature. We now have demonstrated that, at least insofar as temperature is concerned, we shall be able to provide a habitable environment for man in space.

The rate of decay of the orbit, particularly that of Explorer III, which lasted in orbit for about three months, has provided a measure of the density of the upper regions of the atmosphere. Explorer III completed approximately 1260 revolutions before its disappearance. Its orbit ranged from a perigee of 116.86 miles and an apogee of 1740.77 miles on its first pass to 107.2 miles and 650.2 miles, respectively, about two weeks before it vanished. The rate of decay of apogee was 11.36 miles per day between March 26 (the date it was launched) and April 11, 11.95 miles per day between April 11 and 25, 14.99 miles per day between April 25 and May 31, 14.16 miles per day from then until June 10, and 16.9 miles per day thereafter. The exact significance of this somewhat erratic path in terms of atmospheric density is still being analyzed.

The measurements of micrometeorite density have substantially confirmed previous estimates based on such in-

direct evidence as the data from high altitude sounding rockets, and the measurement of ocean floor sediment. The results of a partial analysis of the data from Explorer I by the Air Force Cambridge Research Center, which is responsible for this experiment, show for example that the average flow of particles in the 4-μ range is 30 particles per yd^2 per hr, whereas for a larger particle of about 10μ in diameter, the rate is three particles per yd^2 per hr. For the spaceship designer, these numbers offer no problem. However, they take on an interesting meaning when the surface considered is the surface of the Earth. In these terms, we find that cosmic dust accounts for an increase in the mass of the Earth of 2000 tons per year.

It is interesting to note that the Russians carried on a similar experiment aboard the Sputniks. Surprisingly, they have reported a density of particles which is approximately 1000 times as great as that measured by Explorer. This result is difficult to understand not only because it disagrees with the previous estimates, but also because the increase in mass of the Earth at this high rate would be expected to have had a noticeable effect on its rotation speed over the centuries.

In contrast to the micrometeorite measurements which appear to verify preliminary estimates, the measurements of cosmic-ray intensity gave some surprising new results. The first two Explorers indicated that the level of cosmic radiation was about as expected up to 600 miles altitude in the region near the equator. From this altitude up to the highest altitude reached by the satellites, the cosmic-ray intensity increased at a much higher rate than had been expected. At the farthest reaches of the orbits, the count was more than 1000 times the expected value, and the rate of increase showed no tendency to level off.

Preliminary analysis of the data from Explorer IV shows that the number of cosmic-ray particles passing through the unshielded Geiger tube is of the order of 36,000 per cm^2 per sec, from all directions. At least 60 per cent of these particles have enough energy to penetrate the lead shield around the other Geiger tube. In addition to these very energetic particles, there is an even greater density of particles of low energy. At the northern and southern limits of the trajectory, these low energy particles predominate. Here, the flux of particles of low energy at an altitude of about 1400 miles is about one million per cm^2 per sec, from all directions. As the satellite rotates around its axis, the density measurements change. On the basis of this result, it appears that more than 80 per cent of these particles come from one favored direction.

On the basis of the preliminary estimates, it is not possible to separate altitude effects from latitude effects, and, because of the magnetic field, both of these effects should cause changes in cosmic-ray intensity. The data of the first two weeks indicated an increasing intensity with altitude at all latitudes. The radiation has been found to vary both in quantity and in quality with latitude and altitude. A low energy component similar to that suggested on the basis of the results of the first two Explorer satellites is usually present, whereas high energy particles become more and more predominant as the satellite approaches the magnetic equator. Thus radiation intensities in excess of 100 roentgens per hr have been observed by the satellites.

In regard to cosmic radiation, it is interesting to note that, although the Russian satellites also carried instruments for measuring this effect, the preliminary announcements of scientific results made by the Russian scientists did not indicate that they had discovered this high intensity region. Their preliminary information was confined to altitudes below 600 miles. At a recent meeting sponsored by the IGY committee held in Moscow, the Russians entered into a more thorough description of the equipment onboard the Sputniks. They revealed that the Sputniks carried tape recorders which stored scientific information around the orbit and played it back as the Sputnik passed over Russia. Also, the Sputniks carried continuous transmitters which sent the information to Earth steadily for any receiver which the satellite happened to be passing over. The cosmic-ray measurements were being transmitted on the continuous transmitter in the same way that information is telemetered from Explorers I and IV, but the cosmic-ray information was evidently not put on the tape recorders as was done with Explorer III. Thus the Russians could observe cosmic-ray data only when the satellite was near its lowest point. When the satellite was passing through the high altitude region, and presumably detecting the intense cosmic-ray field, the satellite was not over Russia. Instead, when the satellite was passing through this interesting region, it was over some part of the world near or below the equator.

It is true that many radio receiving stations over these portions of the world were recording the signals sent by the Russian Sputniks. However, these signals were meaningless without the telemetering code, and this code was not published by the Russians. Furthermore, in spite of the request by this country and others, the Russians would not enter into any arrangements to exchange preliminary satellite data. Thus, although the Sputnik was observing this surprising high intensity cosmic-ray field, the Soviet government, by its own decision, refused to accept this data or make it possible for anyone else to interpret it. As a result, although the Soviet scientists were the first to launch an artificial Earth satellite, they were the last to learn about this vital discovery of the high intensity cosmic-radiation field. Instead, it remained for the American scientists to discover and announce this completely new geophysical phenomenon.

The Jupiter-C research vehicle then, however unsophisticated it may seem as compared with Vanguard, and however diminutive it may be as compared with Sputnik, has been to date exceedingly successful in accomplishing its objective: The exploration of space and the acquisition of fundamental knowledge of our planet's environment in the universe.

General Solution for Optimization of Staging of Multistaged Boost Vehicles

CARL H. BUILDER[1]

The Marquardt Corporation
Van Nuys, Calif.

A general solution for the optimization of staging of multistaged boost vehicles based upon weight-dependent criteria is presented. Optimization may be in terms of any criterion that can be expressed as proportional to stage or step weight, such as cost, volume, empty weight, propellant weight, as well as the usual criterion of gross weight. The solution is applicable to a vehicle of any number of stages having different performances and characteristics. The possibility of stages with variable performance, such as an air-breathing engine stage, is included. Analytic procedures for the solution of multistage vehicles are outlined, and an example of the optimization of staging for minimum cost is presented.

IN THE past few months, the staging of step rockets for minimum gross weight has received considerable attention (1 to 4).[2] However, these solutions are applicable to only one special case of the general problem of optimum staging: When minimum gross weight is the optimization criterion.

The optimization of rocket staging for minimum gross weight has been treated by a number of authors during the past two years. Malina and Summerfield, in an early paper (5), optimized staging for maximum burnout velocity with homogeneous stages. Vertregt (6) was perhaps the first to outline the general solution for minimum gross weight staging; however, explicit solution was limited to stages having equal specific impulses. Goldsmith (7) offered a solution for two-stage rockets when the structural weights are proportional to the fuel weight and the engine weights proportional to the stage gross weight. Schurmann (8) considered burnout accelerations as a variable in the optimization for minimum gross weight when all stages have equal specific impulses. Weisbord (1), Ten Dyke (2), Subotowicz (3) and Hall and Zambelli (4) have all presented, in the last year, general solutions for minimum gross weight with nonhomogeneous stages. Thus, it would appear that if gross weight were the criterion for optimum staging, solution would now be amenable through any one of nearly a half-dozen papers.

However, minimum gross weight is not likely to be the only criterion of interest in the optimization of staging. Under certain circumstances other criteria, such as cost, volume, empty weight, etc., may be equally important. In the design of boost vehicles for any ambitious space program involving large payloads in orbit or in extraterrestrial trajectories, the cost of the boost vehicle is likely to be one of the most important criteria for staging. While it is recognized that optimized staging does not necessarily result in the optimum system, the ability to optimize the staging for various criteria provides a set of sub-optimum systems which can aid in the final system selection. The ability to define optimum staging for various criteria is the objective of this paper.

A general solution for the optimization of staging for any criterion proportional to stage weight is derived. The solution is applicable to any number of dissimilar (performance-wise) stages, and takes into account the possibility of a stage or stages having variable specific impulse, such as an air-breathing engine stage. Since a large number of pertinent parameters, such as cost, empty weight, propellant tank weight, engine weight, volume, etc., can be approximated over a reasonable range as being proportional to stage weight, this solution provides a means of optimizing staging for many criteria of interest, including the criterion of minimum gross weight.

General Solution for Optimum Staging

The solution is taken to be that set of stage velocity increments ΔV_i which corresponds to a stationary value of the objective function K subject to the constraints imposed by the stage parameters, I_i, β_i, η_i and the system final velocity V_t. The objective coefficients η_i may be specific volume, specific cost or any other parameter per unit weight of stage i. So long as these coefficients are independent of the absolute magnitude of the stage weights

$$K = \sum_{i=1}^{n} \eta_i w_i \qquad [1]$$

If the system is defined for a payload weight of unity, then from momentum considerations, for the ith stage

$$\int_{\sum_{j=1}^{i-1} \Delta V_j}^{\sum_{j=1}^{i} \Delta V_j} \frac{du}{I_i g} = \log_e \left(\frac{1 + \sum_{j=i}^{n} w_i}{1 + \beta_i w_i + \sum_{j=i+1}^{n} w_i} \right) \qquad [2]$$

$$\int_{\sum_{j=1}^{i-1} \Delta V_j}^{\sum_{j=1}^{i} \Delta V_j} \frac{du}{I_i g} \equiv \gamma_i \qquad [3]$$

If the function x_i is defined as

$$x_i \equiv \frac{e^{\gamma_i}(1 - \beta_i)}{1 - \beta_i e^{\gamma_i}} \qquad [4]$$

then Equations [2, 3 and 4] may be combined to yield

$$w_i = (x_i - 1) \prod_{j=i+1}^{n} x_i \qquad [5]$$

Received Dec. 1, 1958.
[1] Senior Research Engineer.
[2] Numbers in parentheses indicate References at end of paper.

Substituting Equation [5] in Equation [1]

$$K = \sum_{i=1}^{n} \left[\eta_i(x_i - 1) \prod_{j=i+1}^{n} x_j\right] \quad [6]$$

The objective function K is a stationary value when, for $i = 1, 2, \ldots n$

$$\partial K/\partial x_i = 0 \quad [7]$$

subject to the constraint

$$V_t = \sum_{i=1}^{n} \Delta V_i \quad [8]$$

However, since x_i is a function only of γ_i(β_i is a constant), Equation [7] is equivalent to

$$\partial K/\partial \gamma_i = 0 \quad [7a]$$

The method of LaGrange's multipliers provides a solution for constrained extrema in terms of n simultaneous equations of the form

$$\frac{\partial K}{\partial \gamma_i} + \lambda \frac{\partial \phi}{\partial \gamma_i} = 0 \quad [9]$$

plus the constraining equation

$$\phi = 0 \quad [10]$$

In this case

$$\phi = \sum_{i=1}^{n} \Delta V_i - V_t \quad [10a]$$

If, by definition

$$y_i \equiv 1/(1 - \beta_i e^{\gamma_i}) \quad [11]$$

then Equation [6] may be differentiated to

$$\frac{\partial K}{\partial \gamma_i} = y_i\left(\prod_{k=i}^{n} x_k\right)\left\{\eta_i + \sum_{j=1}^{i-1}\left[\eta_j(x_j - 1) \prod_{k=j+1}^{i-1} x_k\right]\right\} \quad [12]$$

where the value of the product

$$\prod_{k=j+1}^{i-1} x_k$$

is taken to be unity for $j + 1 > i - 1$.

Differentiating Equation [10a]

$$\frac{\partial \phi}{\partial \gamma_i} = \frac{\partial \Delta V_i}{\partial \gamma_i} \quad [13]$$

The evaluation of this total differential requires examination of Equation [3]. If the impulse of the stage I_i is constant, as is frequently assumed for the rocket motor, then Equation [3] may be integrated to

$$\frac{\Delta V_i}{I_i g} = \gamma_i \quad [3a]$$

and the differential becomes

$$\frac{\partial \phi}{\partial \gamma_i} = \frac{\partial \Delta V_i}{\partial \gamma_i} = I_i g \quad [13a]$$

However, if the impulse varies with velocity, as is characteristic of air-breathing engines, evaluation of the Equation [3] involves differentiation under the integral sign

$$\frac{d\gamma_i}{d\Delta V_i} = \int_{\sum_{j=1}^{i-1} \Delta V_j}^{\sum_{j=1}^{i} \Delta V_j} \frac{\partial(1/I_i g)}{\partial \Delta V_i}\, du + \frac{\partial \sum_{j=1}^{i} \Delta V_j}{\partial \Delta V_i}\left(\frac{1}{I_i g}\right)_{u = \sum_{j=1}^{i} \Delta V_j} - \frac{\partial \sum_{j=1}^{i-1} \Delta V_j}{\partial \Delta V_i}\left(\frac{1}{I_i g}\right)_{u = \sum_{j=1}^{i-1} \Delta V_j} \quad [14]$$

Since the impulse I_i is a function of the velocity u and not the stage velocity increment ΔV_i, the partial differential under the integral is zero. Also

$$\frac{\partial \sum_{j=1}^{i} \Delta V_j}{\partial \Delta V_i} = \frac{\partial \Delta V_i}{\partial \Delta V_i} = 1 \quad [15]$$

and

$$\partial \sum_{j=1}^{i-1} \Delta V_j/\partial \Delta V_i = 0 \quad [16]$$

Thus

$$\frac{d\gamma_i}{d\Delta V_i} = \left(\frac{1}{I_i g}\right)_{u = \sum_{j=1}^{i} \Delta V_j} \quad [14a]$$

For a stage with variable impulse, Equation [13] becomes

$$\frac{\partial \phi}{\partial \gamma_i} = \frac{\partial \Delta V_i}{\partial \gamma_i} = (I_i g)_{u = \sum_{j=1}^{i} \Delta V_j} \quad [13b]$$

Equation [13b] is equivalent to [13a] if the impulse I_i is taken at the burnout velocity of the ith stage. Substituting Equations [12 and 13a] in Equation [9] results in n equations of the form

$$y_i\left(\prod_{k=i}^{n} x_k\right)\left\{\eta_i + \sum_{j=1}^{i-1}\left[\eta_j(x_j - 1) \prod_{k=j+1}^{i-1} x_k\right]\right\} + \lambda I_i g = 0 \quad [17]$$

plus the constraining Equation [8]

$$V_t = \sum_{i=1}^{n} \Delta V_i$$

The LaGrangian multiplier λ may be eliminated from these $n + 1$ equations by substitution, leaving $n - 1$ equations of the form

$$y_i = \frac{y_1\left(\prod_{k=1}^{i-1} x_k\right)\frac{I_i}{I_1}}{\frac{\eta_i}{\eta_1} + \sum_{j=1}^{i-1}\left[\frac{\eta_j}{\eta_1}(x_j - 1) \prod_{k=j+1}^{i-1} x_k\right]} \quad [18]$$

plus the nth equation, Equation [8]. Evaluation of Equation [18] for each of the n stages is relatively simple, since the right-hand side of the equation contains no terms higher than $i - 1$. Thus, if ΔV_1 is assumed, y_2 may be calculated, and subsequently y_3 may be calculated, and so on until y_n. The resulting values of ΔV_i may be substituted in Equation [8] to calculate V_t and, thus, check the validity of the assumed value for ΔV_1. Successive approximations lead to that value for ΔV_1, which, through Equation [18], leads to satisfaction of Equation [8].

Discussion

The procedures for solution of a specific boost system by means of Equations [8 and 18] have been outlined. Solution by successive approximation techniques may be carried out by automatic computers or by hand. Simple iteration methods do not generally converge and must be supplemented by damping the indicated change in ΔV_1 (in computer calculations), or by judgment (in hand calculations). For hand calculations, tables or graphs of the functions x_i and y_i as functions of γ_i, with β_i as a parameter, are very useful. It is

Table 1 Assumed parameters for a three-stage boost vehicle

Stage, i	1	2	3
specific impulse, I_i	285	298	250
residual weight, β_i	0.08	0.11	0.09
objective coefficient, η_i (stage cost in \$/lb)	10	17	7

not feasible to present graphs of the desired precision to accompany this paper. Such graphs are easily prepared using Equations [4 and 11].

Note that the objective coefficients η_i appear in Equation [18] of the solution in ratio form. Thus, the absolute magnitude of the objective coefficient is never required for establishing the optimum staging. This is useful, for example, when agreement on absolute costs is not attainable. Often, agreement may be confined to, "This costs 20 per cent more than that." Under such conditions, optimum staging can be established, even if the total system cost cannot.

Ten Dyke (2) and Hall and Zambelli (4) have proposed simple procedures for taking into account the real effects of drag and gravity when using the ideal rocket equations, such as Equation [2]. These procedures involve the use of an effective terminal velocity which exceeds the real terminal velocity by an amount that corresponds to the energy consumed by drag, gravity and turning. The incorporation of such effective velocities in the optimization techniques presented here is acceptable provided that the relationship between the effective and real velocities is accounted for in the determination of the specific impulse of variable-impulse stages. This may require that the relation between effective and real velocities be established over the boost vehicle spectrum. This, of course, is tantamount to assignment of drag and gravity losses over the entire trajectory.

As an example of the application of optimum staging for minimum vehicle cost, consider a three-stage orbital boost vehicle with the characteristics listed in Table 1. The effective velocity of the system is taken to be 32,000 fps which includes a reasonable allowance for drag and gravity effects along the trajectory.

If the example vehicle is staged for minimum gross weight, by setting

$$\eta_i = \eta_1 = 1 \qquad [19]$$

the resulting mass ratio (gross weight to payload weight) is 79.0. If the assigned cost figures are applied to this staging, the total cost of the booster vehicle is \$850 per lb of payload.

When the vehicle is staged for minimum cost, by setting the η_i values equal to the stage costs per pound in Table 1, the mass ratio is increased to 79.6, but the total cost is reduced to \$842 per lb of payload. However, the differences in mass ratio and cost are sufficiently small, in this case, so that choice between the two sub-optimum systems is probably arbitrary. This is because the assigned costs for each stage are of the same order of magnitude.

Now, however, let us assume that the relative stage costs change markedly by recovering and reusing the first or bottom stage of the booster system. If we assume that recovery incurs no penalty in stage performance and that fuel costs are negligible when compared to hardware costs, then

$$\eta_1 = \frac{\$10}{m} \qquad [20]$$

where m is the number of flights made by the first stage. The differences in mass ratio and cost between vehicles staged for minimum gross weight and for minimum cost increase steadily with m, as shown in Table 2.

Although the example illustrates optimum staging for minimum cost, optimization could as easily have been for minimum empty weight, minimum volume, minimum fuel weight or any other parameter which can be expressed per pound of stage weight.

Nomenclature

g = acceleration due to gravity
I_i = propellant specific impulse of the ith stage
K = objective function of the booster system per unit weight of payload
n = total number of stages in the booster system
u = velocity
ΔV_i = velocity increment due to the ith stage
V_f = final velocity attained by the payload
w_i = net weight of the ith stage, including propellant, but excluding payload and all stages above the ith stage. Expressed as weight per unit weight of payload
x_i = function of γ_i and β_i
y_i = function of γ_i and β_i
β_i = fractional weight of non-propellants of the ith stage which is jettisoned at the burnout of the ith stage
γ_i = integral function of u and I_i
η_i = objective coefficient of the ith stage. Expressed as volume, cost, etc., per unit weight of the ith stage
λ = LaGrangian multiplier
ϕ = constraining function = 0

The mathematical symbols d, ∂, Σ, Π, e, etc., are used in their usual contexts.

References

1 Weisbord, L., "A General Optimization Procedure for N-Staged Missiles," JET PROPULSION, vol. 28, March 1958, pp.164–167.
2 Ten Dyke, R. P., "Computation of Rocket Step Weights to Minimize Initial Gross Weight," JET PROPULSION, vol. 28, May 1958, pp. 338–340.
3 Subotowicz, M., "The Optimization of the N-Step Rocket With Different Construction Parameters and Propellant Specific Impulses in Each Stage," JET PROPULSION, vol. 28, July 1958, pp. 460–463.
4 Hall, H. H. and Zambelli, E. D., "On the Optimization of Multistage Rockets," JET PROPULSION, vol. 28, July 1958, pp. 463–465.
5 Malina, F. J. and Summerfield, M., "The Problem of Escape from the Earth by Rocket," *J. Aeron. Sci.*, vol. 14, Aug. 1947, pp. 476–478.
6 Vertregt, M., "A Method of Calculating the Mass Ratio of Step Rockets," *J. Brit. Interplanet. Soc.*, vol. 15, March-April 1956, p. 95.
7 Goldsmith, M., "On the Optimization of Two-Stage Rockets," JET PROPULSION, vol. 27, April 1957, pp. 415–416.
8 Schurmann, E. E. H., "Optimum Staging Technique for Multistaged Rocket Vehicles," JET PROPULSION, vol. 27, Aug. 1957, pp. 863–865.
9 Michelson, I., "Ultimate Design of High Altitude Sounding Rockets," JET PROPULSION, vol. 27, Oct. 1957, pp. 1107–1108.

Table 2 Comparison of weight-optimized and cost-optimized systems

Number of flights for first stage, m	1	2	3	5	10	20
System optimized for gross weight:						
mass ratio, lb/lb of payload	79.0	79.0	79.0	79.0	79.0	79.0
cost, \$/lb of payload	850	525	416	330	265	232
System optimized for cost:						
mass ratio, lb/lb of payload	79.6	82.7	85.9	91.6	104.0	124.0
cost, \$/lb of payload	842	494	369	261	172	118
System comparison:						
difference in mass ratio, lb/lb of payload	0.6	3.7	6.9	12.6	25.0	45.0
difference in cost, \$/lb of payload	8	31	47	69	93	114

The Useful Life of Solid Propellants at Very High Temperatures—Part 1

M. VISNOV[1]

Frankford Arsenal
Philadelphia, Pa.

The advent of the heating problem associated with supersonic speeds directs attention to the thermal stability of propellants under unusual conditions. It requires a sharp definition of the point in time-temperature coordinates where the propellant ceases to function correctly. The autoignition point is not sufficient to meet the designer's needs, as there are two successive zones of danger in the decomposition of propellants. The first zone is where propellant function is faulty; the second is where the propellant becomes a hazard to adjacent equipment. Knowledge of these zones is vital to the design of propellant powered devices. Examples are given of the data which the problem demands. Typical data obtained to date are presented, as well as a brief description of automatic equipment employed in the current project for obtaining the data.

THE HEAT that accompanies the operational conditions of current and planned supersonic aircraft and missiles has added still another problem area to the list of those facing technical personnel in these fields. Survival and reliable functioning under such extremes are now required of the compact source of work we know as the propellant powered or cartridge actuated device (CAD). For those that deal in structures, the emphasis has been on the search for materials which maintain form and strength over the increased temperature range. The field of propellant powered devices faces an even more pressing problem. Here, relatively sensitive chemical compositions which are inherently unstable to various degrees must not only maintain form and strength at these high temperatures, but, in addition, when called upon must decompose into specified volumes of gas at controlled rates. When it is realized that there exist today high temperature requirements for propellant actuated devices severe enough to pose the hazard of spontaneous ignition, then some appreciation of the problem facing the propellants field can be obtained.

A study of the high temperature problem as applied to propellants for cartridge actuated devices must deal with certain conditions peculiar to these systems which tax the stability of a propellant to an unusual degree. The severity of these conditions provides a virtual proving ground for propellant life under extremes of exposure. These factors include:

Location of cartridge actuated devices.
Extension of high temperature range of performance.
Repetition of high temperature exposures (recycling).
The sealed cartridge case.
Limitations for protection of propellant powered devices.

Some idea of how each of these factors contributes to the unique demands on propellants for CADs will be discussed.

Location of Cartridge Actuated Devices

Where possible, personnel ejection devices are placed in areas served by forced cooling and hence have some means of protection against heat. However, certain cartridge powered initiators and thrusters for canopy removal and related functions are placed by necessity close to the canopy itself. Other propellant systems perform multiple functions simultaneously or in series at divergent points. It is unavoidable that parts of this network of devices must lie in uncooled compartments. Here, the rise in temperature which the propellant must withstand depends upon its distance from the skin. For those CADs which must be mounted a few inches from the skin, the problem is, of course, aggravated. A related problem is the potential mounting of propellant devices to perform certain functions close to heat producing mechanisms, such as engines or afterburners. More severe temperature extremes are encountered by stores or payload ejection devices. Such devices are often mounted with a minimum of shielding close to the skin directly exposed to air flow. Specifications exist today for such devices to withstand temperatures higher than 300 F. There are requirements for certain CADs now under development for exposure to 500 F for periods in excess of 4 hr.

Requirements for propellant powered devices for missiles vary with use. Gas generators for fuel pressurization are usually positioned within the interior of the body and require little protection. Certain designs, however, must be shielded from internal heat effects. Nose cone and warhead detaching devices, if skin mounted, require protection from aerodynamic heating. A current specification for a cartridge powered device that manipulates missile airfoils bears a high temperature requirement of 350 F for 1 hr. A potential application for propellant devices is in the functioning of components to alter flight during atmospheric re-entry. These devices could be actuated by temperature sensing mechanisms. For such a system, it follows that a greater resistance to high temperature by the propellant would allow a wider latitude in increments of time and, consequently, distance, within which the necessary flight adjustment could be made.

Extension of the High Temperature Operation Range

For most rocket or gun applications, ordnance requirements stipulate satisfactory performance over a temperature span of −65 to 160 F. In addition, it is desired that temperature coefficients of performance be at a minimum. However, it is not uncommon for performance at either extreme to be marginal. Propellant devices exposed to much higher temperatures than described may also be required to function at the peak of heat exposure. Propellants for this application face a temperature range of performance hitherto unknown to the field.

Presented at the ASME-ARS Aviation Conference, Dallas, Texas, March 17–20, 1958. Revised April 1959.

[1] Physical Chemist, Research and Development Group.

Recycling

Propellant powered devices which are an integral part of the operation or mission of supersonic vehicles are subjected to only one thermal cycle before being fired. But other CADs, such as personnel ejection or certain stores ejection devices serve an emergency purpose. As such, they are required to undergo an unknown number of missions and attendant high temperature cycles. If this is coupled with potential ground soak exposures between missions, then the heat problem as applied to CAD propellants assumes its real, albeit disturbing, proportions. Although this possibility of continuous cycling and its additive destructive effects on propellants could be kept under control by a frequent replacement program, a high temperature resistant propellant could keep such a program within reasonable bounds or else do away with it altogether. In reference to ground soak, studies show that in parked aircraft, temperatures well over 200 F have been observed beneath the closed canopy at pilot heat level.[2] In one day, under these conditions, data show temperatures exceeding 160 F for 6 hr and exceeding 200 F for 3 hr. The number of times that this cycle may be repeated cannot be determined, since it depends on the operational status of the aircraft and ground handling procedures, among other factors. The fact remains that, whether the aircraft is flown or not, the CAD propellant, unlike weapons propellants, is a fixed aircraft component subject to whatever extremes occur.

Sealed Cartridge Case

A specification requirement for CADs is that the case containing the propellant be sealed to withstand 14 psi pressure differential. This is to forestall moisture condensation within the cartridge case due to extremes of humidity and temperature, between ground level and flight altitude. Sealing, however, works to disadvantage at elevated temperatures, since this accelerates the decomposition rate of many propellants.

Limitations for Protection of Propellant Powered Devices

The possibility of protection against heat by insulation has been considered and in certain instances is feasible. However, it is difficult to extend insulation over a broad range of application, since CADs are designed under sharp limits of allotted space, usually within fractions of an inch. Dimensional increases due to the addition of thermal barriers must be brought into line with with the ever-present drive toward miniaturization.

The Research and Development Group of Frankford Arsenal is charged with the mission of research and development in the field of cartridge actuated devices. The need for propellant-initiator systems capable of operation at temperatures far above the presently accepted maximum of 160 F has been recognized for some time. As a result, a program is currently under way for the Air Force whose object is the development of propellant-initiator systems for use in environments up to 400 F. This program is divided into five phases which can be summed up as follows:

1 Determine the useful life at high temperatures and auto-ignition hazard time-temperature relationship of currently standard propellants for CADs.

2 Determine the same limits for other existing propellant types.

3 Establish the feasibility of substituting more thermally stable existing propellants for the present ones in CADs.

4 Develop new and radical propellant-initiator systems for high temperature resistant CADs.

5 Establish the safe operating time-temperature limits of standard and new systems in propellant powered devices.

This paper describes some of the data required, the approach taken to obtain this data, and some of the equipment developed for that purpose.

Discussion

Nitrate Ester Propellants

The bulk of high temperature work on propellants in the past has usually taken either of two directions—research on storage stability and surveillance procedures or direct work on the phenomena of auto-ignition or cookoff.

For storage stability, the maximum temperature of work is in the area of the 160 F requirement imposed by the armed services. In this work as in stability tests conducted above this temperature, heat is employed as a means of further accelerating those propellant decomposition processes which would normally take long periods of time to bring about. Norms are set in terms of these accelerated results, and estimates of propellant life at ambient temperatures are made by correlating the results obtained under these extreme test conditions. For work at temperatures higher than the 160 F range, investigators over the years have resorted to rigorously defined empirical test procedures to obtain reproducible results at these accelerated conditions. These include the well-known methyl violet heat stability test at 274 F (134.5 C) for nitrocellulose single-base propellants, and at 248 F (120 C) for double-base propellants, and the gas evolution tests, such as the Taliani test at 230 F (110 C) or the vacuum stability test at 212 F (100 C) for single-base and 194 F (90 C) for double-base propellants.

The literature shows lesser emphasis on high temperature work dealing with auto-ignition of propellants. The hazard of spontaneous ignition during propellant manufacture has provided the impetus for most of this work. Some research of a more basic nature deals not with auto-ignition as an end in itself, but, under controlled conditions, as a means of determining physico-chemical constants of propellant compositions. Typical is the establishment of the apparent activation energy for ignition by applying the Arrhenius equation for the influence of temperature on rate of reaction, in this case reduced to

$$\log t = \frac{E_a}{2.303R}\left(\frac{1}{T}\right) + \text{constant}$$

where

t = time to ignition
E_a = activation energy
R = gas constant
T = absolute temperature

A plot of log t vs. the reciprocal of the absolute temperature yields a straight line from whose slope the activation energy E_a can be calculated.

Composite Propellants

The variety of fuels developed for composite propellants since World War II pose an extremely difficult problem to those concerned with correlating propellant stability under various conditions. The complicating factor is that the accepted chemical stability tests of today, either the color indicator or gas evolution types, are applicable only to the nitrate ester family of propellants. Unfortunately, the chemical basis for applying these tests and norms to the composite propellants does not appear to exist, since in many cases the latter do not evolve gaseous nitrogenous decomposition products. In the absence of a standard yardstick, other means of comparison must be employed. For the program described in

[2] Fendick, R. B. and Stuck, D. H., "Phase V High Temperature Climatic Test of an F101A Aircraft," Directorate of Flight and All-Weather Testing, Wright Air Development Center, Technical note no. WADC-TN-56-404, Nov. 1956.

this paper, progressive degradation of different propellant types under severe heating is being measured by infrared spectrophotometry and by mass spectrometry techniques.

Factors Affecting CAD Propellant Life at High Temperature

For our purpose the title "propellant life at high temperatures" may be subdivided. We can describe the profile of high temperature life as in Figs. 1a and 1b. If we raise the temperature surrounding the device above 200 F, there is first an interval where, outwardly, nothing takes place. But it is during this period that present CAD propellants begin to change. So long as these changes are not significant enough to affect ballistics when fired, the propellant can be said to still retain "useful life." Useful life is terminated when this decomposition has increased to the point where ballistics fall outside of minimum or maximum tolerances. Beyond this point, as exposure to heat continues, the rate of decomposition increases sharply. Though seemingly intact, the propellant device is now useless. Ultimately, of course, if the time-temperature conditions are severe enough, the zone of auto-ignition hazard is entered.

The earlier heating stage where useful life may be measured in minutes or hours, depending on heat input history, is an unexplored area. This useful life can fall well within one or more flight times of supersonic vehicles. The changes in the propellant in these exposures short of auto-ignition include chemical degradation, migration of ingredients, or plastic deformation of calculated grain geometries. Any one can render the charge incapable of functioning as originally designed.

Various factors are being investigated for their effects on the time-temperature coordinates of the propellant life zones pictured above. These factors are:

Rate of temperature rise.
Rate of rise plus exposure time at a series of temperature levels.
Thermal lag through the case wall.
Composition of the propellant.
Propellant dimensions and mass

What is unique is that their influence is being exerted in this system under constant-volume conditions within the limits of the CAD seal. For nitrate ester propellants, at least, it is known that if the products of decomposition remain in contact with the propellant under pressure, the decomposition rate will be accelerated.

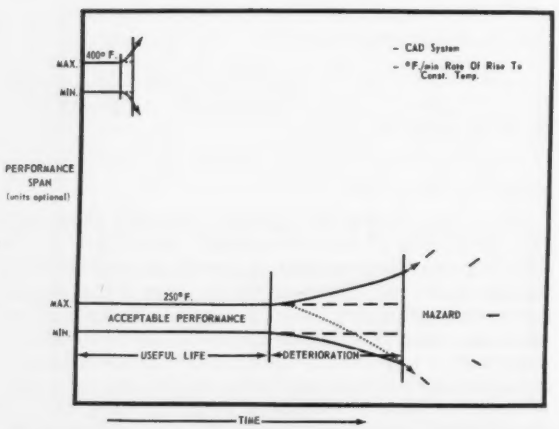

Fig. 1a Propellant life at high constant-temperature levels, one system

Experimental Methods

Procedure

The hazard zone of potential auto-ignition is determined under actual sealed CAD cartridge case conditions. The auto-ignition time-temperature relationship is evaluated from heat runs at various rates of temperature rise and rate of rise coupled with sustained constant temperatures. The latter are carried out at regular intervals beginning at 200 F and extending to auto-ignition maximum. The next step is the determination of the zone of useful life. This is obtained from simultaneous exposures of numbers of loaded CAD cartridges. The specific time-temperature schedules are in the safe zone determined from the foregoing auto-ignition determinations, but are arranged to become increasingly severe, ending just short of the indicated auto-ignition conditions. From each exposure, certain of the cartridges are then tested ballistically for change in performance, while others are examined chemically and microscopically for extent of decomposition and physical deformation of propellant. Concurrently, study is made of the heat transfer characteristics of the system and effect on primer and igniter.

Materials and Equipment

Propellants

The propellant types currently under study include:

Nitrate ester types, single-base compositions (nitrocellulose) and double-base compositions (including both high and low nitrogen nitrocellulose and a range of nitroglycerin contents and additives).

Composite propellant types (including perchlorate and nitrate oxidizers and rubber, plastisol, resinous, nitropolymer, and newer, more exotic fuels).

Thermal Programmer

Valid and reproducible data for this program require the closely controlled application of heat. To accomplish this, an electronically controlled thermal programmer was designed. The unit is capable of providing linear rates of rise from 0.5 to 30 F per min. It can be preset to level off at any temperature up to 750 F and maintain that temperature for any time interval from 1 min to 12 hr. Time-temperature history and auto-ignition point are recorded on a strip chart. Accessory devices include a delayed start timer for lengthy overnight runs and a signal actuated at shutoff to operate safety and cooling devices.

Auto-Ignition Apparatus

This device is operated by the thermal programmer. In it,

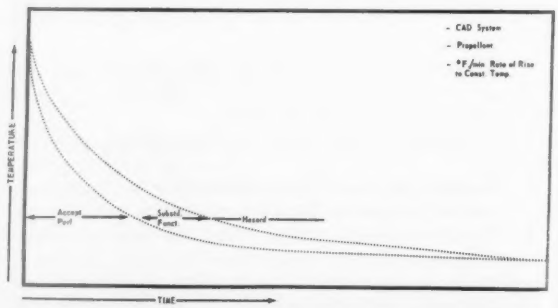

Fig. 1b Propellant life at constant-temperature levels, one system

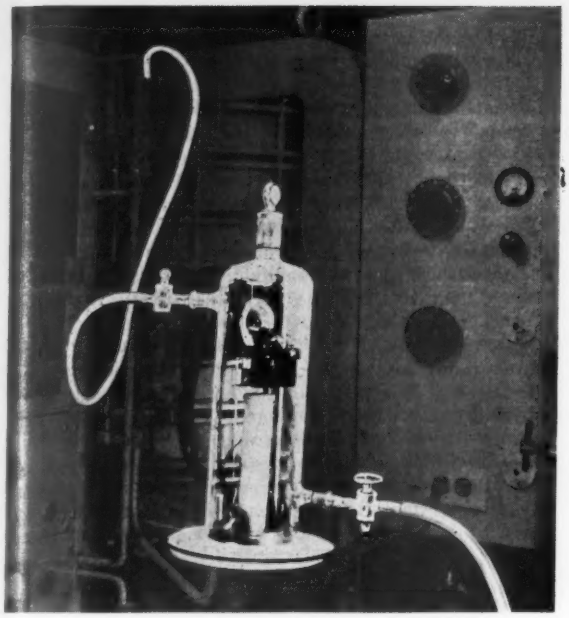

Fig. 2 Gas release chamber

a loaded cartridge can be safely heated until auto-ignition occurs. The heated vessel is a solid block of commercially pure copper containing a deep 1-in. diameter well. Within the well, the cartridge is supported by a retainer which permits the case wall surrounding the propellant to be suspended in air. The control thermocouple from the programmer is in contact with the cartridge wall. Heating is accomplished by a dual system, one system comprised of helically wound elements in a heating jacket, the other, a set of six cartridge heaters buried in the copper block radially surrounding the well. The standard M38 cartridge case serves as a test container. For this purpose, it is modified to permit the gases from the ignited propellant to rupture the sealing disk. At auto-ignition, the blast of gases actuates a trigger, which, through a microswitch, instantly shuts off the entire heating, controlling and recording mechanisms. The operation is automatic and is carried out in an armored cubicle.

Apparatus for Estimation of Propellant Useful Life

For the determination of the zone of useful life of propellants, fully loaded cartridges are used. Safety considerations dictate that personnel cannot be present during these tests. For this purpose, a specially designed oven, located in an armored room, is operated by remote control from the programmer. The severe heating schedules are relatively short, and must be terminated abruptly. When a particular schedule ends, the programmer shuts off the oven, signals a device which opens the oven door, and a blower purges the oven of heated air. Since the exposed cartridges are sealed, they still retain gaseous decomposition products. To transfer these products to the mass spectrometer for analysis, the cartridge is opened in a sealed-off chamber designed for this purpose (Fig. 2). The sealed chamber is first flushed with helium. A sharp pin driven by a solenoid positioned above the cartridge ruptures the cartridge sealing disk, and the gases are released. The chamber is then opened to an evacuated line leading to the mass spectrometer, and the gases are drawn into the instrument for analysis.

Results

The first phase of the program is approaching completion with the establishment of time vs. temperature auto-ignition hazard data for CAD cartridges loaded with the most widely used solid propellant types. Over eight hundred runs have been made covering various rates of temperature rise and elevated constant temperature "soak." Due to the precise programming of heat input by the apparatus described above, reproducible data have been obtained. Typical individual run data are shown in Table 1 for a CAD cartridge loaded with various propellants.

The effect of rate of temperature rise on auto-ignition temperature for nitrate ester propellants is shown in Fig. 3. In general, a lower rate will result in a lower auto-ignition tem-

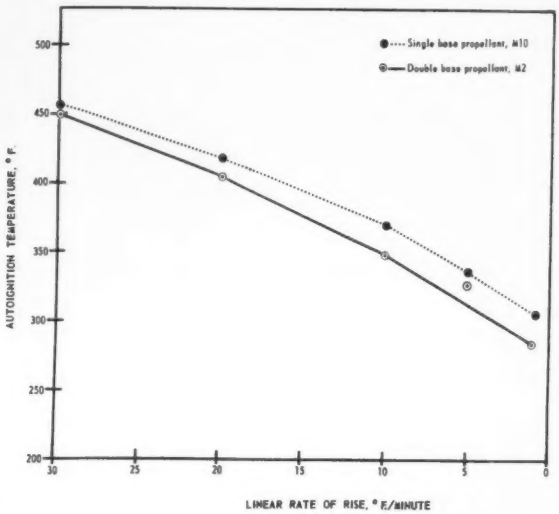

Fig. 3 Auto-ignition temperature vs. linear rate of rise, sealed CAD cartridge

Table 1 Auto-ignition temperature individual run data, sealed CAD cartridge

	Auto-ignition temperature, F —Linear rate of rise, F/min—				
Propellant type	1	5	10	20	30
double base	284	325	354	414	441
	284	325	350	411	442
	283	324	350	412	440
	284	325	355	410	441
	282	325	350	412	445
ammonium perchlorate/ polymer	460	514	554	602	637
	460	516	552	598	637
	460	515	553	601	647
	457	513	555	612	637
	463	516	559	596	652
ammonium nitrate/ polymer	382	402	437	497	527
	382	401	437	493	542
	387	400	437	496	532
	379	398	438	497	532
	387	399	438	485	527
black powder	529	554	572	594	616
	522	553	575	598	617
	522	550	573	598	615
	522	554	573	594	609
	520	550	571	590	611

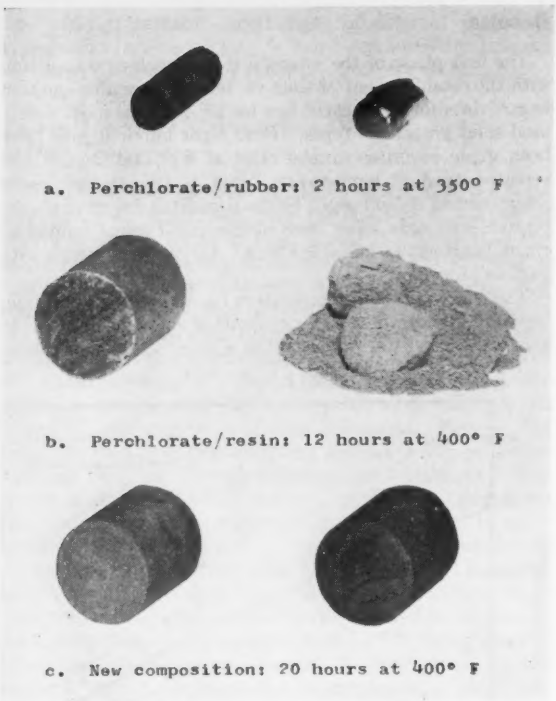

Fig. 4 Composite propellants before and after high temperature exposure: a. perchorate/rubber—2 hr at 350 F. b. perchlorate/resin—12 hr at 400 F. c. new composition—20 hr at 400 F

Table 2 Auto-ignition temperature, sealed CAD cartridge case

Propellant type	Grain dimensions, in. OD	Length	Auto-ignition temperature, F Linear rate of rise[a] F/min 5	10	20	30
M2, double base	0.040	0.046	321	347	403	436
	0.073	0.243	322	351	399	430
	0.203	0.432	329	349	403	449
	0.245	0.478	326	350	396	447
	0.495	0.600	319	352	403	442
M10, single base	0.049	0.135	336	364	410	446
	0.202	0.475	337	369	418	455

[a] Values represent averages of five runs.

Table 3 Auto-ignition time, min, at constant temperature, sealed CAD cartridge

Propellant	Constant temperature level, F[a] 225	250	275	300	325	350
double base	720+	286	30	11	6	4
single base	720+	720+	480[b]	19	8	4

[a] Values represent averages of five runs.
[b] Average of seven cartridges. Eight cartridges survived 720 min. Fifteen tests made due to this anomalous behavior.

perature. At these low rates of rise, the temperature gradient induced by the cartridge case is minimized, and the observed auto-ignition temperature is more a characteristic of the propellant itself. At high rates of rise, the indicated auto-ignition temperature reflects the heat transfer rate of the cartridge system. (In this connection, it should be borne in mind that the work described herein is necessarily the study of a cartridge exposed to a heated environment. As a result, the values obtained are not ascribed to propellant alone, but rather to the propellant-cartridge system.) As shown in Table 2, the grain size of the nitrate ester propellant described here had no significant effect upon auto-ignition temperatures. It should be noted, however, that the grain sizes are relatively small.

Other data obtained show that nitrate ester propellants now standard for CAD will not meet 400 F exposure. Several series of propellant loaded sealed cartridges were heated at one rate of rise at 30 F per min up to level-off at predetermined constant temperatures. Isothermal exposures were terminated at 12 hr if auto-ignition did not occur sooner. The sharp drop in total life at constant temperature exposures above the 250 F level is shown in Table 3. Note the slight advantage of single-base over double-base propellants below the 300 F level.

When tested under similar conditions, the composite propellants as a class show greater tolerance for elevated temperatures prior to auto-ignition. Many can be held at 300 F or somewhat higher for considerable periods. (Exact data and compositions are, of course, classified.) Some of these, however, do not survive these exposures in usable condition. Upon examination after exposures up to 400 F, they have shown slumping, melting, exudation of ingredients or such general degradation as to be unrecognizable as propellant grains. Some are pictured in Fig. 4 before and after exposure. New composite propellants specifically tailored for high temperature resistance are now being developed. Some are being evaluated in this program and to date are a marked improvement over earlier compositions. One is pictured in Fig. 4 for comparison.

An interesting sidelight is the resistance to auto-ignition shown by black powder, various grades of which are used as igniter charges in CAD. A sample of the data is shown in Table 1. On a temperature rate of rise basis, there was little difference between the various granulations.

Summary

The first phase of this program can be summed up as a search for propellant systems capable of simple survival at high temperatures. By-products of this evaluation are the data necessary for establishment of auto-ignition hazard zones. With the completion of this phase, some observations can be made. Present nitrate esters fall short of the new high temperature requirements for propellant actuated devices. Certain composites show promise up to 400 F exposures for moderate durations. Even here the composite propellants face certain problems at high temperatures. Oxidizers must survive these temperatures without phase change or other phenomena. Fuels or binders will require changes in their formulations. Propellant curing cycles may need adjustment. (For this program, one of the earlier composites which showed exudation of one of the fuel ingredients was reformulated and now shows promise of increased high temperature life.) For CAD application, composite propellant grains in very small sizes and burning web thicknesses of close tolerance will have to maintain these dimensions without swelling or slump over the increased temperature range. There is some difficulty in obtaining composite propellants in small geometries, but some new extrudable high temperature resistant formulations have been obtained. Similar difficulty exists in obtaining burning rate data of composite propellants at the high pressures characteristic of some cartridge actuated devices. A very difficult problem is an acceptable temperature coeffi-

cient of performance over a temperature spread of approximately 460 F.

The second phase of this work is the delineation of zones of substandard ballistic functioning at high temperature exposure levels short of auto-ignition. Concurrently, these heated propellants are being studied by instrumental techniques to determine the mechanism of ballistic failure. This requires matching the ballistic performance of nitrate esters with the new propellants (phase 3 of the program). Some of this has already been accomplished, and firings of CADs exposed to high heat schedules are now in progress. It is hoped that a report on the completion of this phase will be made in the near future.

In this problem of propellant actuated devices exposed to severe heat, a great deal of data must be obtained and examined. Elevated temperature conditions are now real, and these data must come from a considerable amount of work in areas previously subjects for theoretical study. Stability and performance problems in these areas must be overcome if we are to make use of the merits of propellant power packages at high temperatures. The approach described here encompasses such a study with a view toward end item development.

Vaporization Rate Limited Combustion in Bipropellant Rocket Chambers

E. MAYER[1]

Rocketdyne Division,
North American Aviation, Inc.
Canoga Park, Calif.

A one-dimensional model of the bipropellant rocket combustion chamber is analyzed on the assumption that vaporization of liquid droplets is the rate controlling step in the combustion process. The dependence of the gas flow variables on position coordinate in the chamber is determined in elementary analytic form subject to the assumptions that the vaporized propellants are instantaneously mixed and reacted in stoichiometric ratio, and that droplet motion is governed by full entrainment in the product gas flow; i.e., droplet velocity is equal to local gas velocity. The formal solutions obtained permit comparison and contrast with the more fundamental case of monopropellant combustion. It is concluded that in the bipropellant system gas velocity distribution is determined primarily by the droplet spectrum and volatility of the more slowly vaporizing species, and that the temperature distribution is strongly dependent on the droplet size spectrum and volatility of the more rapidly vaporizing species. Depression of the temperature levels associated with the presence of excess unreacted propellant gas near the injector implies the existence of flame-holding stability limits due to excessive mismatch in the local vaporization rates. The possible scope of applications and limitations of the vaporization rate controlled combustion model is discussed on the basis of relevant data available in the literature on combustion in rockets.

DURING the past decade a great deal of experimental and theoretical work has been accomplished in basic studies of droplet and spray combustion (1)[2] with the objective of elucidating a variety of combustion problems in jet propulsion. However, applications of these basic studies to combustion in liquid propellant rocket chambers have been lagging because of complexities arising from the interactions among the atomization, fluid dynamic and chemical effects. In recent investigations Priem (2,3) obtained successful correlations of combustion efficiency with chamber length based on a theoretical combustion chamber model in which vaporization of hydrocarbon droplets was the rate controlling process. It is the purpose of this paper to present a general description of the vaporizaton rate limited bipropellant combustion chamber by analysis of a representative model which retains the essential features of the bipropellant process without undue mathematical complications. Elaborate treatment does not appear warranted at this time, owing to uncertainties in droplet size and velocity distributions obtained upon injection of liquid propellant streams into the prevalent gas environment in the rocket chamber. Nevertheless, by the use of simplified representations of droplet distributions and vaporization laws, it is possible to ascertain the effects of bipropellant volatilities on the gas velocity, efficiency and temperature steady-state distributions in rocket combustion governed by vaporization rates. The simplified treatment herein presented permits the comparison and contrast of the bipropellant process with the more elementary case of vaporization rate controlled monopropellant combustion.

The applicability of the results obtained is limited to high temperature reaction under relatively rapid mixing conditions. Consideration of published data on the internal chemical and flow conditions in experimental chambers (4,5) reveals the importance of mixing and chemical time

Presented at the ARS 13th Annual Meeting, New York, N. Y., Nov. 17–21, 1958.

[1] Engineering Specialist, Advance Design. Member ARS.

[2] Numbers in parentheses indicate References at end of paper.

lags which, to some extent, mask the role of vaporization rates in the dependence of combustion efficiency on combustor length. Nevertheless, as shown by Priem (2,3), useful technical correlations may be deduced by treatment of a vaporization rate limited combustor model. More generally, it is reasonable to expect that clarification of bipropellant combustion governed by vaporization rates will simplify the interpretation of combustion phenomena arising from mixing and chemical time lags present in the rocket combustion chamber.

Model of the Vaporization Rate Limited Combustion Chamber

In the combustion process limited by vaporization rates, the continuous, steady-state conversion of liquid propellants to reacted gases is visualized to occur in the following sequence. Upon injection of the liquid jets at the upstream end of the chamber, a droplet spray is formed here with initial droplet size and velocity distributions dependent on both jet impingement configurations and prevalent "steady-state" gasdynamic conditions. In the subsequent history of the droplets, evaporation is governed by heat transfer from the surrounding gas stream, and velocity modifications ensue by entrainment in the product gas flow. The vaporized propellants are rapidly mixed and promptly reacted (in stoichiometric ratio) wherever they are formed, thus providing for a continuous increase of the gaseous mass flow rate with increasing distance along the flow direction. The combustion is completed downstream of the injector where all liquid droplets capable of providing reactants have been vaporized; i.e., in a bipropellant, with nonstoichiometric overall oxidant-to-fuel ratio, combustion is complete when the deficient propellant has been vaporized.

An idealized model of the combustion chamber representing the features described above is analyzed in this paper on the basis of the following assumptions:

(a) One-dimensional, constant-pressure gas flow.

(b) Ideal gas law.

(c) Instantaneous mixing and (stoichiometric) chemical reaction of the vaporized propellants within the local product gas flow.

(d) Negligible axial heat conduction and radiation effects.

(e) Vaporization rate independent of instantaneous location of droplet, i.e., dependent primarily on the time elapsed after injection.

(f) Droplet motion governed by full entrainment in the main gas flow, i.e., droplet velocity equal to the local gas velocity.

The idealizations listed in these assumptions appear to be more applicable to large-scale, high performance rocket engines than to small-scale model combustion chambers, where the nonrepetitive pattern of injected jets and the influence of relatively nearby chamber walls impair the validity of the one-dimensional treatment. To be sure, even in the large-scale engine with planar injector face, the presence of discrete liquid jets creates complex multidimensional flow conditions near the injector face. In particular, the continuous effective ignition of the vaporized propellants in the large-scale engine must be accomplished by anchoring the reaction process in the low velocity recirculation zones created in the neighborhood of the solid portions of the injector face. Although details of the recirculation process are not accounted for in assumptions (a), (b), (c) and (d), the one-dimensional treatment does permit an appraisal of the relative importance of bipropellant vaporization rates on flameholding against the injector face, which is a necessary condition for combustion stability in the large-scale, high performance engine (see discussion of flameholding stability).

In regard to assumption (e), basic investigations of both combustion (1,6) and vaporization of droplets (1,7) indicate that the diameter vs. time relation of typical propellant droplets of initial diameter D_i can be approximately represented by the parabolic form

$$D^2 = D_i^2 - Kt \qquad [1]$$

where K is a rate parameter dependent on physico-chemical properties of the droplet and of its ambient atmosphere. In application to rocket combustion, use of K data pertaining to vaporization of droplets in turbulent surroundings is more appropriate than use of rate parameter data determined from droplet combustion in quiescent atmospheres (see next section).

Finally, in regard to assumption (f), it is clear that rapid entrainment of the droplets in the main gas can be expected only for the small droplet component of the spray formed upon injection. In high performance engines, this spray component appears to be of particular importance in achieving the high gas generation rates and heat release rates present in the zone adjacent to the injector. Full entrainment in one-dimensional gas flow is an essential assumption for avoiding mathematical complications which arise if drag effects due to relative velocities between droplets and gas flow are taken into account. A more realistic treatment of the entrainment problem appears to be further complicated by the unknown initial droplet velocity distribution within the spray formed upon impingement.

Representative Vaporization Rate Data

In rocket engineering practice, a basic datum in the design of a combustion chamber adequate for efficient combustion of given propellants is the characteristic length defined by

$$L^* = V_c/A_t$$

where

V_c = chamber volume (including the converging section of the nozzle)

A_t = nozzle throat area

Empirical values of L^* are listed in Table 1 reproduced from (8).

Table 1 Empirical values of L^* at P_c = 300 psia

Propellants	L^*, in. (Approximate values)
LOX-alcohol	50–100
nitric acid-aniline	40–175
nitric acid-JP_3	50–60
nitromethane	>190
LOX-JP_4	35–55

The extended ranges of L^* values indicated in the table arise from such complicating hydraulic factors as initial axial velocities, droplet size distribution and mixing pattern of the injected propellant present under the experimental conditions yielding the listed data. Further complications arise from chemical lags incurred in the conversion of gas phase propellants to product gases. In spite of these complications, the influence of vaporization rates on the reported L^* values becomes apparent in view of representative vaporization rate data as given, for example, by Penner (7), shown in Fig. 1. The solid curves in Fig. 1 describe the dependence of droplet radius on time calculated in (7) on the assumption that heat transfer from the product gases to the vaporizing droplet occurs across a film thickness approximately equal to the instantaneous droplet radius. The dotted curve in the figure is obtained by application of Spalding's transfer-number method (9), whereby droplet lifetimes under comparable

Table 2 Lifetimes of fuel droplets of initial diameter, $D_i = 200\ \mu$

Fuel	Process	Lifetime, t_f, sec	$K = D_i^2/t_f$, cm²/sec	Source
n-heptane	Quiescent combustion in O_2 at	0.008	0.050	Goldsmith's (10) experimental data corrected for
ethanol	$P_g = 300$ psi	0.009	0.045	pressure level by 0.25 pressure exponent (11)
n-octane	Vaporization in product gas at	0.003	0.133	Ref. (7), see also Fig. 1
ethanol	$T_g = 3000$ K, $P_g = 300$ psia	0.004	0.100	

product gas conditions are interrelated by the transfer numbers[3] B dependent on the vaporizing species.

Comparison of the empirical L^* data with the calculated droplet lifetimes indicates that both quantities increase in the propellant sequence, 1 hydrocarbon, 2 alcohol, 3 aniline, suggesting the importance of vaporization as a rate controlling step in the overall combustion process for these high performance propellants.

The dominant role of the vaporization process is also revealed in the relatively long L^* of monopropellants as nitromethane and hydrazine ($L^* > 200$ in.). However, low performance monopropellants of this type are known to undergo slow gas phase reactions which preclude the applicability of single rate controlling step (see discussion).

It may be noted here that the droplet vaporization rates calculated in (7) are considerably greater than those obtained when vaporization occurs under quiescent conditions of droplet burning governed by molecular diffusion of vapor from the droplet surface to a surrounding reaction front, established across an intervening vapor film of some 3 to 10 radii in thickness (1,6). Although an abundance of quiescent droplet burning data has become available during the past decade (1,6), the applicability of such data to the interpretation of rocket combustion is questionable because of turbulent conditions in the rocket chamber. These conditions preclude the existence of an extended molecular diffusion field surrounding the droplet. It is likely that the high temperature gaseous products penetrate within a radius or less of the droplet surface, thus increasing heat and mass transfer rates severalfold as compared with droplet burning.

For purposes of orientation, lifetime data on hydrocarbon and alcohol droplets of initial diameter $D_i = 200\ \mu$, vaporizing under quiescent and turbulent conditions, are compared in Table 2. The rate constants K listed in this table are related to the lifetime t_f by the parabolic law Equation [1], i.e., by $K = D_i^2/t_f$ which, on theoretical grounds, is applicable to droplet combustion. For the vaporization rates calculated in (7), use of the parabolic law is only approximately valid as indicated in the nondimensional diameter vs. time curves in Fig. 2. The agreement shown in this curve is sufficiently close to warrant the application of the parabolic form for vaporization rates in the illustrative calculations of the next two sections.

An order-of-magnitude estimate of injected droplet diameters based on $D_i = \sqrt{Kt_f}$ may be made from droplet lifetime data inferred from photographic studies of combustion in transparent experimental rocket chambers. The growth of gas velocity in the axial direction, associated with the progress of combustion, is conveniently determined by fast photography of moving luminous pockets, as described by Berman and Logan (12). Gas velocity data obtained under severe atomization conditions in liquid oxygen/alcohol combustion at $P_g = 300$ psi (12) indicate that combustion is accomplished within 3 in. of the injector with an approximate droplet lifetime of $t_f = 0.002$ in transit through the combustion zone. With the vaporization parameter $K = 0.1$ cm² per sec (see Table 2), the estimated maximum droplet diameter is $D_i \simeq 1.4 \times 10^{-2}$ cm.

[3] The transfer numbers $B_{\text{octane}} = 5.02$, $B_{\text{ethanol}} = 2.95$ ((9) p. 130) inserted into

$$\frac{t_{\text{ethanol}}}{t_{\text{octane}}} = \frac{\log (1 + B_{\text{octane}})}{\log (1 + B_{\text{ethanol}})}$$

interrelate the times required for a given decrease in the droplet radius in curves (c) and (d) of Fig. 1.

Combustion of Uniform Droplets

Many of the essential features of vaporization rate limited combustion are readily deduced by treatment of the elementary case of uniform initial droplet size D_i for each propellant type. The influence of droplet size distribution is conveniently discussed in terms of the elementary results derived in this section.

Monopropellants

Since the heat released per unit mass of the vaporized (and reacted) monopropellant is constant, the gas temperature T_g and density ρ_g are also constant under the assumptions (a) and (b). If N liquid droplets of diameter D_i are injected per unit area per unit time, the mass flux $\dot{m}$, consisting of liquid

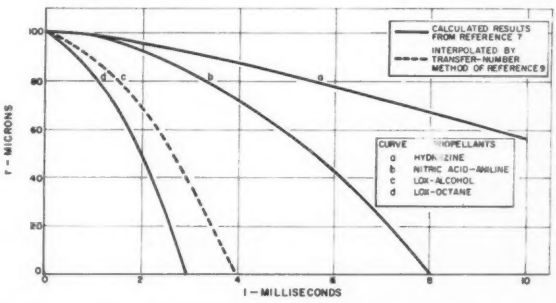

Fig. 1 Radius vs. time data for vaporizing fuel droplets (T_g = 3000 K, P_g = 300 psia)

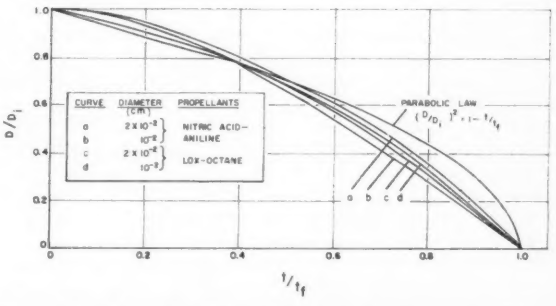

Fig. 2 Nondimensional diameter vs. time dependence of vaporizing fuel droplets based on data in (7)

and gas phase fluxes $\dot{m}_l$ and $\dot{m}_g$, is

$$\dot{m} = \dot{m}_l + \dot{m}_g = (\pi/6)D_i^3\rho_l N \quad [2]$$

where ρ_l is the liquid density. The gaseous mass flux at any station along the combustion chamber

$$\dot{m}_g = \dot{m} - \dot{m}_l = \rho_g u_g \quad [3]$$

is readily calculated from given vaporization rate laws (e) under the assumption of full entrainment (f) of liquid droplets in the product gas velocity u_g.

Full entrainment implies that the droplet flux N is constant at any section of the one-dimensional chamber, hence $\dot{m}_l$ for the species is

$$\dot{m}_l = \frac{\pi}{6} D^3\rho_l N = \dot{m}\left(\frac{D}{D_i}\right)^3 \quad [4]$$

where D is the local droplet diameter.

It is convenient in the calculations to employ the time elapsed after injection t as a parameter which connects u_g and the coordinate x downstream of the injector

$$x = \int_0^t u_g\, dt \quad [5]$$

Thus, if the droplet history is given by the vaporization law $D = D(t)$, Equation [3] yields immediately

$$\frac{\dot{m}_g}{\dot{m}} = 1 - \frac{D^3(t)}{D_i^3} = \frac{u_g}{u_f} \quad [6]$$

where u_f is the final gas velocity attained after an interval t_f corresponding to the droplet lifetime defined by $D(t_f) = 0$. In accordance with the assumed ideal gas law (b), u_f is determined from

$$u_f = \frac{\dot{m}}{\rho_g} = \frac{\dot{m}\, RT_g}{P_g} \quad [7]$$

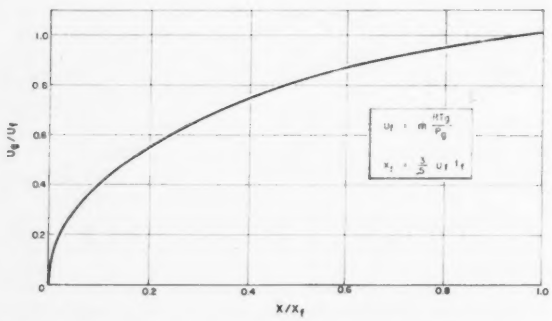

Fig. 3 Nondimensional gas velocity vs. coordinate in monopropellant combustion chamber with uniform injected droplet size

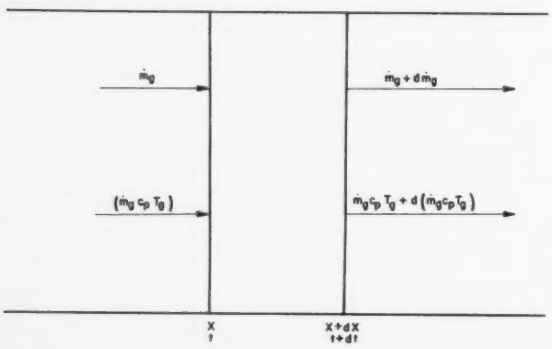

Fig. 4 Sketch of incremental relations for elementary zone of combustion chamber model

The velocity u_g in Equation [6] is attained at the coordinate determined from Equation [5]

$$x = u_f\left(t - \frac{\int_0^t D^3 dt}{D_i^3}\right) \quad [8]$$

For the special form $D(t)$ in Equation [1], we have in nondimensional form with $\tau = t/t_f = Kt/D_i^2$ as a parameter

$$\frac{u_g}{u_f} = 1 - (1 - \tau)^{3/2} \quad [9]$$

$$\frac{x}{x_f} = \frac{5}{3}\left\{\tau - \frac{2}{5}\left[1 - (1 - \tau)^{5/2}\right]\right\} \quad [10]$$

where

$$x_f = \frac{3}{5} u_f t_f \quad [11]$$

is the distance traversed by the droplet in its lifetime $\tau = 1$, i.e., the combustion length. These results are illustrated in Fig. 3 showing the dependence of the velocity on coordinate along the monopropellant combustion chamber. With suitable modifications, the prototype parametric results in Equations [9 and 10] prove to be useful in calculating velocity and coordinate results for bipropellant systems with inclusion of the droplet size distribution effects, as will be shown.

Bipropellants

In this case we distinguish between the histories of fuel and oxidant droplets $D_F(t)$ and $D_O(t)$ as they may be characterized by different vaporization parameters K_F and K_O, respectively. Since the chemical reaction is assumed to occur in a stoichiometric mixture ratio, $M_{st} = (O/F)_{st}$, the presence of excess unreacted propellant sharing in the local heat release may, in general, lead to spatial dependence of the steady-state temperature T_g. For the sake of simplicity, we shall assume further that the local vaporization rates always provide excess oxidant, so that the heat release rate is expressible in proportion to the local fuel vaporization rate.

Consider now the steady-state gas mass balance and relations for the elementary zone between the planes X and $X + dX$, as sketched in Fig. 4. The incremental mass flux, consisting of both reacted products and unreacted excess gas (oxidant in this instance), is

$$d\dot{m}_g = d\dot{m}_{g,F} + d\dot{m}_{g,O} = d(\rho_g U_g) \quad [12]$$

The incremental enthalpy flux is referred to the heat value of the fuel $H_{F,B}$ under standard conditions at temperature $T = T_B$

$$d(\dot{m}_g c_p T) = (H_{F,B} - \Delta H_F)\, d\dot{m}_{g,F} - \Delta H_O d\dot{m}_{g,O} \quad [13]$$

where the enthalpy corrections ΔH_F and ΔH_O are so determined as to allow for possible nonstandard initial conditions of the fuel and oxidant, respectively. (These corrections are small compared with $H_{F,B}$ for most propellant combinations.)

Integration of Equations [12 and 13] yields the continuity equation

$$\dot{m}_g = \dot{m}_{g,F} + \dot{m}_{g,O} = \rho_g U_g \quad [14]$$

and the energy equation

$$\dot{m}_g(c_p T_g - c_{p,B} T_B) = (H_F - \Delta H_F)\dot{m}_{g,F} - \Delta H_O \dot{m}_{g,O} \quad [15]$$

wherein the integration constant $c_{p,B}\, T_B$ has been introduced to refer the enthalpy of the product gas to the standard temperature T_B. With ρ_g eliminated by means of the equation of state

$$\rho_g = P_g/RT_g \quad [16]$$

Equations [14 and 15] yield the following results for gas

velocity and temperature

$$U_g = q_F \dot{m}_{g,F} - q_O \dot{m}_{g,O} \quad [17]$$

$$T_g = \frac{P_g}{R}\left(\frac{q_F \dot{m}_{g,F} - q_O \dot{m}_{g,O}}{\dot{m}_{g,F} + \dot{m}_{g,O}}\right) \quad [18]$$

where

$$q_F = \frac{R}{c_p P_g}(H_F - \Delta H_F + c_{p,B}\, T_B) \quad [19]$$

$$q_O = \frac{R}{c_p P_g}(\Delta H_O - c_{p,B}\, T_B) \quad [20]$$

The changing chemical composition within the bipropellant chamber produces changes in c_p, R, q_F, q_O, which, on the basis of simplified reaction kinetics, can be expressed as functions of the auxiliary variables $\dot{m}_{g,F}$ and $\dot{m}_{g,O}$ (see Appendix). These variables, in turn, are implicitly dependent on the time t elapsed after injection, in analogy with the monopropellant case

$$\dot{m}_{g,F} = \dot{m}_F\left(1 - \frac{D_F^3(t)}{D_{F,i}}\right) \quad [21]$$

$$\dot{m}_{g,O} = \dot{m}_O\left(1 - \frac{D_O^3(t)}{D_{O,i}}\right) \quad [22]$$

where $\dot{m}_F$ and $\dot{m}_O$ designate total mass flux of the injected species. Thus, with t as a parameter Equations [17, 18] and

$$X = \int_0^t U_g dt \quad [23]$$

constitute the parametric relations connecting U_g and T_g with the coordinate X downstream of the injector.

In order to express the salient features of the bipropellant combustion field in simple analytic form, we now assume constant gas properties c_p and R. The coefficients q_F, q_O are then also constant, in view of Equations [19 and 20]. Introducing the terminal values attained upon complete vaporization of the fuel at $t = t_F \geq t_O$

$$U_f = q_F \dot{m}_F - q_O \dot{m}_O \quad [24]$$

$$T_f = \frac{P_g}{R}\left(\frac{q_F \dot{m}_F - q_O \dot{m}_O}{\dot{m}_O + \dot{m}_F}\right) \quad [25]$$

$$X_f = \int_0^{t_F} (q_F \dot{m}_{g,F} - q_O \dot{m}_{g,O}) dt \quad [26]$$

and employing the dimensionless notation

$$M = \dot{m}_O/\dot{m}_F \qquad Q = q_O/q_F$$
$$\eta_F(t) = \dot{m}_{g,F}/\dot{m}_F \qquad \eta_O(t) = \dot{m}_{g,O}/\dot{m}_O \quad [27]$$

we arrive at the parametric relations for assumed constant gas properties

$$\frac{U_g(t)}{U_f} = \frac{\eta_F - QM\eta_O}{1 - QM} \quad [28]$$

$$\frac{T_g(t)}{T_f} = \left(\frac{1+M}{\eta_F + M\eta_O}\right)\left(\frac{\eta_F - QM\eta_O}{1 - QM}\right) \quad [29]$$

$$\frac{X(t)}{X_f} = \frac{\int_0^t (\eta_F - QM\eta_O)\, dt}{\int_0^{t_F} (\eta_F - QM\eta_O)\, dt} \quad [30]$$

For liquid oxygen/hydrocarbon systems, the overall mixture ratio M ranges from 2 to 3, whereas the enthalpy correction ratio Q is of the order of 10^{-2}, tending to make $QM\eta_O \ll \eta_F$, even though, due to the greater volatility of oxygen, $\eta_O > \eta_F$ in the early stages of droplet vaporization. With $QM \ll 1$, Equations [28–30] indicate that the principal effect of early

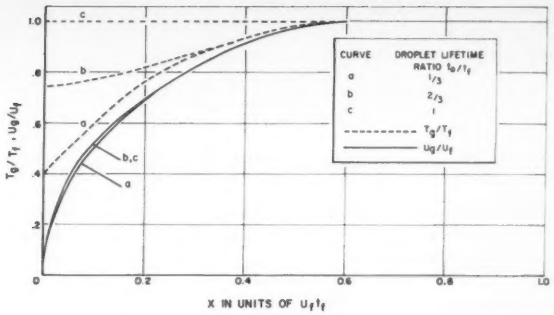

Fig. 5 Influence of relative vaporization rates on temperature and velocity distributions in bipropellant combustion chamber (mixture ratio $M = 2.5$)

vaporization of the oxidant is on the temperature distribution T_g vs. X, whereas U_g vs. X is determined primarily by the fraction of fuel vaporized η_F. It is to be noted that parametric relations of the type Equations [28 and 29] expressing U_g and T_g in terms of the vaporized propellant fractions η_F and η_O may be derived, in general, from aerothermodynamic principles. However, the connection between X and the vaporized fractions can be determined only by taking into account the kinetics of gas generation, i.e., the motion of vaporizing droplets. The assumption of equal droplet and gas velocities (f), whereby η_F and η_O are interrelated by a single parameter t, yields the particularly simple expression for X in Equation [30]. The present treatment can be readily extended to account for the influence of propellant droplet velocity lags under representative frictional entrainment laws.

A graphical illustration of the gas flow conditions described by Equations [28 to 30] is illustrated in Fig. 5 based on the vaporization law

$$D_F^2 = D_{F,i}^2 - K_F t \quad [31]$$

$$D_O^2 = D_{O,i}^2 - K_O t \quad [32]$$

with the assumption that the oxidant droplet lifetime $t_O = D_{O,i}^2/K_O$ is not greater than $t_F = D_{F,i}^2/K_F$. The influence of relative vaporization rates is illustrated for three different values of the droplet lifetime ratio, $t_O/t_F = \frac{1}{3}, \frac{2}{3}$ and 1, at a given overall mixture ratio $M = 2.5$ and $Q = 0.01$.

It is seen from Fig. 5 that the changes in t_O/t_F have a far greater influence on the temperature distribution (dotted curves) than on the velocity development (solid curves) in the combustion chamber. This is readily understood on the following physical grounds. Reduction of the ratio t_O/t_F increases the oxidant-to-fuel vaporization rates, and, since the heat release depends primarily on the vaporized fuel, less heat will be released per unit mass of the vaporized mixture. The consequent reduction of temperature at constant chamber pressure results in increased gas density. Thus, the greater mass flux due to increased oxidant vaporization with lower temperature and greater density in the chamber can be accommodated without large changes in the gas velocity.

It is to be noted that the monotonic increase of T_g vs. X shown in Fig. 5 is predicated on the assumption that, in the oxidant-rich gas stream considered here, $t_F > t_O$. If $t_F < t_O$, a temperature peak in excess of T_f (see Eq. [25]) is attained at the end of fuel vaporization. More generally, it is readily seen from Equation [29] that temperature maxima and minima along the vaporization rate limited bipropellant combustion chamber can occur if

$$\frac{dT_g}{dt} = 0 = \eta_O \frac{d\eta_F}{dt} - \eta_F \frac{d\eta_O}{dt} \quad [33]$$

Finally, we note that at injector, $X = 0$, $\eta_F \to 0$, $\eta_O \to 0$, the temperature ratio in Equation [29] is calculated by a limiting process: $t \to 0$, $\eta_O/\eta_F \to t_F/t_O$, which yields

$$\frac{T_g(0)}{T_f} = \left(\frac{1+M}{1+M\,t_F/t_O}\right)\left(\frac{1-QM\,t_F/t_O}{1-QM}\right) \qquad [34]$$

The Influence of Droplet Size Distributions

If the number of droplets injected per unit area per unit time N contains a spectrum of initial droplet sizes specified by the distribution function $n(D_i)$, we have

$$dN = n(D_i)\,dD_i \qquad [35]$$

as the component of the spectrum in the size range from D_i to $D_i + dD_i$. Let the time history of droplets in this size range be designated by $D(i, t)$ with lifetime $t_{f,i}$ determined from $D(i, t_{f,i}) = 0$. Let, further, the identity of droplets be fixed upon injection in the flux component dN defined by Equation [35]. As the droplets in this group move along the chamber with the velocity of the product gases, the droplet flux remains constant at the value dN, while the associated elementary liquid mass flux is

$$d\dot{m}_l = (\pi/6)D^3(i, t)\rho_l\,dN \qquad [36]$$

Hence, for the model under consideration with total mass flux

$$\dot{m} = \frac{\pi}{6}\rho_l \int_{D_i=0}^{D_i=D_m} D_i^3\,n(D_i)\,dD_i \qquad [37]$$

the liquid mass flux surviving up to a time t after injection is given by

$$\frac{\dot{m}_l(t)}{\dot{m}} = \frac{\displaystyle\int_{D(i,\,t)=0}^{D_m} D^3(i, t)\,n(D_i)dD_i}{\displaystyle\int_0^{D_m} D_i^3\,n(D_i)dD_i} \qquad [38]$$

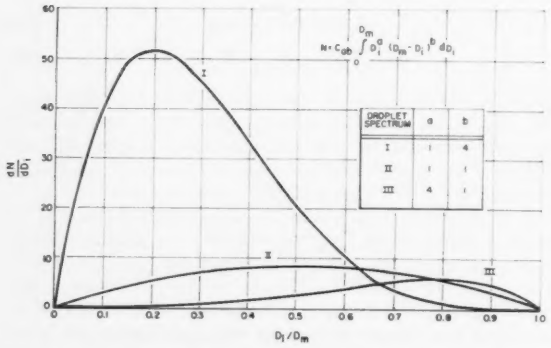

Fig. 6 Comparison of droplet size spectra for constant mass flux $\dot{m}$ and maximum diameter D_m. $[\dot{m}/D_m = (\pi/6)\rho_l D_m^3]$

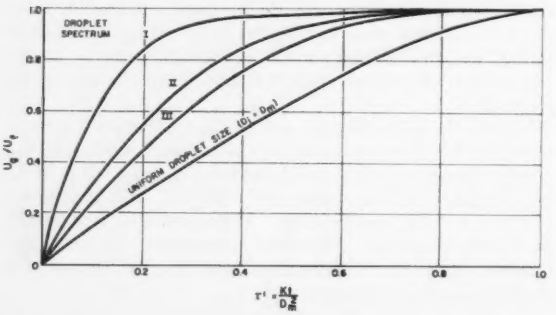

Fig. 7 Velocity vs. time elapsed after injection for various injected droplet spectra with maximum droplet diameter D_m

Table 3 Specification of droplet size distribution functions

Spectrum	a	b	$\frac{\pi}{6}\frac{\rho_l}{\dot{m}} C_{ab} D_m^{a+b+4}$
I	1	4	630
II	1	1	30
III	4	1	72

where D_m is the maximum diameter in the injected spectrum. In exhibiting the role of droplet size distribution, the surviving liquid fraction $\dot{m}_l/\dot{m}$ in Equation [38] replaces the fraction $D^3(t)/D_i^3$ appearing in the previously derived expressions for uniform injected droplet size (Eqs. [6, 8, 21, 22]).

The droplet size distribution produced by the atomization process is generally described by empirically determined distribution functions sufficient to specify such basic features of the spray as mean droplet size, skewness and dispersion about the mean. In the illustrative calculations below we shall employ for each propellant species a polynomial representation of the injected distribution function in the form

$$n(D_i) = C_{ab} D_i^a (D_m - D_i)^b \qquad [39]$$

where a, b are integers, and C_{ab} is a constant related to the injected mass flux of the species by

$$\dot{m} = \frac{\pi}{6}\rho_l C_{ab} \int_0^{D_m} D_i^{a+3}\,(D_m - D_i)^b dD_i \qquad [40]$$

Equation [40] is adequate for approximate representation of some actual distribution functions, such as, for example, the Nukiyama-Tanasawa equation ((1), pp. 4 to 53). Moreover, it is of great convenience in treating a broad class of possible distribution functions without entailing undue mathematical complexities.

The influence of the injected droplet spectrum is illustrated for three distribution functions (Spectra I, II and III in Table 3) having peak droplet populations respectively at $\frac{1}{5}$, $\frac{1}{2}$ and $\frac{4}{5}$ of a reference maximum diameter D_m. Graphical comparison of these spectra referred to fixed values of $\dot{m}$ and D_m is shown in Fig. 6.

Monopropellants

Applying the distribution functions to a monopropellant obeying the vaporization law (Eq. [1])

$$D^2(i, t) = D_i^2 - Kt \qquad [41]$$

we obtain from Equation [38]

$$\frac{\dot{m}_l(\tau')}{\dot{m}} = \frac{\displaystyle\int_{\xi=\sqrt{\tau'}}^1 (\xi^2 - \tau')^{3/2}\xi^a(1-\xi)^b d\xi}{\displaystyle\int_0^1 \xi^{a+3}(1-\xi)^b\,d\xi} \qquad [42]$$

where

$$\tau' = Kt/D_m^2$$
$$\xi = D_i/D_m$$

The integrals required here are readily evaluated from standard formulas (13) for

$$\int (\xi^2 - \tau')^{3/2}\,\xi^p d\xi$$

where p is an integer. The results showing nondimensional gas velocity vs. τ'

$$\frac{u_g(\tau')}{u_f} = \frac{\dot{m}_g(\tau')}{\dot{m}} = 1 - \frac{\dot{m}_l(\tau')}{\dot{m}} \qquad [43]$$

are given in Fig. 7. A second integration with respect to

time indicated in Equation [5] leads to

$$\frac{x}{x_f} = \frac{\int_0^{\tau'} u_g \, d\tau'}{\int_0^1 u_g \, d\tau'} \qquad [44]$$

in which the required integrals are also readily evaluated by standard methods.

Based on Equations [43 and 44] with τ' as a parameter, the calculated results for the velocity dependence in a monpropellant combustion chamber are shown in Fig. 8. This figure, in effect, represents the efficiency vs. length for the combustor model considered here. In the high efficiency regime, $u_g/u_f \sim 0.9$ significant reductions in length are indicated by improvement of atomization. However, since complete combustion depends on vaporization of the largest injected droplet (D_m is the same for the distributions considered here), failure to reduce the maximum droplet size under enhanced atomization results in increasing the combustion length required for 100 per cent efficiency.

Bipropellants

In the bipropellant combustion field given by Equations [28 to 30], the role of the injected droplet size spectra is implicit in the vaporized fractions η_F and η_O defined by Equation [27]. The latter quantities can be alternatively defined in terms of the surviving liquid fractions

$$\eta = 1 - (\dot{m}_l/\dot{m}) \qquad [45]$$

and, hence, can be calculated by application of Equation [38] to each species. Insertion of the results for η_F and η_O based on Equations [38 and 45] into Equations [28 to 30] yields the parametric equations connecting U_g, T_g and X corresponding to droplet size distributions $n_F(D_{F,i})$, $n_O(D_{O,i})$ and vaporization laws $D_F(i,t)$, $D_O(i,t)$.

In view of the role of η_F and η_O in the parametric equations, the influence of bipropellant droplet size distributions may be summarized as described below. The conclusions in the next paragraph refer to the assumed oxidant-rich conditions in the derivation of the prototype solutions in Equations [28 to 30].[4]

Since for typical bipropellant combinations $Q \ll 1, MQ \ll 1$, the effect of the droplet spectrum on U_g/U_f vs. X/X_f appears primarily through the modified η_F. However, the modified η_O has a strong influence on the T_g/T_f vs. X/X_f distribution.

The terminal values U_f and T_f are determined independently of vaporization by given propellant injection rates, heat released per unit mass of the overall mixture, and the pressure level in the combustion chamber. The combustion length X_f depends primarily on η_F, i.e., on the vaporization rates and droplet size spectrum of the fuel. Graphical illustrations of these results are shown in Fig. 9 for oxidant and fuel droplet spectra corresponding to the droplet spectra I and III, in Table 3, with assumed lifetime ratio $t_O/t_F = \frac{1}{2}$ and mixture ratio $M = 2.5$.

Flameholding Stability

The previously derived results were obtained on the assumption that vaporization is followed by prompt local mixing and chemical reaction. The latter can occur only if the locally vaporized propellants mixture ratio is within sufficiently close limits about the stoichiometric ratio and the local temperature is sufficiently high, dependent on the propellant combination. For oxygen-inert-hydrocarbon systems in particular, fundamental experiments indicate that flame propagation can be achieved only if the resultant flame

[4] Analogous results are readily obtained within the scope of the present analysis if the local vaporization rates provide excess fuel everywhere, or if transitions occur from oxidizer-rich to fuel-rich vaporization rates along the combustion chamber.

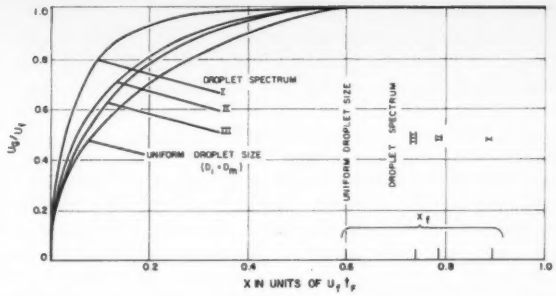

Fig. 8 Velocity vs. coordinate in chamber for various injected droplet spectra with maximum droplet diameter D_m

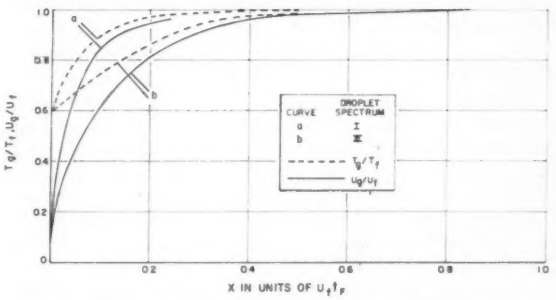

Fig. 9 Influence of injected droplet size spectrum on temperature and velocity distributions in bipropellant combustion chamber (lifetime ratio $t_O/t_F = \frac{1}{2}$; mixture ratio $M = 2.5$)

temperature is above ~1200 K (14). If we introduce such a minimum temperature as a threshold temperature at which reaction is achieved in the bipropellant combustion chamber, we arrive at a stability condition necessary for continuous ignition of the propellants (i.e., flameholding) in the low velocity region near the injector face

$$T(0) \geq T_{\min} \qquad [46]$$

In view of Equation [29] the flameholding stability condition can be expressed as

$$T_f \lim_{t \to 0} \frac{(1+M)}{(\eta_F + M\eta_O)} \frac{(\eta_F - QM\eta_O)}{(1-QM)} \geq T_{\min} \qquad [47]$$

where the T_f is the terminal temperature, dependent on the overall mixture ratio $M = \dot{m}_O/\dot{m}_F$. For the particular case of uniform oxidant and fuel droplet size with lifetimes t_O and t_F, the stability condition yields

$$T_f \frac{(1+M)}{(1+Mt_F/t_O)} \frac{(1-QMt_F/t_O)}{(1-QM)} \geq T_{\min} \qquad [48]$$

In application to oxygen/hydrocarbon systems with assumed $T_{\min} = 1200$ K and typical data $M \sim 2.5$, $T_f \sim 3500$ K, Equation [48] implies that the stability limit is reached if $t_F/t_O \sim 3$.

Discussion

The idealized conditions of the vaporization rate controlled combustor model are approached when mixing and chemical time lags, present in actual combustion chambers, are at a minimum. The limitations and possible scope of application of the theoretical results are briefly discussed on the basis of relevant experimental data.

Monopropellants

By injection of fuel and oxidant in chemically homogeneous or physically premixed liquid jets, as in the case of monopropellants, the mixing lags are minimized; high flame temperature (~3000 K) and associated reduction of chemical lags are additional prerequisites for the emergence of vaporization as a rate controlling step. A survey of available monopropellant combustion data (15) reveals that the latter prerequisites are not satisfied, inasmuch as currently familiar low performance monopropellants generally undergo slow gas phase chemical reactions. It would be interesting to ascertain the applicability of the vaporization model to recently developed high performance monopropellants (16). In particular, the vaporization model implies that the product gas in monopropellant combustion is at a constant temperature (flame temperature); this result could be most simply ascertained by noting to what extent the exhaust gas temperature is independent of combustion efficiency determined under experimental conditions.

Bipropellants

In regard to bipropellant combustion, if vaporization rate is the slow step in the combustion process, unreacted gaseous propellants of both species cannot coexist in the product gas flow. However, the latter may be diluted by the presence of an excess, unreacted gas phase propellant. As the results summarized in Equations [28 to 30] and illustrated in Figs. 5, 8 and 9 indicate, the velocity or efficiency distribution is primarily determined by the droplet spectrum and vaporization rate of the slowly vaporizing species. The principal effect of varying the droplet size spectrum of the more rapidly vaporizing species appears in the temperature distribution which, in general, is depressed by the presence of excess unreacted propellant gas.

In Priem's (2,3) combustion model it had been assumed that hydrocarbon vaporization is rate controlling while the product gas remains constant at the flame temperature T_g. Although the gas temperature variations influence the vaporization rates to some extent, in view of the results summarized in the preceding paragraph, Priem's assumptions appear satisfactory for the calculation of gas velocity or combustion efficiency vs. combustor length.

Experimental data on temperature and chemical distributions have been obtained by sampling of the gas flow with pneumatic probes in liquid oxygen-ammonia (4) and nitric acid-hydrocarbon (5) combustion chambers. The investigations reported were done under comparable pressure (P_g ~300 psia) and thrust (ca 1000 lb) conditions with a variety of hydraulic injection patterns. Evidence of mixing delay is shown in both investigations. The temperatures reported appear to be generally well above the ignition temperature and increase progressively in the axial direction from the injector toward the exhaust nozzle, but radial variations are observed associated with the hydraulic injection patterns. In the oxygen-ammonia combustion investigated by Baker (4), coexistence of unreacted fuel and oxidizer did not occur except in some low temperature gas pockets associated with poor mixing. On the other hand, the nitric acid-hydrocarbon combustion data obtained by Trent (5) shows the existence of nonequilibrium concentrations of nitric oxide at high temperatures, suggesting, as a rate controlling step, the chemical process whereby the intermediate nitric oxide is converted to product gases. Similar investigations of oxygen-hydrocarbon combustion might be expected to reveal the role of carbon monoxide conversion as a rate controlling step under sufficiently rapid mixing conditions.

From the preceding considerations it is concluded that a fundamentally adequate account of rocket combustion phenomena cannot be based solely on the vaporization rate controlled model. However, the latter model provides a rational approach to the determination of technically useful correlations between rocket combustion and vaporization data, particularly in high performance combustors. High performance, characterized by high volumetric reaction rates in the combustion chamber, is achieved in practice with highly reactive chemical propellants under adequately rapid mixing conditions favoring the emergence of vaporization as a rate controlling process.

Appendix

The influence of variable gas properties is treated by considering the presence of product gases and excess gas (oxidant in the example treated) with molecular weight $\mathfrak{M}_{pr}$ and $\mathfrak{M}_O$, respectively. With reaction rate occurring at assumed constant stoichiometric ratio M_{st}, the species referred to have the flow rates

$$\dot{m}_{pr} = \dot{m}_{g,\,F}(1 + M_{st}) \qquad [A\text{-}1]$$

$$\dot{m}'_{g,\,O} = \dot{m}_{g,\,O} - \dot{m}_{g,\,F}M_{st} \qquad [A\text{-}2]$$

Expressing the additivity laws for c_p and R in terms of species flow rates (to which the densities are proportional by virtue of the common transport velocity U_g), we have

$$\dot{m}_g c_p = \frac{C_{p,\,O}}{\mathfrak{M}_O}\dot{m}'_{g,O} + \frac{C_{p,\,pr}}{\mathfrak{M}_{pr}}\dot{m}_{pr} \qquad [A\text{-}3]$$

$$\dot{m}_g R = R_{\mathfrak{M}}\left(\frac{\dot{m}'_{g,\,O}}{\mathfrak{M}_O} + \frac{\dot{m}_{pr}}{\mathfrak{M}_{pr}}\right) \qquad [A\text{-}4]$$

where

C_p = molal specific heat at constant pressure
$R_{\mathfrak{M}}$ = universal gas constant

Elimination of $\dot{m}_{pr}$ and $\dot{m}'_{g,\,O}$ from Equations [A-3 and A-4] by substitution from Equations [A-1 and A-2] yields the expressions for c_p and R in terms of the auxiliary variables $\dot{m}_{g,\,F}$ $\dot{m}_{g,\,O}$, and hence in terms of the time parameter t implicit in $\dot{m}_{g,\,F}$, $\dot{m}_{g,\,O}$ (see Eqs. [21 and 22]). In this manner, variable gas properties c_p and R can be treated within the system of parametric Equations [17, 18 and 23] which connect U_g and T_g with the coordinate X.

In particular, we note that the preceding modifications lead to a simple expression for the enthalpy ratio (see Eq. [29])

$$\frac{c_p(T_v)T_v}{c_p(T_f)T_f} = \left(\frac{1+M}{\eta_F + M\eta_O}\right)\left(\frac{\eta_F - QM\eta_O}{1 - Q_f M}\right) \qquad [A\text{-}5]$$

from which the temperature T_g may be evaluated by suitable iterative procedures if temperature dependence of the molal specific heats $C_p(T_g)$ is taken into account in the calculation of $C_p(T_g)$. Application of Equation [A-5] to the flameholding stability limit considered in the example shows that, because of lowered gas specific heats at $T_{\min}$ = 1200 C, the stability limit is reached if the fuel-to-oxidant lifetime ratio is increased to $t_F/t_O \sim 3.5$.

Nomenclature

a, b	=	exponents in polynomial representation of dimensionless droplet size distribution,
c_p	=	gas specific heat at constant pressure, cal/gm K
$\dot{m}$	=	injected propellant mass flux, gm/cm² sec
$\dot{m}_g$	=	gas phase mass flux, gm/cm² sec
$\dot{m}$	=	liquid phase mass flux, gm/cm² sec
$\dot{m}_F$	=	total fuel mass flux, gm/cm² sec
$\dot{m}_O$	=	total oxidant mass flux, gm/cm² sec
n	=	droplet size distribution function, no./cm³ sec
q	=	velocity coefficient, cm³/gm
t	=	time elapsed after injection (droplet age), sec
t_f	=	droplet lifetime, sec
t_F	=	maximum fuel droplet lifetime, sec
t_O	=	maximum oxidant droplet lifetime, sec
u_f	=	terminal gas velocity (monopropellant), cm/sec

u_g = velocity in chamber (monopropellant), cm/sec
x = coordinate in chamber (monopropellant), cm
x_f = combustion length (monopropellant), cm
C_{ab} = rate constant in polynomial representation of injected droplet size distribution, no./sec $cm^{(a+b+3)}$
C_p = molal specific heat at constant pressure, cal/mole K
D = instantaneous droplet diameter, cm
D_i = injected droplet diameter, cm
D_m = maximum injected droplet diameter, cm
$H_{F,B}$ = heat value of fuel referred to standard temperature T_B, cal/gm
ΔH_F, ΔH_O = enthalpy corrections for fuel and oxidant, cal/gm
K = vaporization rate constant, cm^2/sec
L^* = characteristic combustor length, cm
M = $\dot{m}_O/\dot{m}_F$ = overall mixture ratio, dimensionless
$\mathfrak{M}$ = molecular weight, gm/mole
N = injected droplet flux, no./cm^2 sec
P_g = combustion chamber pressure, gm/cm^2
Q = q_O/q_F = ratio of velocity coefficients, dimensionless
T_f = temperature at the end of combustion zone, K
T_g = local gas temperature, K
U_f = terminal velocity (bipropellant), cm/sec
U_g = velocity in chamber (bipropellant), cm/sec
X = coordinate in chamber (bipropellant), cm
X_f = combustion length (bipropellant), cm
η = $\dot{m}_g/\dot{m}$ = vaporized fraction of propellant species, dimensionless
ξ = D_i/D_m = nondimensional initial droplet diameter, dimensionless
ρ_g = gas density, gm/cm^3
ρ_l = liquid density, gm/cm^3
τ = Kt/D_i^2 nondimensional time (uniform initial droplet size), dimensionless
τ' = Kt/D_m^2 nondimensional time (initial droplet spectrum with maximum diameter D_m), dimensionless

Subscripts

f = final, completely vaporized
g = gas
pr = product gas
B = refers to standard conditions
F = fuel
O = oxidant

References

1 Battelle Memorial Institute Personnel, "Injection and Combustion of Liquid Fuels," WADC TR 56-344, 1957.

2 Priem, R. J., "Propellant Vaporization as a Criterion for Rocket-Engine Design; Calculations of Chamber Length to Vaporize a Single n-Heptane Drop," NACA TN 3985, 1957.

3 Priem, R. J., "Propellant Vaporization as a Criterion for Rocket Engine Design; Calculations Using Various Log-Probability Distributions of Heptane Drops," NACA TN 4098, 1957.

4 Baker, D. I., "Mixture Ratio and Temperature Surveys of Ammonia-Oxygen Rocket Motor Combustion Chambers," JET PROPULSION, vol. 25, 1955, p. 217.

5 Trent, C. H., "Investigation of Combustion in Rocket Thrust Chambers," *Ind. Engng. Chem.*, vol. 48, 1956, p. 721.

6 Bolt, J. A. and Saad, M. A., "Combustion Rates of Freely Falling Fuel Droplets in a Hot Atmosphere," in "Sixth Symposium on Combustion," Reinhold, 1957, p. 717; *see also* Kumagai, S. and Isoda, H., "Combustion of Fuel Droplets in a Falling Chamber," in "Sixth Symposium on Combustion," Reinhold, 1957, p. 726.

7 Penner, S. S. "On Maximum Evaporation Rates of Liquid Droplets in Rocket Motors," JOURNAL OF THE AMERICAN ROCKET SOCIETY, vol. 23, 1953, p. 85.

8 Besserer, C. W., "Missile Engineering Handbook," van Nostrand, Princeton, 1958.

9 Spalding, D. B., "Some Fundamentals of Combustion," Academic Press, New York, 1955.

10 Goldsmith, M., "Experiments on the Burning of Single Drops of Fuel," JET PROPULSION, vol. 26, 1956, p. 172.

11 Hall, A. R. and Diederichsen, J., "An Experimental Study of the Burning of Single Drops of Fuel in Air Pressures up to Twenty Atmospheres," in "Fourth Symposium on Combustion," Williams and Wilkins, Baltimore, 1953, p. 837.

12 Berman, K. and Logan, S. E., "Combustion Studies with a Rocket Motor Having a Full-Length Observation Window," JOURNAL OF THE AMERICAN ROCKET SOCIETY, vol. 22, 1952, p. 78.

13 Dwight, H. B., "Tables of Integrals and Other Mathematical Data," Macmillan Co., Inc., 1951.

14 Egerton, A. C., "Limits of Inflammability," in "Fourth Symposium on Combustion," Williams and Wilkins, Baltimore, 1953, p. 4.

15 Altman, D. and Penner, S. S., "Combustion Processes," Vol. 2, in "High Speed Aerodynamics and Jet Propulsion," Princeton University Press, 1956, p. 489.

16 Clark, J. D., "Dark Horse in the Propellant Race," ASTRONAUTICS, vol. 3, no. 9, 1958, p. 34.

Correlation and Prediction of Flame Properties With Special Reference to Liquid Hydrazine

MELVIN GERSTEIN[1]

NASA,
Lewis Flight Propulsion Laboratory
Cleveland, Ohio

A large background of experimental data, analytical studies and correlations exist for hydrocarbon air flames. Much less work has been done with propellants of interest in the rocket field. It is possible, however, that some of the experimental and analytical techniques developed for flames of fuels burning in air will be useful when applied to the fuels and oxidants used in rockets. This paper presents a summary of some of the predictions and correlations which have been reported. A brief discussion of the application of some of these correlations to the liquid hydrazine decomposition flame is also included. Such a flame, using a propellant with relatively simple flame kinetics and which can support a flame when introduced either as a liquid or a gas, may well serve to bridge the gap between gas phase combustion studies and combustion of condensed phases, such as liquid and solid monopropellants.

Flame Velocity

LAMINAR flame velocities have been calculated for several systems in which the chemical reactions can be represented by relatively simple kinetics. Typical of these are the hydrazine and ozone decomposition flames and the hydrogen-bromine flame. It is particularly fortunate that chemistry has, in this case, favored rocket combustion interests, hydrazine and ozone being of obvious importance, whereas the hydrogen-bromine flame may well be a better introduction to the hydrogen-fluorine flame than to the much more complicated hydrogen-air flame.

The equations used in predicting flame velocity involve straightforward use of the equations of conservation for a chemically reacting system. An example of the results obtained from such calculations is compared with experimental data in Table 1.

Table 1 Flame velocity, cm/sec

System	Calculated	Experimental
H_2-Br_2 (40 per cent Br_2, 60 per cent H_2) (1)	34	20–32
O_3 (25 per cent O_3, 75 per cent O_2 (2)	47	55
N_2H_4 (3)	184	185

Considering the approximations required to obtain solutions and the lack of good high temperature kinetics and gas property data, the agreement is good.

Attempts to calculate the laminar flame velocity of systems having more complicated reactions have not been very successful, although it has been possible to predict changes in flame velocity produced by changes in initial mixture temperature and to some extent fuel-air ratio and pressure.

Quenching Distance

Recently, quenching distances have been calculated for the same flames (Table 1) which have been the subject of flame velocity calculations. Although quenching distances may be of limited interest in most practical combustion systems, it will be shown later that the quenching distance is a relatively easily measured property, which can be used in conjunction with the flame velocity to obtain information related to the chemical reaction rates in flames. A simplified model of flame quenching suggests that the flame is quenched when sufficient energy has been removed, so that the chemical reactions are no longer self-sustaining. The heat loss can be calculated using conventional heat transfer methods, and the rate of chemical reaction can be obtained when the kinetics are known. A further criterion is needed, the quantity of energy which must be abstracted before the flame reactions are no longer self-sustaining. The criterion used in (4)[2] was the temperature of the inflection point in the temperature-distance curve through a plane flame. The results obtained in this way are shown in Table 2.

For the H_2-Br_2 flame, the agreement is excellent, not only for the calculated quenching distance at 1 atm shown in the

Table 2 Quenching distance, cm

System		Calculated	Experimental
H_2-Br_2	(55 per cent H_2, 45 per cent Br_2)	0.66	0.6–0.7
O_3	(25 per cent O_3, 75 per cent O_2)	0.35	0.25
N_2H_4	...	0.05	0.12

Presented at the ARS 13th Annual Meeting, New York, N. Y., Nov. 17–21, 1958.

[1] Assistant Chief, Propulsion Chemistry Division. Member ARS.

[2] Numbers in parentheses indicate References at end of paper.

table, but also the pressure dependence is calculated to be

$$Q.D. \propto P^{-0.88}$$

which can be compared to the experimental value

$$Q.D. \propto P^{-0.86}$$

The agreement for ozone and hydrazine is not as good. The experimental data for ozone are open to some questions, so that the validity of the comparison is not certain. The only experimental quenching distance found for hydrazine involved the limiting tube diameter for flame propagation through a column of liquid hydrazine. The experimental value is 2.4 times the calculated value. The reaction rate used in the calculation involved gaseous hydrazine. If the combined evaporation and reaction required for the liquid column is a slower process, then the deviation is in the proper direction. The liquid hydrazine flame will be discussed in more detail later.

Those who have attempted to calculate quenching distances for flame reactions more complex than those involved in Table 2 have been troubled by the same problem mentioned in connection with the calculation of flame velocity, namely, the lack of suitable knowledge about the chemical kinetics. The use of a simplified model has been reasonably successful in predicting the effects of pressure, temperature and tube geometry on quenching distance. The relationship between reaction order and pressure dependence of quenching distance has been useful in obtaining approximate reaction orders for the overall process occurring in a flame. The failure of these reaction orders to predict the effects of changes in fuel-air ratio (5) indicates that a single overall reaction is not adequate for the description of hydrocarbon-air flame properties.

Relation Between Flame Velocity and Quenching Distance

Dimensionally, flame velocity may be considered proportional to the square root of the ratio of a transport property a and a reaction time τ; the quenching distance may be considered proportional to the square root of the product of a and τ, where τ is related to the reaction rate W and initial fuel concentration A_0 by the relation

$$W = A_0/\tau$$

The ratio of flame velocity U_f to quenching distance D should then be given by

$$\frac{U_f}{D} \propto \frac{1}{\tau} \propto \frac{W}{A_0}$$

and the product $U_f D \propto a$.

Reaction rates calculated from the first expression are found to give reasonable reaction orders and rates comparable with those deduced from other flame properties (6).

It is shown in (7) that the second expression is in reasonable agreement with experiment. Large deviations were found for hydrocarbon-nitric oxide flames and the ethylene oxide decomposition flame. Whether these represent failures of the correlation or experimental errors is not certain.

Liquid Hydrazine Flames

The rate of burning of a liquid column of hydrazine varies directly with pressure and the limiting tube diameter inversely with pressure for sub-atmospheric pressures (8). The ratio U/D thus varies with the pressure squared at low pressures, indicating that a second order reaction is involved. Since the rate of the gas phase decomposition of hydrazine is second order (9), it is suggested that the gas phase reaction rate may be a controlling factor at low pressures, a conclusion drawn in (8) from the burning rate study alone. The inverse pressure dependence of the limiting tube diameter is also consistent with a second order reaction.

Using the relationship between U/D and W developed in (7), and including a factor for the ratio of moles of product to moles of reactant, one can estimate a reaction rate of 0.036 mole/cm³-sec, which is three-fifths of the value necessary to predict the quenching distance in Table 2. Since the quenching distance depends on the square root of the reaction rate, the actual error in predicting quenching distance would be about 30 per cent. Note that while the pressure dependence of both burning rate and limiting tube diameter suggests that the gas phase reaction rate may control, the estimated value of the reaction rate for liquid hydrazine is an order of magnitude slower than that calculated for the gas phase reaction (4). This suggests that an additional process depending only slightly on pressure may be involved.

It has been suggested that the burning of solid propellants is a two-step process (10) involving the gasification of the propellant followed by a gas phase reaction. If the same concept is applied to the liquid hydrazine flame, the additional process required, evaporation of the liquid, is only slightly dependent on pressure (11).

A very simple model produces some interesting results. Consider that the rate of disappearance of the liquid U, which is also the burning rate, is determined by the rate of heat transfer from the gas phase to the liquid surface

$$U = \frac{\lambda}{\rho_0 \Delta H_0} \frac{\Delta T}{\Delta X}$$

where

λ = mean thermal conductivity
ρ_0 = liquid density
ΔH_0 = heat absorbed by the liquid
$\Delta T/\Delta X$ = assumed linear temperature gradient

Since the flame temperature is relatively independent of pressure, the change in gradient required to make U vary linearly with the pressure is that ΔX vary inversely with pressure, where ΔX is now the thickness of the reaction zone. For a second order reaction, the thickness of a gas phase flame does vary approximately as $1/P$ (12), which is then consistent with the low pressure experimental data. At higher pressures (1 to 8 atm) the burning rate of liquid hydrazine varies roughly as $P^{1/2}$, while above 8 atm the burning rate remains constant or may even drop slightly (13). Since the gas phase reaction rate varies as P^2 and the evaporation rate is relatively independent of pressure, it is not unreasonable that at low pressures the rate is controlled by the gas phase reaction and at high pressures by evaporation. In a simple way, one can assume that the flame thickness is made up of two factors, $\Delta X = h_0 + h_1/P$, where h_0 is controlled by heat and mass transfer and is relatively independent of pressure, while h_1 is thickness of the gas phase reaction zone at 1 atm and for a second order reaction varies as $1/P$. The data for the burning rate of liquid hydrazine from (8 and 13) are plotted in Fig. 1. The curve drawn through the data was calculated from the relation

$$U = \frac{0.0017}{h_0 + h_1/P}$$

The values of h_0 and h_1 were obtained empirically from experimental values of U at $\frac{1}{3}$ and at 16 atm. It is seen that the simple model produces a curve of the proper shape.

The addition of small amounts of water should not change the evaporation characteristics of the liquid mixture but should affect the rate of the gas phase reaction. Examination of Table 3 shows that there is no systematic variation of burning rate with water content at high pressure, whereas at 1 atm the burning rate decreases as the water content increases.

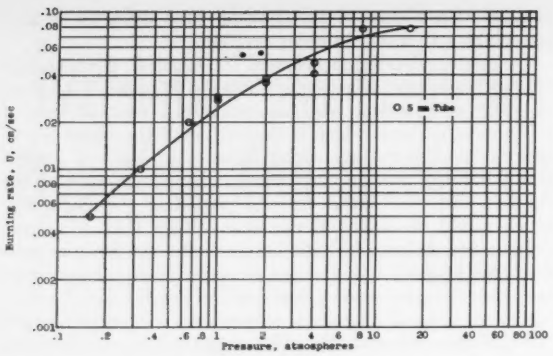

Fig. 1 Variation of the burning rate of liquid hydrazine with pressure for 98.9 per cent N_2H_4. Ordinate—burning rate U, cm/sec. Abscissa—pressure, atm

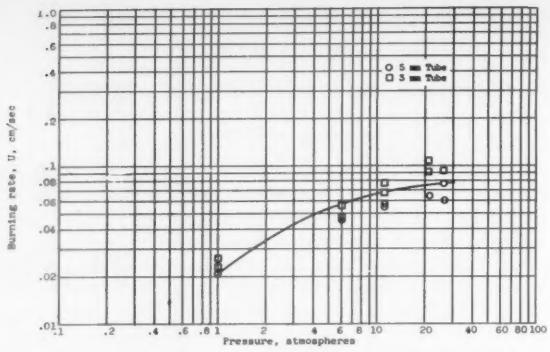

Fig. 2 Variation of the burning rate of liquid hydrazine with pressure for 94 to 95 per cent N_2H_4. Ordinate—burning rate U, cm/sec. Abscissa—pressure, atm

Table 3 Effect of N_2H_4 concentration on burning rate

N_2H_4 concentration	Average burning rate (13) 1 atm	Plateau
98.9	0.028	0.077
97	0.028	0.092
~~94~~–95	0.024	0.098
94.5	0.022	0.069

The calculated curve is compared with the experimental data of (13) in Fig. 2, assuming that h_0 is independent of pressure and obtaining h_1 from the 1-atm burning rate for a 94 to 95 per cent N_2H_4-H_2O mixture.

The agreement is encouraging. Certainly, the model is oversimplified, but it suggests that the liquid hydrazine flame cannot be treated in terms of the gas phase reaction alone or as a simple evaporation problem neglecting chemical reaction rate over a wide pressure range. It also appears that the rate of the gas phase chemical reaction is not a controlling factor at high pressure.

References

1 Von Kármán, T., Penner, S. S. and Millan, G., "The Theory of One Dimensional Laminar Flame Propagation for Hydrogen Bromine Mixtures. Part 1: Dissociation Neglected. Part 2: Dissociation Included," Technical Rep. no. 16 on contract no. DA 04-495-Ord-446, TR 446, California Institute of Technology, Aug. 1956; *see also* Gilbert, M. and Altman, D., "The Chemical Steady State in HBr Flames," in "Sixth Symposium (International) on Combustion," Reinhold Publishing Corp., New York, 1957, pp. 222–236.

2 Hirschfelder, J. O., Curtiss, C. F. and Bird, R. B., "Molecular Theory of Gases and Liquids," John Wiley and Sons, New York, 1954, pp. 756–783.

3 Millan, G. and Sanz, S., "Hydrazine Decomposition Flame," Office of Scientific Research Rep. on contract no. AF61(514)-734C, June 1956.

4 Gerstein, M. and Potter, A. E., Jr., "Considerations Related to the Quenching of Flames with Simple Kinetics," Heat Transfer and Fluid Mechanics Institute Preprint, Berkeley, Calif., June 19–21, 1958, pp. 67–79.

5 Potter, A. E., Jr. and Berlad, A. L., "The Effect of Fuel Type and Pressure on Flame Quenching," in "Sixth Symposium (International) on Combustion," Reinhold Publishing Corp., New York, 1957, pp. 27–36.

6 Gerstein, M., "Review of Some Recent Combustion Experiments," Third AGARD Combustion and Propulsion Panel Colloquium, Palermo, Sicily, March 17–21, 1958.

7 Potter, A. E., Jr. and Berlad, A. L., "A Relation Between Burning Velocity and Quenching Distance," NACA Technical Note 3882, Nov. 1956.

8 Gray, P., Lee, J. C., Leach, H. A. and Taylor, D. C., "The Propagation and Stability of the Decomposition Flame of Hydrazine," in "Sixth Symposium (International) on Combustion," Reinhold Publishing Corp., New York, 1957, pp. 255–263.

9 Spalding, D. B., "Theory of Flame Phenomena with a Chain Reaction," Phil. Trans. of the Royal Society, vol. 249, Series A, no. 957, pp. 1–25.

10 Geckler, R. D., "The Mechanism of Combustion of Solid Propellants," in "Selected Combustion Problems," Butterworths Scientific Publications. London, 1954, pp. 289–339.

11 Spalding, D. B. and Jain, V. K., "Theory of the Burning of Mono-Propellant Droplets," Aeronautical Research Council Rep. 20,176, Imperial College, London, May 19, 1958.

12 Gaydon, A. G. and Wolfhard, H. G., "Flames, Their Structure, Radiation and Temperature," Chapman and Hall Ltd., London, 1953.

13 Adams, G. K. and Stocks, G. W., "The Combustion of Hydrazine," in "Fourth Symposium (International) on Combustion," The Williams & Wilkins Co., Baltimore, 1953, pp. 239–248.

Comparison Between Hot Gas Ignition and Limit Flame Temperatures[1]

M. VANPÉE[2] and
H. G. WOLFHARD[3]

Bureau of Mines,
U.S. Department of the Interior
Pittsburgh, Pa.

Hot gas ignition temperatures of a variety of fuels have been determined and compared with limit flame temperatures of the same fuels. The ignition temperatures were taken under two conditions: A continuous jet of hot nitrogen flowing into a cold fuel-air mixture, and a continuous jet of hot air flowing into cold fuel. Limiting flame temperatures were determined by producing a diffusion flame in an atmosphere of air diluted with nitrogen. The nitrogen concentration required to extinguish the flame was noted and the limiting flame temperature calculated assuming stoichiometric combustion. It was found that, with the exception of a few combustibles, a correlation holds between hot gas ignition temperature and limit flame temperature. The effects of various additives, such as bromine, chlorine and methyl bromide were also studied and corroborated this conclusion.

IN A SYSTEM containing a combustible gas mixture, ignition may occur through contact with hot burned gases. One such condition may occur when a laminar stream of a combustible gas mixture flows adjacent and parallel to a laminar stream of hot burned gases, as treated theoretically by Marble and others (1,2).[4] Experimental ignition data are available for ignition of a virtually quiescent cold mixture by continuous hot inert jets (3). It is the purpose of our research to establish the parameters influencing ignition and thus to evaluate the extent to which present theoretical treatments are justified.

In a previous paper (3) it was found that the ignition temperatures of a variety of fuels (for ignition by hot inert continuous jets) arranged themselves into an order which was very different from that known to exist for spontaneous ignition or spark ignition. However, there was a close relation to hot wire ignition temperatures. Hot gas ignition temperatures are much lower than the adiabatic flame temperatures of stoichiometric mixtures; they are close, however, to flame temperatures for limit mixtures. Thus, there is a possibility that the reactions governing limit flames are the same as those leading to hot gas ignition. If this is true, different fuels should show the same order of temperature in both cases.

A close relation between lean or rich limit flame temperatures and hot gas ignition temperatures was not anticipated, as the fuel-air ratios are very different. A better relation was to be expected for the temperature of stoichiometric mixtures which had been diluted with inert gas until a limit of flame propagation was reached. For convenience, a diffusion flame was adopted for comparison, and its limit temperature by dilution was determined. The influence of characteristic inhibitors on flame propagation or spontaneous ignition was also explored.

Experimental Setup and Procedure

Hot Gas Ignition

The experimental procedure was the same as that described earlier (3). Air or nitrogen was heated in a ceramic furnace; it formed a continuous jet of hot gas flowing into the outer explosive mixture at room temperature. Two new platinum-wound ceramic furnaces which were less subject to cracking and aging (see (3)) were used, and results were more reproducible. Furnace A was 2-ft long and had an inner diameter of 10 mm; furnace B was 1-ft long and 4 mm in inner diameter. The gas flow for furnace A was 100 cc/sec, as this gave the flattest possible temperature distribution of the jet near the furnace exit. Furnace B was used for the work on additives, with gas flows at 35 cc/sec.

As in our previous work, no corrections were made for the emissivity of the platinum-platinum rhodium thermocouple (wire, 0.005-in. diam) owing to the uncertainties of the relevant heat transfer numbers. The temperatures recorded were measured directly above the furnace exit in the center of the jet. The outer chamber containing the room-temperature explosive mixture was about 50-cm long and 9 cm in diameter. A slow flow of mixture (200 cc/sec) purged the vessel sufficiently to prevent dilution. Liquid fuels were introduced by saturating air with the fuel and admitting further air to get the desired concentration.

Limiting Flame Temperatures

Limiting flame temperatures were determined by producing a diffusion flame around a sintered stainless steel hemisphere (4). The fuel entered the flame from within the hemisphere, and air flowed slowly upstream against the hemisphere. This gave rise to a very stable flame. The air was diluted progressively with nitrogen until extinction occurred. This resembled the bursting of a soap bubble, as the flame extinguished first at the stagnation point. The oxygen index of

Received Dec. 11, 1958.
[1] This work was sponsored by Project SQUID which is supported by the office of Naval Research under Contract Nonr 1858 (25) NR-098-038. Reproduction in full or in part is permitted for any use of the United States Government.
[2] Research Scientist, Division of Explosives Technology.
[3] Formerly Research Scientist, Division of Explosives Technology. Present address: Reaction Motors Division, Thiokol Chemical Corp., Denville, N.J.
[4] Numbers in parentheses indicate References at end of paper.

the air at the extinction point was noted (oxygen index = oxygen in air divided by total amount of oxygen and nitrogen), and the limiting flame temperature calculated, assuming stoichiometric combustion. The burner system employed could be used for both gaseous and liquid fuels without modification.

All gases used in this study were taken from cylinders (Matheson Co. cp grade). Benzene, methyl alcohol and ethyl alcohol were also of cp grade. Iron carbonyl and tetraethyl lead were obtained from the Ethyl Corp.

Experimental Results

Ignition Temperatures

Ignition temperatures were measured for the 10-mm jet under two conditions: (a) 100 cc/sec hot air going into pure fuel. This leads to an ignition zone 7 to 10 cm above the furnace exit, and a conventional diffusion flame strikes back and settles on the furnace exit; (b) 100 cc/sec hot nitrogen going into a fuel-air mixture. A luminous column forms in the center of the jet for temperatures below ignition temperatures. The column grows in length and width as the temperature of the jet is increased. At the ignition temperature the column branches out, and a propagating flame moves throughout the explosive mixture. All ignition temperatures refer to the temperature in the center of the jet directly above the furnace exit.

Tables 1 and 2 give the ignition temperatures for cases (a) and (b) together with older values (3) for comparison. The values of Table 2 refer in both cases to the ignition temperatures of the most favorable mixture strength, which is always close to stoichiometric (3). The values with the 10-mm jet are as much as 150 C less than the previous values with smaller jets.

Table 1 Ignition temperatures for hot air jet into fuel, C

Fuel	Jet diam, 10 mm 100 cc/sec air	Jet diam, 4 mm 35 cc/sec air (3)
methane	1040	1190
ethane	840	945
propane	885	1010
n-butane	910	1025
ethylene	765	875
propylene	930	1060
butylene	960	1070
acetylene	655	755
carbon monoxide (cp)	785	not tested
CO (cp+ 5 per cent H_2)	660	not tested
CO (commercial)	not tested	765
hydrogen	640	670

Table 2 Ignition temperatures for a jet of hot nitrogen into fuel-air mixtures, C

Fuel in fuel-air mixture	N_2 jet 10 mm 100 cc/sec	N_2 jet 7 mm 60 cc/sec (3)
methane	1325	$\gg$ 1200
ethane	915	1015
propane	990	1110
n-butane	990	1095
ethylene	900	985
propylene	1060	1150
iso-butylene	1070	1155
CO (cp)	870	not tested
CO (+ 10 per cent H_2)	720	not tested
CO (commercial)	not tested	795
hydrogen	not tested	<755
benzene	1018	not tested
methyl alcohol	946	not tested
ethyl alcohol	964	not tested
diethyl ether	956	not tested

Effect of Additives on Hot Gas Ignition Temperature

The 4-mm-diameter furnace was used in these experiments; the igniting jet was either nitrogen or carbon dioxide of 35 cc/sec total flow.

Ethane-Air Mixtures

Lead tetraethyl and iron carbonyl, when mixed with the outer explosive mixture and with carbon dioxide used as hot igniting jet, had no influence on the hot gas ignition temperature within ±5 C. In the case of iron carbonyl, a bright yellow luminous column formed before ignition, indicating the effective introduction of the additive.

The results for chlorine and methyl bromide are shown in Fig. 1 for a hot nitrogen jet. Chlorine in the outer mixture raises hot gas ignition temperatures only slightly. For comparison, Fig. 1 also shows the influence of chlorine on the ignition temperature when added to the hot jet. It is apparent that this additive is more effective when present in the hot jet where the critical reactions leading to ignition occur. Methyl bromide has a strong inhibiting effect. Two per cent of this compound in the outer mixture raises the ignition temperature by nearly 150 C. Nitric oxide when added to the outer mixture in small concentrations lowers the ignition temperature slightly; in larger concentrations a small inhibiting effect becomes noticeable.

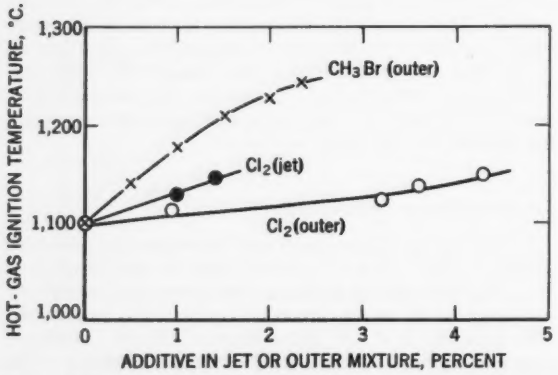

Fig. 1 Influence of additives on ignition temperature of ethane-air mixtures

Carbon Monoxide-Air Mixtures

Both chlorine and methyl bromide had a strong inhibiting effect on the ignition of carbon monoxide-air mixtures. In both cases a concentration of 4 per cent of the additive in the outer mixture raised the ignition temperature by about 400 C.

Limit Flame Temperatures

The limiting oxygen indexes as measured with the hemispher-

Table 3 Limiting oxygen indexes for various fuels

Fuel	Limiting oxygen index, this paper	Limiting oxygen index, from (4)	Limit temperature, C
methane	0.142	0.139	1518
ethane	0.119	0.118	1363
propane	0.129	0.127	1422
n-butane	0.128	...	1434
ethylene	...	0.105	1335
propylene	0.127	...	1489
iso-butylene	0.130	...	1494
CO (+10 per cent H_2)	0.065	...	1041
CO (cp)	...	0.076	1177
hydrogen	0.051	0.054	811
benzene	...	0.133	1540
methyl alcohol	...	0.111	1258
ethyl alcohol	...	0.126	1405
diethyl ether	0.124	...	1386

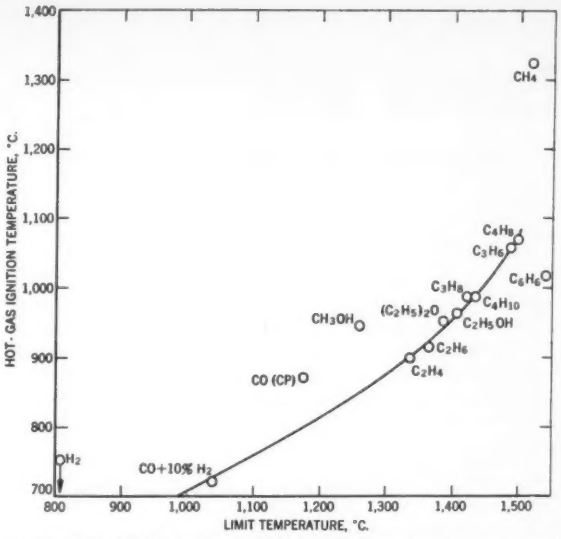

Fig. 2 Correlation between hot gas ignition temperature and limit temperature of flames

ical diffusion flame burner are given in Table 3. This table also contains values for relevant fuels from an earlier publication (4). These values are in close agreement with those of the present investigation. Limit adiabatic flame temperatures are listed in the third column.

Discussion

A comparison between Tables 2 and 3 shows that a relation exists between hot gas ignition temperatures and limit temperatures of stoichiometric flames. In both cases reactions occur under near-stoichiometric conditions in a large dilution with nitrogen. The implication of this relationship is that the same reactions are responsible for both flame propagation under limiting conditions and hot gas ignition under critical conditions. Fig. 2 shows a plot of hot gas ignition temperature against limit flame temperature. Although as a general rule it can be seen that high limit temperature always goes with high ignition temperature, exceptions do exist. Methane clearly has an exceptionally high hot gas ignition temperature. Methyl alcohol and benzene also deviate from the proposed relationship.

Accordingly, the correlation between hot gas ignition and limit temperature of stoichiometric flames must be considered a relatively loose one, and activation energies as calculated from the limit data are not directly applicable to hot gas ignition. Limit temperatures calculated from lean limit data show no improvement when plotted against hot gas ignition temperatures. The correlation is, in fact, much worse.

Although the correlation between ignition temperature and limit temperature is only a loose one, it applies to observations made other than in direct ignition experiments. The influence of additives on ignition temperature can be understood from this correlation. Methyl bromide added to fuel-air mixtures narrows the region of flame propagation and increases the limit temperatures for all fuel-air mixtures (see for example (5)). Even smaller details of flame inhibitions reflect themselves in hot gas ignition. Chlorine is much less effective in inhibiting hydrocarbon flames than methyl bromide (see (6)) and the same tendency can be seen for the ignition temperature in Fig. 1. Carbon monoxide flames, on the other hand are strongly inhibited by chloride (6), and again it was found that both methyl bromide and chlorine increase the ignition temperature of carbon monoxide drastically and by about the same amount. The effects of iron carbonyl and lead tetraethyl on limit temperature are unknown but are presumably negligible, as no influence on burning velocity could be found (7). Similarly, these two compounds have no influence on the hot gas ignition temperature, whereas both compounds are known to influence spontaneous ignition temperatures greatly.

References

1 Marble, F. E. and Adamson, T. C., Jr., "Ignition and Combustion in a Laminar Mixing Zone," in "Selected Combustion Problems I," Butterworths Scientific Publications, London, 1954, p. 111.

2 Cheng, S. I. and Kovitz, A. A., "Ignition in the Laminar Wake of a Flat Plate," in "Sixth Symposium (International) on Combustion," Reinhold Publishing Corp., New York, 1957, p. 418.

3 Wolfhard, H. G., "The Ignition of Combustible Mixtures by Hot Gases," JET PROPULSION, vol. 28, no. 12, Dec. 1958, pp. 798–804; *see also*. Wolfhard, H. G. and Vanpée, M., "The Ignition of Fuel-Air Mixtures by Hot Gases and Its Application to Firedamp Explosions," in "Seventh Symposium (International) on Combustion," in publication.

4 Simmons, R. F. and Wolfhard, H. G., "Some Limiting Oxygen Concentrations for Diffusion Fames in Air Diluted with Nitrogen," *Combustion and Flame*, vol. 1, 1957, p. 155.

5 Simmons, R. F. and Wolfhard, H. G., "The Influence of Methyl Bromide on Flames. Part 1. Pre-Mixed Flames," Trans. Faraday Soc., vol. 51, 1955, p. 1211.

6 Simmons, R. F. and Wolfhard, H. G., "The Structure of Chlorine Flames," JET PROPULSION, vol. 27, 1957, p. 44.

7 Sachsse, H. and Bartholomé, E., "Beiträge zur Frage der Flammengeschwindigkeit," *Z. Elektrochem.*, vol. 53, 1949, p. 183.

Technical Notes

Hypersonic Viscous Shock Layer

SINCLAIRE M. SCALA[1]

General Electric Co., Philadelphia, Pa.

A DECADE ago Tsien (1)[2] (as well as others) and, more recently, Adams and Probstein (2) have attempted to define the different regimes of gaseous interactions during high altitude flight. In this note some results are presented which are pertinent to the flight of hypersonic lifting vehicles composed of axially symmetric and two-dimensional elements; see Fig. 1.

Analysis

It may readily be shown that in the continuum regime the nominal boundary layer thickness at a stagnation point is directly proportional to the square root of the nose radius, i.e.

$$\delta/\sqrt{R_B} = f\,(V_\infty, \text{Alt}, T_w) \qquad [1]$$

while the shock layer thickness or shock detachment distance at a stagnation point is directly proportional to the nose radius, i.e.

$$\delta_s/R_B = f\,(V_\infty, \text{Alt}) \qquad [2]$$

It follows that a suitable parameter useful in defining the flow regime where incipient merging of the shock layer and boundary layer occurs is

$$\delta\sqrt{R_B}/\delta_s = f\,(V_\infty, \text{Alt}, T_w) \qquad [3]$$

Upon restricting the flight Mach number and surface temperature at high altitude to the limits

$$16 \leq M \leq 24$$

$$1000 \leq T_w \leq 3000 \text{ R} \qquad [4]$$

and employing values of the nominal boundary layer thickness at the stagnation point (3,4) based on recent exact numerical solutions of the hypersonic boundary layer equations and the results of Li and Geiger (5) for the shock detachment distance, one obtains the results shown in Fig. 2. That is, for the regime of interest defined by Equation [4], all the data fall on curves, all of which lie within the bands depicted in Fig. 2. It is seen that at a given altitude the value of the merged layer parameter is larger for axially symmetric bodies than for two-dimensional bodies. This follows because, although the boundary layer thickness δ_{2D} is of the order of $\sqrt{2}$ times larger than δ_{3D}, the shock layer thickness δ_{s2D} is considerably larger than δ_{s3D} for a given value of the nose radius, consequently

$$\left(\frac{\delta\sqrt{R_B}}{\delta_s}\right)_{2D} < \left(\frac{\delta\sqrt{R_B}}{\delta_s}\right)_{3D} \qquad [5]$$

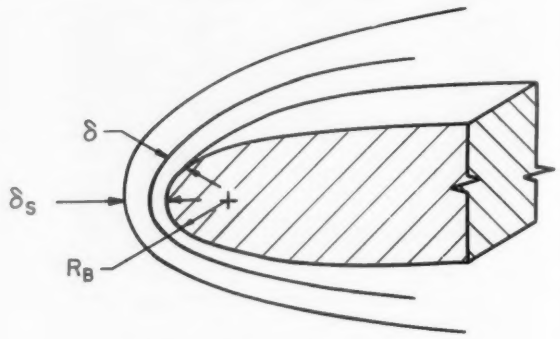

TWO-DIMENSIONAL FLOW

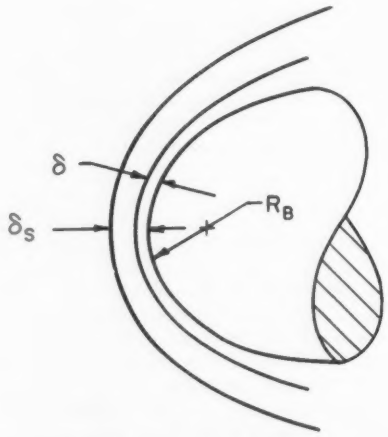

AXIALLY-SYMMETRIC FLOW

Fig. 1 Schematic of merged hypersonic viscous layer for two-dimensional and axially symmetric flow

For convenience, the mean free path λ was calculated upstream of the shock, at the outer edge of the boundary layer, and at the wall. By definition

$$\lambda = \frac{1}{\sqrt{2}\,\pi\, nN\sigma^2} \qquad [6]$$

and hence, if one takes $\sigma = 3.6$Å (constant), then in fps units there follows

$$\lambda = 9.196 \times 10^{-7}\,\frac{T(\text{deg R})}{p(\text{lb/ft}^2)},\ \text{ft} \qquad [7]$$

The initial decrease in the mean free path, as a free stream particle crosses the shock, is due to the shock compression, whereas, in the boundary layer, which is assumed to be at constant pressure, the mean free path drops directly with the temperature (for constant σ). Thus, in Fig. 3 are shown λ_∞,

Received April 20, 1959.

[1] Consulting Research Engineer, High Altitude Gas Dynamics. Member ARS.

[2] Numbers in parentheses indicate References at end of paper.

EDITOR'S NOTE: The Technical Notes and Technical Comments sections of ARS JOURNAL are open to short manuscripts describing new developments or offering comments on papers previously published. Such manuscripts are published without editorial review, usually within two months of the date of receipt. Requirements as to style are the same as for regular contributions (see masthead page).

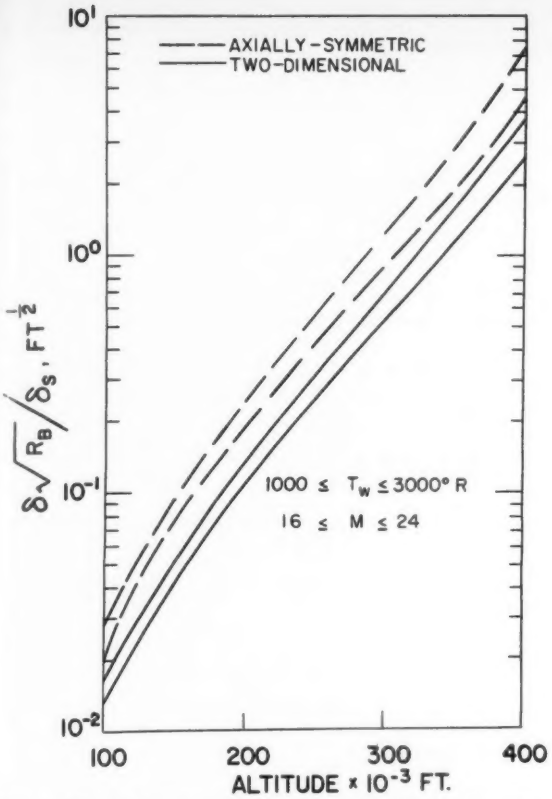

Fig. 2 **Merged layer parameter at the hypersonic stagnation point**

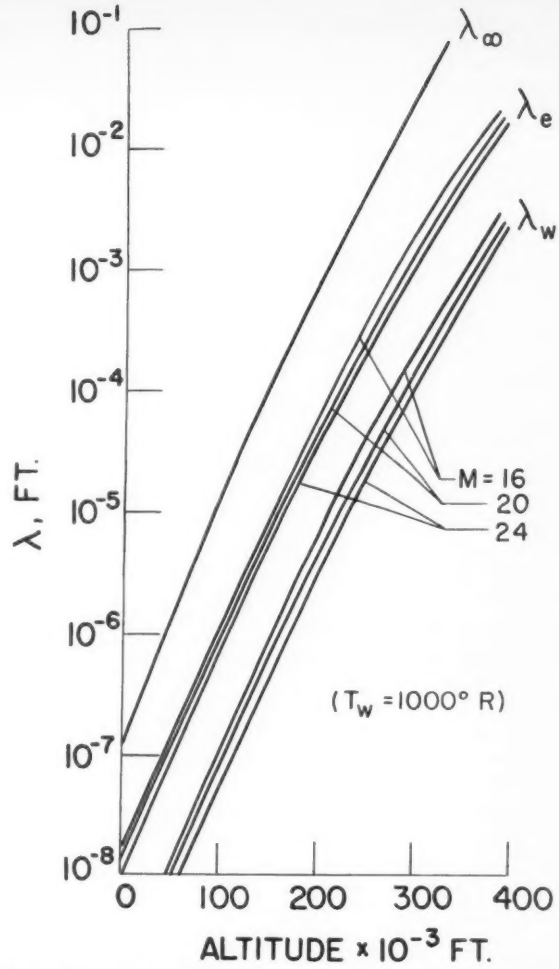

Fig. 3 **Mean free path, upstream, local and at the surface of the body**

λ_e as functions of Mach number, and λ_w as a function of Mach number for a surface temperature $T_w = 1000$ R.

In these calculations, the free stream conditions were based on a model of the Earth's atmosphere proposed by ARDC (6). Normal shock tables were averaged based on work by Logan (7), Feldman (8) and Huber (9).

Discussion

The merged layer parameter shown in Fig. 2 immediately indicates the limits of applicability of the standard aerodynamic technique of separating the flow field into a shock wave, influscid flow and boundary layer flow for the high altitude hypersonic flight regime.

If preferred, one can also combine the data of Figs. 2 and 3 to form a critical Knudsen number. Thus, if one sets the ratio δ/δ_s equal to unity, the data of Fig. 2 may be interpreted as a relationship between $\sqrt{R_B}$ and the altitude at which merging occurs. Then a critical Knudsen number may be defined which is based on the free stream mean free path λ_∞ or on either λ_e or λ_w.

For example, if one selects

$$Kn_\infty = \lambda_\infty / R_B \qquad [8]$$

then the data taken from Figs. 2 and 3 yield the limits

$$6 \times 10^{-2} \leq Kn_{\infty_{2D}} \leq 10^{-1}$$

$$2 \times 10^{-2} \leq Kn_{\infty_{3D}} \leq 3 \times 10^{-2} \qquad [9]$$

Similarly, based on λ_e one obtains

$$2 \times 10^{-3} \leq Kn_{e_{2D}} \leq 5 \times 10^{-3}$$

$$7 \times 10^{-4} \leq Kn_{e_{3D}} \leq 1.7 \times 10^{-3} \qquad [10]$$

Other definitions can also be used, of course.

In general, a small nose radius promotes the formation of a viscous shock layer. However, in view of inequality [5], it is possible for different portions of composite bodies to be operative simultaneously in different flow regimes with catastrophic consequences. Fortunately, the trend indicates that with proper care two-dimensional lifting surfaces can be thinner than the center body and still operate in the same flight regime.

It is understood, of course, that when $\delta/\delta_s = 0(1)$, ordinary continuum concepts must be replaced by a new continuum model, such as perhaps the one recently considered by Probstein and Kemp (10), and independently by Hoshizaki (11).

Acknowledgment

The author would like to acknowledge the assistance of Leon Gilbert and Miss Eileen Foxhill in performing the computations and in preparing the graphs. The analysis is based on work performed under the auspices of the U. S. Air Force, B.M.D. contract no. AF 04(647)-269.

Nomenclature

Alt = altitude
Kn = λ/R_B, Knudsen number, based on nose radius
M = Mach number
n = moles per unit volume

N = Avogadro number
p = pressure
R_B = nose radius of body
T = temperature
V_∞ = flight speed
δ_s = shock layer thickness
δ = boundary layer thickness
σ = collision diameter
λ = mean free path

Subscripts

$2D$ = two-dimensional flow
$3D$ = three-dimensional flow
e = edge of boundary layer
w = wall
∞ = free stream, upstream of shock

References

1 Tsien, H. S., "Superaerodynamics, Mechanics of Rarefied Gases," *J. Aeron. Sci.*, vol. 13, no. 12, Dec. 1946, pp. 653–664.

2 Adams, M. C. and Probstein, R. F., "On the Validity of Continuum Theory for Satellite and Hypersonic Flight Problems at High Altitudes," JET PROPULSION, vol. 28, no. 2, Feb. 1958, pp. 86–89.

3 Scala, S. M. and Baulknight, C., "Transport and Thermodynamic Properties in a Hypersonic Laminar Boundary Layer, Part II Applications," General Electric Co. (MSVD), Aerophysics R.M. no. 24, (R59SD306), Jan. 1959.

4 Scala, S. M. and Ashley, W., to be published.

5 Li, Ting Yi and Geiger, R., "Stagnation Point of a Blunt Body in Hypersonic Flow," *J. Aeron. Sci.*, vol. 24, no. 1, Jan. 1957, pp. 25–32.

6 AFCRC, The ARDC Model Atmosphere, General Electric Co. (MSVD), no. 56SD233, Sept. 1956.

7 Logan, J. G., Jr., "Normal Shock Calculations in Air (Altitudes 10,000 ft. to 240,000 ft.)," Cornell Aeronautical Lab., Jan. 1957.

8 Feldman, S., "Hypersonic Gas Dynamic Charts for Equilibrium Air," Avco Research Laboratory, Jan. 1957.

9 Huber, P. W., "Tables and Graphs of Normal Shock Parameters at Hypersonic Mach Numbers and Selected Altitudes," NACA T.N. no. 4352, Sept. 1958.

10 Probstein, R. F. and Kemp, N. H., "Viscous Aerodynamic Characteristics in Hypersonic Rarefied Gas Flow," IAS 27th Annual Meeting, Rep. no. 56-62, Jan. 1959.

11 Hoshizaki, H., "Shock-Generated Vorticity Effects at Low Reynolds Numbers," Lockheed Missile Systems, Rep. LMSD 48331, Jan. 1959.

3 The time rate and maximum time rate of average heat input per unit area

$$\frac{dH_{av}}{dt} = \frac{1}{2}\frac{C_F' mg}{(L/D)C_D A} V\left(1 - \frac{V^2}{gr_0}\right) \quad [3]$$

$$\left(\frac{dH_{av}}{dt}\right)_{max} = \frac{1}{3\sqrt{3}}\frac{C_F' mg}{(L/D)C_D A}\sqrt{gr_0} \quad [4]$$

$$V_{\left(\frac{dH_{av}}{dt}\right)_{max}} = \sqrt{\frac{gr_0}{3}} \quad [5]$$

4 The time rate and maximum time rate of local stagnation region heat input per unit area

$$\frac{dH_s}{dt} = 6.8 \times 10^{-4}\sqrt{\frac{2mg}{C_D A(L/D)\sigma}}\left(1 - \frac{V^2}{gr_0}\right)^{1/2} V^2 \quad [6]$$

$$\left(\frac{dH_s}{dt}\right)_{max} = \frac{2}{3\sqrt{3}}\, 6.8 \times 10^{-4}\sqrt{\frac{2mg}{C_D A(L/D)\sigma}}\,(gr_0) \quad [7]$$

$$V_{\left(\frac{dH_s}{dt}\right)_{max}} = \sqrt{\frac{2}{3}gr_0} \quad [8]$$

At large angles of inclination, the differential equation of motion is

$$\frac{dV^2}{ds} + \left[\frac{d\theta}{ds} - \frac{\cos\theta}{r}\right]\frac{2}{(L/D)}V^2 + \frac{2g}{(L/D)}\left(\cos\theta - \frac{L}{D}\sin\theta\right) = 0$$

When the angle of inclination is large but constant, closed form approximate solutions may be obtained as follows[3]:

1 Flight range

$$R = \left(\frac{r_0}{2}\right)\left(\frac{L}{D}\right)\ln\left\{\frac{gr_0[1 - (L/D)\tan\theta] - V_e^2}{gr_0[1 - (L/D)\tan\theta] - V_f^2}\right\} \quad [9]$$

2 Total aerodynamic heat input to the vehicle from the beginning to the end of the flight

$$\frac{Q}{(1/2)mV_f^2} = \frac{1}{2}\frac{C_F' S}{C_D A}\left\{\left(\frac{L}{D}\right)\left(\frac{gr_0}{V_f^2}\right)\tan\theta\ln\frac{gr_0[1 - (L/D)\tan\theta] - V_e^2}{gr_0[1 - (L/D)\tan\theta] - V_f^2} - \left(\frac{V_e}{V_f}\right)^2 + 1\right\} \quad [10]$$

3 The time rate and maximum time rate of average heat input per unit area

$$\frac{dH_{av}}{dt} = \frac{1}{2}\frac{C_F' mg\cos\theta}{(L/D)C_D A} V\left(1 - \frac{V^2}{gr_0}\right) \quad [11]$$

for $V_f \geq \sqrt{(1/3)\,gr_0}$[4]

$$\left(\frac{dH_{av}}{dt}\right)_{max} = \frac{1}{3\sqrt{3}}\frac{C_F'\, mg\cos\theta}{(L/D)C_D A}\sqrt{gr_0} \quad [12]$$

$$V_{\left(\frac{dH_{av}}{dt}\right)_{max}} = \sqrt{\frac{1}{3}gr_0} \quad [13]$$

4 The time rate and maximum time rate of local stagna-

Hypervelocity Vehicles at Large Angles of Inclination

W. H. T. LOH[1]

Chance Vought Aircraft, Inc., Dallas, Texas

RESULTS on hypervelocity vehicles, either from boost glide or orbital re-entry, at small angles of inclination and constant lift-drag ratio were obtained recently by Allen and Eggers[2]; they are:

1 Flight range

$$R = \left(\frac{r_0}{2}\right)\left(\frac{L}{D}\right)\ln\left(\frac{gr_0 - V_e^2}{gr_0 - V_f^2}\right) \quad [1]$$

2 Total aerodynamic heat input to the vehicle from the beginning to the end of the flight

$$\frac{Q}{(1/2)mV_f^2} = \frac{1}{2}\frac{C_F' S}{C_D A} \quad [2]$$

Received March 30, 1959.

[1] Staff Engineer to assistant chief engineer, technical.

[2] Eggers, A. J. and Allen, H. J., "A Comparative Analysis of the Performance of Long Range Hypervelocity Vehicles," NACA TN 4046, Oct. 1957.

[3] Other assumptions are the same as those in the Allen-Eggers paper. However, theoretically speaking, constant angle of inclination can only be maintained by continuous programming of lift-drag ratio with velocity according to

$$\left(\frac{L}{D}\right) \cong \left(\frac{2\cot\theta}{\beta r_0}\right)\frac{[1 - (V^2/gr_0)]}{(V^2/gr_0)\ln(V/V_f)^2}$$

But for regions of our interest, it may be treated approximately here as a constant. This is because, numerically, the maximum variation of (L/D) is only about 20 per cent for (V^2/gr_0) from 0.8 to 0.3 at $(V_f^2/gr_0) = 0.9$; and it reduces to about 15 per cent for (V^2/gr_0) from 0.6 to 0.2 at $(V_f^2/gr_0) = 0.7$. Therefore, within the said regions of interest, (L/D) is approximately treated as constant in this derivation. Note also it is a function of θ.

[4] When V_f is smaller than the quantity, the maximum occurs at the start of the unpowered flight.

tion region heat input per unit area

$$\frac{dH_s}{dt} = 6.8 \times 10^{-4} \sqrt{\frac{2mg \cos\theta}{(L/D)AC_D\sigma}} \left(1 - \frac{V^2}{gr_0}\right)^{1/2} V^2 \quad [14]$$

for $V_f \geq \sqrt{(2/3)gr_0}$

$$\left(\frac{dH_s}{dt}\right)_{max} = \frac{2}{3\sqrt{3}} \times 6.8 \times 10^{-4} \sqrt{\frac{2mg \cos\theta}{(L/D)AC_D\sigma}} (gr_0) \quad [15]$$

$$V_{\left(\frac{dH_s}{dt}\right)_{max}} = \sqrt{\frac{2}{3} gr_0} \quad [16]$$

5 Total time of flight

$$t = \frac{1}{2} \frac{L/D}{\cos\theta} \sqrt{\frac{r_0}{g}\left(1 - \frac{L}{D}\tan\theta\right)^{-1}} \ln \left\{ \left[\frac{\sqrt{gr_0\left(1 - \frac{L}{D}\tan\theta\right)} - V_s}{\sqrt{gr_0\left(1 - \frac{L}{D}\tan\theta\right)} - V_f} \right] \left[\frac{\sqrt{gr_0\left(1 - \frac{L}{D}\tan\theta\right)} + V_f}{\sqrt{gr_0\left(1 - \frac{L}{D}\tan\theta\right)} + V_s} \right] \right\} \quad [17]$$

When the angle of inclination is small

$$\cos\theta \cong 1 \qquad \tan\theta \cong 0$$

Equations [9–16] reduce, respectively, to Equations [1–8].

Nomenclature

- A = reference area for lift and drag expressions
- C_D = drag coefficient
- C_F' = equivalent skin friction coefficient = $\frac{1}{S}\int_S C_{Fl} \frac{\rho_l}{\rho} \frac{V_l}{V} dS$
- C_F = skin friction coefficient
- D = drag, lb
- g = acceleration due to force of gravity, fps²
- H = convective heat transferred per unit area
- L = lift, lb
- m = mass of vehicle
- r = distance of glider measured from center of Earth, ft. When altitude of the glider is small in comparison with Earth radius, r may be taken approximately as r_0
- r_0 = radius of Earth, ft
- Q = convective heat transferred
- R = range, ft
- s = distance along flight path, ft
- S = surface area
- t = time, sec
- V = velocity, fps
- ρ = air density
- θ = angle of inclination or angle of flight path to local Earth horizontal, deg
- σ = nose or leading edge radius of body or wing
- β = constant in density-altitude relation: $\rho = \rho_0 e^{-\beta y}$. Here ρ_0 = reference density, and y = altitude

Subscripts

- e = condition at end of unpowered glide
- f = condition at end of powered boost or condition at beginning of unpowered glide
- l = local conditions
- s = stagnation conditions
- av = average values
- max = maximum values

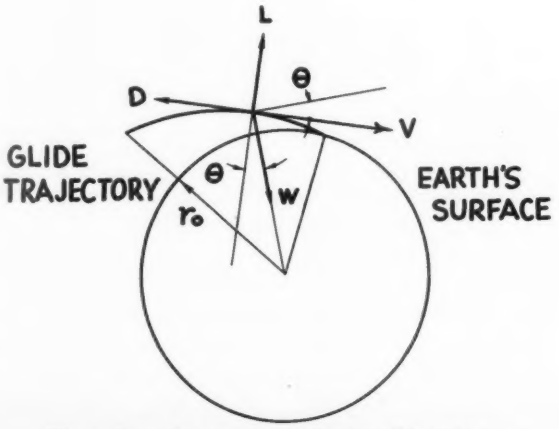

Fig. 1 Large but constant inclination glide trajectory

Stagnation Point Heat Transfer in a Subsonic Jet of Arc-Heated Air[1]

R. R. JOHN[2] and W. L. BADE[3]

Avco Research and Advanced Development Div., Wilmington, Mass.

Heat transfer from a free subsonic jet of arc-heated air to the stagnation region of a plane surface has been determined experimentally. The enthalpy, pressure and velocity gradient of the flow at the edge of the boundary layer were estimated on the basis of mass flow and energy balance measurements. Heat flux values predicted by a correlation formula for stagnation point heat transfer in dissociated air agree approximately with the experimental values.

Description of Experiments

THE RECENT development of arc jet and arc tunnel facilities (1)[4] has provided a means for continuously heating a gas stream to the enthalpy and temperature levels associated with hypersonic flight. The present note reports preliminary measurements of heat transfer from a free subsonic jet of arc-heated dissociated air to the stagnation region of a plane surface.

The arc jet unit used in the experiments is shown schematically in Fig. 1. The gas to be heated is injected tangentially into the chamber. The arc discharge is ignited by exploding a tungsten bridge wire which initially connects the carbon cathode and water-cooled copper anode. The injected gas flows through the region occupied by the arc discharge, momentarily becomes part of the discharge, and then leaves the system through a plenum chamber and a subsonic exit nozzle. The entire arc chamber, including the anode, plenum chamber, exit nozzle and cathode holder, is water-cooled.

For the measurements reported below, the arc jet unit was connected in series with a direct current diesel generator (rated output 1500 amp at 250 v) and a 0.12-ohm ballast re-

Received March 27, 1959.

[1] The work reported here was supported by the U. S. Air Force, Ballistic Missile Division, under Contract no. AF 04(645)-30.

[2] Group Leader, Arc Physics Group. Member ARS.

[3] Senior Scientist, Theoretical Physics Group. Member ARS.

[4] Numbers in parentheses indicate References at end of paper.

sistor. The internal diameter of the exit nozzle was 0.50 in. The jet was exhausted into the open laboratory.

The steady-state heat flux from the plasma jet to the stagnation region of a plane surface was determined using the constant-flow water calorimeter shown schematically in Fig. 2. Measurements were made of the rate of heat transfer through the central circular area, which was aligned coaxially with the arc jet nozzle. The water-cooled annular guard ring surrounding the calorimeter had the dual purpose of preventing heat transfer to the sides of the calorimeter and of establishing an "infinite plate" geometry, for which velocity distribution information was available in the literature. Stagnation region heat transfer from the plasma jet was measured as a function of air mass flow; the results are shown in Fig. 3. It is noted that the observed heat flux is almost independent of air mass flow.

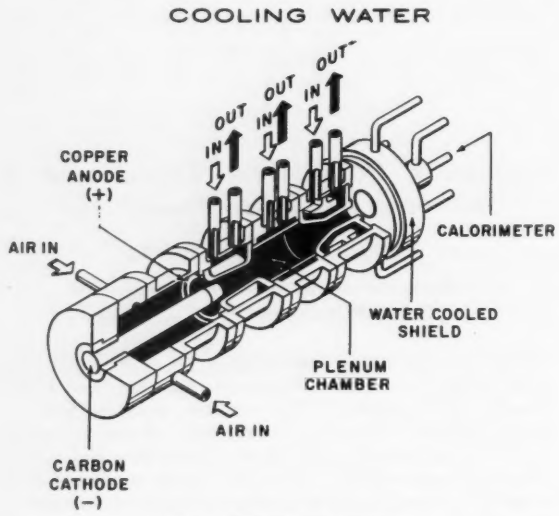

Fig. 1 Electric arc heater

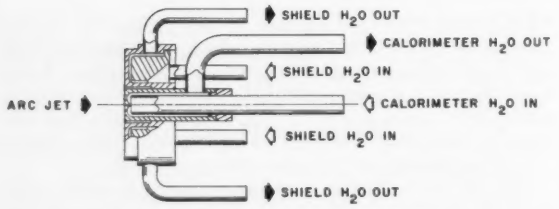

Fig. 2 Constant-flow water calorimeter

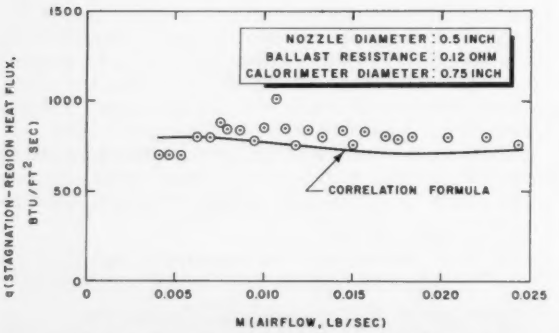

Fig. 3 Stagnation region heat flux vs. air flow

Estimation of Jet Properties

In order to compare these results with existing information about heat transfer in dissociated air, it is necessary to consider the pertinent properties of the plasma jet. These are, as indicated in Equation [4a], the stagnation point velocity gradient and the thermodynamic state of the air at the outer edge of the boundary layer. These quantities were estimated for the plasma jet in the manner described below.

The mean stagnation enthalpy of the air in the jet was calculated from the relation

$$h_s = P_{air}/M = \eta P/M = 0.948 \times 10^{-3}\,\eta VI/M \qquad [1]$$

The power absorbed by the air was estimated from an arc energy balance, in which the power to the arc was determined from measurements of arc voltage and current, and the power loss to the cooling water from the weight flow and temperature rise of the water. The air mass flow was measured using a flowmeter.

The mean velocity of the jet was estimated from the measured air mass flow and the mean stagnation enthalpy, assuming the subsonic exit flow to be quasi one-dimensional and in thermal equilibrium, by simultaneous iterative solution of the equations of continuity and energy

$$M = (\pi/4)\, D^2 \rho_0 U \qquad [2a]$$

$$h_s = h_0 + U^2/2Jg \qquad [2b]$$

and the equation of state (2) for equilibrium dissociated air

$$\rho_0 = f(h_0, p_0) \qquad [2c]$$

The stagnation pressure was estimated from the jet velocity by assuming an isentropic compression (2) of the air flowing from the nozzle exit to the stagnation point. The stagnation pressure and the stagnation enthalpy [1] determine the thermodynamic state of the gas at the edge of the boundary layer.

Finally, on the basis of information available in the literature (3,4) for the incompressible flow of a free jet against a large plane surface, the stagnation point velocity gradient was approximated by the expression

$$\beta \simeq U/D \qquad [3]$$

The variation of estimated jet properties with air mass flow is shown in Table 1.

Table 1 Variation of estimated jet properties with air mass flow

M lb/sec	h_s Btu/lb	p_s atm	β sec^{-1}	T R
0.004	8800	1.02	31,000	11,800
0.008	6500	1.08	49,000	10,800
0.012	5100	1.18	62,000	9800
0.016	4200	1.29	72,000	8600
0.020	3700	1.42	81,000	7700
0.024	3400	1.56	89,000	7400

Comparison With Theory

Fay and Riddell (5) have established from numerical boundary layer solutions that stagnation point heat transfer can be represented by the correlation formula

$$q = 0.763\, N_{Pr}^{-0.6} (\rho\mu)_w^{0.1} (\rho\mu)_s^{0.4} \times [1 + (N_{Le}^{0.52} - 1)(h_D/h_s)]\, \beta^{1/2} (h_s - h_w) \qquad [4a]$$

This formula agrees with heat transfer rates measured in shock tubes (6) if the following nominal transport property values are used

$$N_{Pr} = 0.71 \qquad N_{Le} = 1.4 \qquad [4b]$$

$$\mu = \mu_0 (T/T_0)^{3/2} (T_0 + S)/(T + S) \qquad [4c]$$

where

$\mu_0 = 1.16 \times 10^{-5}$ lb/ft-sec
$T_0 = 492$ R
$S = 204$ R

Equations [4] have been applied to the plasma jet situation, using the estimated jet properties shown in Table 1. The curve of predicted heat flux is shown superimposed on the experimental results in Fig. 3. The correlation formula [4] is in reasonably good agreement with the measured values, and successfully accounts for the empirical observation that heat flux is nearly independent of air flow.

Work is currently under way on the measurement of heat flux at other arc power levels, jet diameters and exit pressures. These results will be published shortly.

Acknowledgment

The authors wish to acknowledge many helpful discussions with Dr. Malin, Dr. Polestra and Dr. Barriault of Avco, RAD. R. N. Schweiger designed the original Avco, RAD electric arc air heater, using a water-cooled copper anode first designed and used by T. Brogan of Avco Research Laboratory.

Nomenclature

D = nozzle diameter, ft
g = gravitational constant, 32.2 ft/sec^2
h = enthalpy, Btu/lb
h_D = dissociation enthalpy per unit mass of air, Btu/lb
I = arc current, amp
J = Joule's constant, 778 ft-lb/Btu
M = air mass flow, lb/sec
N_{Le} = Lewis number for atom-molecule binary diffusion in air
N_{Pr} = Prandtl number for air
p = pressure, lb/ft^2
P = power to arc, Btu/sec
q = stagnation point heat flux, Btu/ft^2 sec
T = absolute temperature, R
U = jet velocity, fps
V = arc voltage, v
β = stagnation point velocity gradient, sec^{-1}
η = arc efficiency = 1 − (power loss to cooling water)÷(power to arc)
μ = viscosity of air, lb/ft-sec
ρ = density of air, lb/ft^3

Subscripts

0 = static conditions at nozzle exit
s = stagnation conditions
w = wall conditions

References

1 Brogan, T., "Electric Arc Gas Heaters for Re-entry Simulation and Space Propulsion," ARS preprint 724-58.
2 Bade, W. L., "Simple Analytical Approximation to the Equation of State of Dissociated Air," ARS JOURNAL, vol. 29, no. 4, 1959, pp. 298–299.
3 Leclerc, A., "Déviation d'un jet liquide par une plaque normale à son axe," *La Houille Blanche*, Nov.-Dec. 1950, p. 816.
4 Sogin, H. H., "Sublimation from Disks to Air Streams Flowing Normal to Their Surfaces," Trans. ASME, vol. 80, 1958, pp. 61–69.
5 Fay, J. A. and Riddell, F. R., "Theory of Stagnation Point Heat Transfer in Dissociated Air," *J. Aeron. Sci.*, vol. 25, 1958, pp. 73–85.
6 Rose, P. H. and Stark, W. I., "Stagnation Point Heat Transfer Measurements in Dissociated Air," *J. Aeron. Sci.*, vol. 25, 1958, pp. 86–97.

Long Period Oscillations During Atmospheric Entry

GEORGE S. CAMPBELL[1]

Hughes Aircraft Co., Culver City, Calif.

An approximate theory is presented for the oscillatory characteristics of the long period motion during atmospheric entry at constant C_L and C_D. Comparison with numerical results for the complete equations of motion indicates that the approximate theory provides an accurate description of the time-varying amplitude decay and frequency during entry.

Received April 7, 1959.

[1] Member of the Technical Staff.

THE PROBLEM of atmospheric entry has been discussed in a number of papers, such as Chapman's recent study of the problem (1).[2] Numerical solutions of the equations of motion have shown that the use of lift during entry may cause a skipping motion. This motion has a long period but is quite different from the classical phugoid motion.

It is the purpose of this note to present simple approximations describing the oscillatory characteristics of the long period motion. The analysis presented is intended to provide an understanding of the oscillatory behavior rather than a detailed computation of the trajectory path. It is hoped that the results obtained will be useful in the design of control systems for re-entry vehicles.

Average Trajectory

Before oscillatory characteristics can be described, it is necessary to have a simple description of the "average" trajectory during descent. Sänger's gliding trajectory appears adequate for this purpose, but for the sake of clarity the derivation is repeated.

The full equations of motion for descent at constant angle of attack are

$$\begin{aligned} m\dot{V} &= -C_D qS + W \sin \gamma \\ -mV\dot{\gamma} - (mV^2/r) \cos \gamma &= C_L qS - W \cos \gamma \end{aligned} \qquad [1]$$

where γ, the flight-path angle, is positive downward and is related to the altitude y

$$\sin \gamma = -\dot{y}/V$$

An exponential density-altitude relation is used (1)

$$\rho = \bar{\rho}_0 e^{-\beta y}$$

and the dynamic pressure is

$$q = \rho V^2/2$$

The basic glide trajectory is calculated by omitting the terms $(mV\dot{\gamma})$ and $(W \sin \gamma)$ from Equations [1] and by assuming small flight-path angles. Under these approximations the above equations are satisfied by

$$V_{avg} = \sqrt{gr} \tanh T \qquad [2]$$

$$\beta y_{avg} = \log (\lambda_0 \sinh^2 T) \qquad [3]$$

$$\frac{\rho_{avg}}{\bar{\rho}_0} = \frac{1}{\lambda_0} \operatorname{csch}^2 T \qquad [4]$$

$$q_{avg} = (W/C_L S) \operatorname{sech}^2 T \qquad [5]$$

in which

$$T = \frac{C_D}{C_L} \sqrt{\frac{g}{r}} (t_c - t)$$

$$\lambda_0 = \frac{C_L S r \bar{\rho}_0}{2m}$$

The constant of integration t_c must be determined so that the proper solution of the singular perturbation problem is chosen. For a trajectory such as that shown in Fig. 1, this parameter was determined by matching Equation [3] with the machine-calculated time for 30 miles altitude.

[2] Numbers in parentheses indicate References at end of paper.

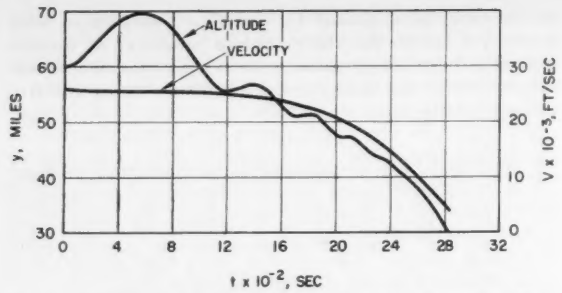

Fig. 1 Altitude and velocity history for entry from 60 miles; $\gamma_0 = 0$; $V_0 = 25753$ fps; $W/S = 18$ lb/ft²; $C_L = 0.54$; $C_D = 0.52$

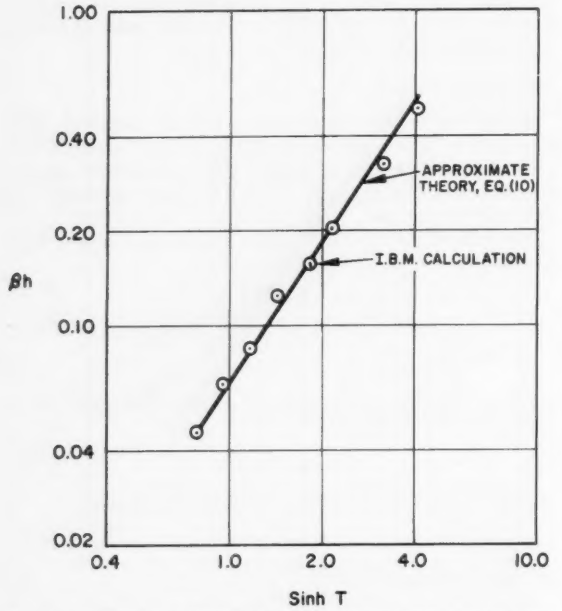

Fig. 2 Amplitude of long period oscillations during entry from 60 miles; $\gamma_0 = 0$; $V_0 = 25753$ fps; $W/S = 18$ lb/ft²; $C_L = 0.54$; $C_D = 0.52$

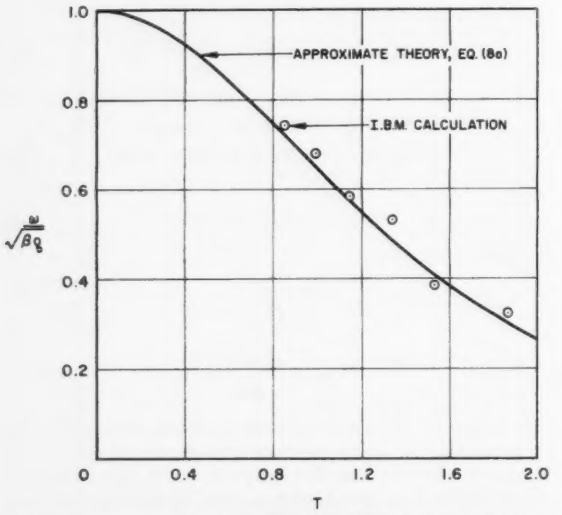

Fig. 3 Frequency of long period oscillations during entry from 60 miles; $\gamma_0 = 0$; $V_0 = 25753$ fps; $W/S = 18$ lb/ft²; $C_L = 0.54$; $C_D = 0.52$

Oscillatory Motion

Superimposed on the average trajectory are altitude and velocity oscillations of the type shown by Chapman and in Fig. 1. In order to describe these oscillations, Equations [1] are linearized about the average trajectory

$$y = y_{avg} + h \qquad h \ll y_{avg}$$

$$V = V_{avg} + w \qquad w \ll V_{avg}$$

When these substitutions are made in Equations [1], the relations for w and h are obtained

$$\frac{\dot{w}}{g} + \left(2\frac{q}{W/C_DS} - \frac{\dot{y}}{V}\right)\frac{w}{V} = -\frac{\dot{h}}{V} + \frac{q}{W/C_DS}\beta h$$

$$\frac{\ddot{h}}{g} - \frac{\dot{V}}{g}\frac{\dot{h}}{V} + \frac{q}{W/C_LS}\beta h = \frac{\dot{y}}{V}\frac{\dot{w}}{g} + \left(2\frac{q}{W/C_LS} + 2\frac{V^2}{gr} - \frac{\dot{V}}{g}\frac{\dot{y}}{V}\right)\frac{w}{V} \qquad [6]$$

The subscript avg has been omitted from q, V and y for purposes of clarity. The exponential term $e^{-\beta h}$ was replaced by $(1 - \beta h)$, so that the analysis, to be strictly valid, only applies when $\beta h \ll 1$.

In computing frequency of the oscillations, only two terms of the lift equation are required

$$\frac{\ddot{h}}{g} + \frac{q}{W/C_LS}\beta h = 0 \qquad [7a]$$

Substitution of average dynamic pressure, Equation [5], gives the equation

$$\frac{d^2h}{dT^2} + (K^2\,\mathrm{sech}^2\,T)\,h = 0 \qquad [7b]$$

in which

$$K = \sqrt{\beta r}\,(C_L/C_D)$$

Since $\sqrt{\beta r} = 30$ for the Earth's atmosphere (1), K is large for (C_L/C_D) of order unity. An approximate solution to Equation [7] may therefore be obtained by the $W\,B\,K$ method (2)

$$\beta h = e^{\pm iK\int \mathrm{sech}T\,dT}$$

The frequency of the altitude oscillations, obtained from $\dot{h}/h$, is

$$\omega = \sqrt{\beta g}\,\mathrm{sech}\,T \qquad [8a]$$

or

$$\omega = \sqrt{\beta g}\sqrt{\frac{q}{W/C_LS}} \qquad [8b]$$

The second relation serves as a basis for simplifying Equations [6], since $\dot{w}/w$ and $\dot{h}/h$ are of order ω. If it is assumed that $q_{avg}/(W/C_DS)$, $V_{avg}/\sqrt{gr}$ and (C_L/C_D) are of order unity, Equations [6] become, for small γ_{avg}

$$\ddot{h} + \frac{C_DS}{m}\frac{q}{V}\dot{h} + \frac{C_LS}{m}q\beta h = 2\left(\frac{C_LS}{m}\frac{q}{V} + \frac{V}{r}\right)w \qquad [9a]$$

$$\dot{w} = \frac{C_DS}{m}q\beta h \qquad [9b]$$

Equation [7a] is substituted into Equation [9b], and the resulting relation is integrated to give

$$w = -(C_D/C_L)h$$

The altitude oscillations are therefore given by

$$\ddot{h} + \left(3\frac{C_DS}{m}\frac{q}{V} + 2\frac{C_D}{C_L}\frac{V}{r}\right)\dot{h} + \frac{C_LS}{m}q\beta h = 0$$

or, after substituting the average trajectory quantities q and V

$$\frac{d^2h}{dT^2} - 2\lambda \frac{dh}{dT} + (K \operatorname{sech} T)^2 h = 0$$

$$\lambda = 3 \operatorname{csch} 2T + \tanh T$$

The damping term may be eliminated by the transformation

$$h = He^{\int \lambda dT}$$

and the resulting equation solved approximately by the $W B K$ method (2) to give

$$\beta h = (\sinh T)^{3/2} e^{\pm iK \int \operatorname{sech} T dT} \qquad [10]$$

Equation [10] is the basic result describing the character of the long period oscillations of a re-entry vehicle. The amplitude envelope depends on density according to

$$\beta h \sim (\bar{\rho}_0/\rho)^{3/4}$$

so that the oscillations die out at the lower altitudes. Frequency of the oscillations is given by Equation [8a].

Numerical Results

In order to check the validity of Equation [10], results from this equation have been compared with numerical solutions of the full equations of motion, Equations [1]. One of the trajectories analyzed is shown in Fig. 1. The average trajectory is described quite accurately by Equations [2 and 3], with $t_c = 2965$ sec.

The amplitude decay and frequency of the altitude oscillations of Fig. 1 are presented in Figs. 2 and 3, respectively. The approximate theory is compared with IBM results, and good agreement is shown. Similar agreement has been obtained for other lift-drag ratios, initial altitudes and flight-path angles. It is noted that the approximate equations, which were derived for small amplitudes ($\beta h \ll 1$), give reasonable results even for relatively large-amplitude oscillations.

References

1 Chapman, D. R., "An Approximate Analytical Method for Studying Entry into Planetary Atmospheres," NACA Technical Note 4276, May 1958.

2 Kamke, E., "Differentialgleichungen Lösungsmethoden und Lösungen," Vol. 1, Chelsea Publishing Co., New York, 1948, p. 138.

Viscous Interaction Experiments at Low Reynolds Numbers[1]

S. A. SCHAAF,[2] F. C. HURLBUT,[3] L. TALBOT[4] and J. AROESTY[5]

University of California, Berkeley, Calif.

THE DISTURBANCE in the surface pressure due to the displacement effect of a laminar boundary layer has been the subject of a considerable number of investigations during the past few years. The reader is referred to Bertram (1),[6] and the literature quoted therein, for a recent summary of these investigations.

The effect is most pronounced, and has been most extensively investigated, for the case of a very sharp, leading edge flat plate at zero angle of attack in supersonic flow. For this case, adiabatic laminar boundary layer theory (2) indicates that the surface pressure p should be roughly proportional to the "hypersonic interaction parameter"

$$\bar{X} = M^3 \sqrt{C/Re_l}$$

where

M = free stream Mach number
Re_l = Reynolds number (based on distance from the leading edge)
C = Chapman-Rubesin constant

According to this result, the pressure becomes infinite as the leading edge is approached. Of course, this is not expected actually to take place, since the boundary layer assumptions are not valid in this region. It is presumed that some appropriate modification in the analysis could be carried out, and that—providing the gas does not slip along the surface—such an analysis would result in a predicted value of the surface pressure at the leading edge of the order of that existing behind a normal shock. If, on the other hand, the gas did slip along the surface, according to the well-known slip velocity boundary condition of kinetic theory, a substantially lower value for the predicted surface pressure would be expected.

The indicated analyses are quite formidable, and neither has yet been successfully carried out. In the present note, data are presented which seem to be more in accordance with the latter expectation, i.e., a surface pressure near the leading edge substantially below that existing behind a normal shock.

The new data are presented in Fig. 1, along with previous data by Bertram (1) and Kendall (3). The new data were obtained in the University of California low density wind tunnel. Two sets of data were obtained. In one of these, the Reynolds number Re_l based on the leading edge thickness of 0.01 in. was in the range $10 < Re_l < 85$; in the second, the leading edge thickness was less than 0.001 in., so that $Re_l < 8$. No effect of leading edge was detectable over these ranges, so that the results were presumably equivalent to the ideal "sharp" leading edge case. The flat plates were at recovery temperature; i.e., the data are for the adiabatic wall case. Two Mach number ranges were used, one at $M \sim 3.7$ to 4.1 and the other at $M \sim 5.5$ to 5.8. The higher of these is quite close to that investigated by Kendall (3), and the agreement between his data and the present experimental results is satisfactory in the region of overlap. The present data depart quite abruptly from the general trend exhibited by both the theoretical analyses and the data of Bertram at slightly higher values of $\bar{X}$. For the $M \sim 3.7$ to 4.1 case, the departure is at about $\bar{X} = 5$. For the $M \sim 5.5$ to 5.8 case, the departure is at about $\bar{X} = 7.5$.

Since the disturbance in the pressure is due to the displace-

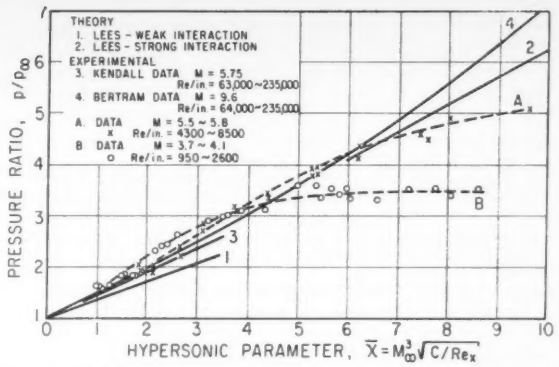

Fig. 1 Induced pressure on flat plate (sharp leading edge)

Received April 22, 1959

[1] This work was supported by the Office of Naval Research, the Air Force Office of Scientific Research and the Bell Aircraft Corp.

[2] Professor, Aeronautical Sciences.
[3] Lecturer, Aeronautical Sciences.
[4] Associate Professor, Aeronautical Sciences.
[5] Graduate Research Engineer, Aeronautical Sciences.
[6] Numbers in parentheses indicate References at end of paper.

ment effect of the boundary layer, it seems reasonable to suppose that any slip flow effect would be associated with the parameter λ_w/δ_*, where λ_w is the mean free path at the wall, and δ_* is the boundary layer displacement thickness. A simple calculation, for air at reasonably high Mach numbers and for the adiabatic boundary layer, leads to the result that $\lambda_w/\delta_* \cong 0.27\bar{X}/M$. Hence both sets of data depart from the no-slip trends for a value of $\lambda_w/\delta_* \cong 0.35$, a not unreasonable value. Conversely, the Bertram data, if this criterion should prove applicable, might be expected to depart for a value of $\bar{X} \cong 12$.

The limiting values of the surface pressure as the leading edge is approached appear to be about 3.5 p_∞ for the case $M \sim 3.7$ to 4.1, and 5.5 p_∞ for the case $M \sim 5.5$ to 5.8. These are substantially below the values of 20 p_∞ and 42 p_∞ at $M = 3.9$ and 5.7, respectively, which would obtain at the stagnation point behind a normal shock. Thus, both the manner in which the data depart from the boundary layer trend and the limiting value approached at the leading edge seem to suggest the existence of slip flow phenomena.

References

1 Bertram, M. J., "Boundary Layer Displacement Effects in Air at Mach Numbers of 6.8 and 9.6," NACA TN-4133, Feb. 1958.

2 Lees, L., "Influence of the Leading Edge Shock Wave on the Laminar Boundary Layer at Hypersonic Speeds," *J. Aeron. Sci.*, vol. 23, no. 6, June 1956, pp. 596–600, 612.

3 Kendall, J. M., Jr., "An Experimental Investigation of Leading Edge Shock Wave-Boundary Layer Interaction at Mach 5.8," *J. Aeron. Sci.*, vol. 24, no. 1, Jan. 1957, pp. 47–50.

Theoretical Study of Recombination Kinetics of Atomic Oxygen[1]

S. T. DEMETRIADES[2] and M. FARBER[3]

Aerojet-General Corp., Azusa, Calif.

Estimates are presented of the rate constants for atomic oxygen recombination due to three-body collisions and other homogeneous and heterogeneous processes.

THIS note presents a summary of a theoretical study (1)[4] of the reaction kinetics of atomic oxygen. Estimates are presented of the mechanism and magnitude of the recombination rates for atomic oxygen in the homogeneous phase as well as of the recombination rates in a heterogeneous system (i.e., on a catalytic wall). A rate constant for the oxygen recombination mechanism $O + O + M \rightarrow O_2 + M$ of the order of 10^{14} to 10^{16} cc^2/mole^2-sec, depending on the temperature, has been derived theoretically. These estimates are based on the results of collision rate theory, absolute reaction rate theory and the interpretation of experimental data available in the literature on other three-body recombination reactions and surface recombination reactions. On the basis of these estimates, Demetriades (2) has made a theoretical study of an upper atmosphere atomic oxygen powerplant.

Homogeneous Recombination Mechanisms

There are two important homogeneous mechanisms which contribute to the production of oxygen molecules in the presence of oxygen atoms, ozone and inert bodies (A, N_2, etc.). These are the triple-body collision mechanism

$$O + O + M \underset{k_{-1}}{\overset{k_1}{\rightleftharpoons}} O_2 + M \qquad [1]$$

and the well-known ozone mechanism

$$O_3 + O \xrightarrow{k_2} 2O_2 \qquad [2]$$

and

$$M + O_3 \underset{k_{-3}}{\overset{k_3}{\rightleftharpoons}} M + O_2 + O \qquad [3]$$

The total rate of production of oxygen molecules due to the combined mechanisms, in moles/cc-sec, is

$$\frac{d(O_2)}{dt} = k_1(O)^2(M)\left[1 - \frac{(O_2)}{K_{c1}(O)^2}\right] + 2\,k_2(O)\,(O_3) + k_3(O_3)\,(M)\left[1 - \frac{(O)\,(O_2)}{K_{c3}(O_3)}\right] \qquad [4]$$

where (O), (O_2) and (O_3) are the concentrations in moles/cc of atomic oxygen, molecular oxygen and ozone, respectively, and (M) is the concentration of third bodies (i.e., usually the total concentration in moles/cc). The equilibrium constants K_{c1} and K_{c3} are given by

$$K_{c1} = \frac{(O_2)}{(O)^2} = 10^{[(25{,}700/T) - 1.390]} \qquad [5]$$

$$K_{c3} = \frac{(O_2)\,(O)}{(O_3)} = 10^{[-(5{,}620/T) + 5.016 - \log_{10} T]} \qquad [6]$$

where T is in deg K. The rate constant k_3 was recently given by Kaufman (3,4). The rate k_2 was studied by Garvin (5) and also by Benson and Axworthy (6). Their experimental results yield

$$k_2 = 1.07 \times 10^{13}\,(T/500)\,10^{-1050/T} \quad \text{cc/mole-sec} \qquad [7]$$

The last two terms of the right-hand side of Equation [4] represent the rate of production of oxygen due to the ozone mechanism. Thus

$$\left.\frac{d(O_2)}{dt}\right|_{\text{ozone}} = 2k_2(O)\,(O_3) + k_3(O_3)\,(M)\left[1 - \frac{(O)\,(O_2)}{K_{c3}(O_3)}\right] \qquad [8]$$

If the concentration of ozone obeys the steady-state approximation and

$$k_{-3}(M)\,(O_2) \gg k_2(O_3)$$

Equation [5] reduces to

$$\left.\frac{d(O_2)}{dt}\right|_{\text{ozone}} \simeq k_2\frac{k_3}{k_{-3}}\frac{(O_2)^2}{(O_2)} = k_2K_{c3}\frac{(O_3)^2}{(O_2)} \qquad [9]$$

If $k_2(O_3) \gg k_3\,(M)\,(O_2)$, Equation [5] reduces to

$$\left.\frac{d(O_2)}{dt}\right|_{\text{ozone}} \simeq -k_3(O_3)\,(M) \qquad [10]$$

On the other hand, if the concentration of atomic oxygen is adjusted so that it obeys the steady-state approximation, and $k_2(M) \gg k_2(O)$, Equation [5] becomes

$$\left.\frac{d(O_2)}{dt}\right|_{\text{ozone}} \simeq \frac{3k_2}{K_{c3}}(O)^2\,(O_2) \qquad [11]$$

If $k_2(O) \gg k_3(M)$, Equation [5] reduces to

$$\left.\frac{d(O_2)}{dt}\right|_{\text{ozone}} \simeq -3k_{-3}(O)\,(O_2)\,(M) \qquad [12]$$

Received March 2, 1959.

1 Presented at the 133rd Meeting of the American Chemical Society, San Francisco, April 14, 1958 (paper no. 10, Sec. A, Div. of Physical and Inorganic Chemistry). This work was supported by the U. S. Air Force through the Directorate of Advanced Studies of the Air Force Office of Scientific Research, Air Research and Development Command, under Contract AF 49(638)-111.

2 Consultant.

3 Present address: Head, Propulsion Laboratory, Hughes Tool Co., Culver City, Calif. Member ARS.

4 Numbers in parentheses indicate References at end of paper.

Finally, if the reaction given by Equation [2] is rate-controlling

$$\left.\frac{d(O_2)}{dt}\right|_{\text{ozone}} \simeq 2k_2(O)\,(O_3) \qquad [13]$$

and if $1 - [(O)\,(O_2)/K_{c3}(O_3)] \simeq 0$

$$\left.\frac{d(O_2)}{dt}\right|_{\text{ozone}} \simeq 2k_2K_{c3}\frac{(O_2)^2}{(O_2)} \qquad [14]$$

It is clear that k_2 and K_{c3} suffice to determine the rate of production of oxygen molecules in the important cases described by Equations [6, 8, 10 and 11]. However, the value of k_1 is required to determine the total rate of production of O_2. The authors of (3 to 6) presented a rate constant k_1 given by

$$k_1 = 3 \times 10^{16}\,(300/T)^{1.5} \qquad \text{cc}^2/\text{mole}^2\text{-sec}$$

$$1000\text{K} \leq T \leq 4000\text{K} \qquad [15]$$

On the basis of the same work, the temperature limits can be extended as follows

$$T < 1000\text{K} \qquad 5.6 \times 10^{15}(T/500)\;10^{-(1050/T)} < k_1 < 3 \times 10^{16}\,(300/T)^{1.5}$$

$$T > 4000\text{K} \qquad k_1 = 3 \times 10^{16}\,(300/T)^{1.5} \qquad [15a]$$

This rate constant was derived in two different ways. First, the order of magnitude of k_1 in the temperature range of interest was established by considering the number of three-body collisions involving two oxygen atoms and one oxygen molecule. The efficiency for these collisions was then assumed to be the same as that for the well-known reaction given by Equation [2], since the activated complex consists of four oxygen atoms and the end products of two oxygen molecules in both cases. That efficiency is of the order of 0.05, and thus k_1 is of the order of 5×10^{15} in the temperature range from 1000 to 2000K. Second, the absolute reaction rate theory of Eyring, Gershinowitz and Sun (7) for the three-body recombination process was modified in such a manner that by employing the experimental rate constants for well-known reactions, such as $H + H + H_2 \rightarrow H_2 + H_2$ and $I + I + M \rightarrow I_2 + M$, an estimate of the rate constant k_1 was derived. At 2000K, the "scaling" on the basis of hydrogen recombination yielded $k_1 = 1.1 \times 10^{15}$, and the "scaling" on the basis of iodine recombination yielded $k_1 = 1.9 \times 10^{15}$. Finally, the temperature dependence of k_1 was assumed to be the same as for the iodine recombination rate constant. The choice of 300K as the base temperature in the quantity $300/T$ was arbitrary. At temperatures lower than about 1300K, the approximations introduced in "scaling" on the basis of the Eyring theory are such that the value of k_1 given by Equation [15] should be slightly higher than the correct value. On the other hand, the collision theory approximation with the efficiency of the reaction $O_3 + O \rightarrow 2O_2$ should provide a definite lower limit.

This estimate is for O_2 as the third body. For N_2, A or other inert molecules acting as third bodies, k_1 is slightly smaller. The rate constant for recombination in high temperature air may be as much as 10 times as great as given by Equation [15] because of the uncertainty in the relative efficiencies of nitrogen and oxygen atoms as third bodies. Further, oxides of nitrogen may be formed and act as chain carriers for oxygen recombination and possibly increase the rate, although no reasonable chain mechanism has been found by these authors. Thus, as already stated by one of these authors (2), the rate constant k_1 for atomic oxygen as a third body is

$$k_1 = 3 \times 10^{17}(300/T)^{1.5} \qquad \text{cc}^2/\text{mole}^2\text{-sec} \qquad [16]$$

with essentially the same temperature limits.

Some values of k_1 as a function of temperature from Equation [12] are presented in Table 1.

Table 1 Present estimate of rate constant k_1 for oxygen recombination by three-body collision mechanism (for O_2 as a third body)

T, K	k_1, cc^2/mole^2-sec
300	$<3 \times 10^{16}$
1000	4.9×10^{15}
1500	2.7×10^{15}
2000	1.7×10^{15}
2500	1.2×10^{15}
3000	9.5×10^{14}
3500	7.6×10^{14}
4000	6.7×10^{14}
5000	4.5×10^{14}
8000	2.2×10^{14}

The integration of Equation [4] has been carried out in closed form for the two limiting cases when the triple-body mechanism or the ozone mechanism predominates, and [4] has also been integrated graphically for various intermediate cases (1). At the higher temperatures and for equilibrium initial concentration of O_3, only triple-body recombination is significant. Tables were also presented (1) of the equilibrium composition of the $O + O_2 + O_3$ system in the range of temperatures from 1000 to 5000K and at 10^{-3}, 5×10^{-5} and 10^{-6} atm.

Heterogeneous Recombination Mechanisms

The concentration of atomic oxygen determines which heterogeneous mechanism is fastest. The first possible mechanism is

$$O + O + \text{wall} \rightarrow O_2 + \text{wall} \qquad [17]$$

i.e., when the wall acts as third body. Then, since the wall is very efficient as a third body

$$\left.\frac{d(O_2)}{dt}\right|_{\text{wall}+2(O)} = 1.5 \times 10^5(O)^2\,(T)^{1/2} \qquad \text{mole/sec-cm}^2 \qquad [18]$$

The second possible mechanism is

$$O + (\text{O adsorbed on wall}) \rightarrow O_2 \qquad [19]$$

This is not a 100 per cent efficient process. The rate of production is

$$\left.\frac{d(O_2)}{dt}\right|_{O+\text{wall}-O} = 9 \times 10^2(O)f(T)^{1/2} \qquad \text{mole/sec-cm}^2 \qquad [20]$$

With an efficiency $f = 0.001$ (for glass, see (8)) this becomes

$$\frac{d(O_2)}{dt} = 0.9(O)\,(T)^{1/2} \qquad \text{mole/sec-cm}^2 \qquad [21]$$

The efficiency f approaches unity for the noble metals and metallic oxides (especially in the presence of traces of OH), and may be low as 10^{-5} for "poisoned" glass surfaces or glass surfaces treated with phosphoric acid. Both heterogeneous mechanisms occur simultaneously, but that given by Equation [19] is faster when (O) is small.

Combined Production Rate

For most practical purposes, the term $(O_2)/K_{c1}(O)^2$ in Equation [4] is small compared to 1, and, at least at high temperatures, the term due to the ozone mechanism is small compared to the triple-body mechanism. Then, at low pressures, the combined rate of production of oxygen becomes

approximately

$$\frac{d(O_2)}{dt} \simeq k_1(O)^2(M) + 9 \times 10^9(O) f \frac{A}{V} (T)^{1/2} \quad \text{mole/sec-cc} \quad [22]$$

where A is the catalytically active surface area in cm² of a control volume V in cc. When the control volume in cc is large compared to its surface area in cm², wall recombination may be neglected.

Conclusions

With the rates presented in this paper, which are not so high as previously thought (9), either flow or static experiments can be designed to measure the specific rate constant k_1. In these experiments, the visualization of the recombination reaction can be enhanced by injection of traces of substances whose reaction rates are known (e.g., NO, NO_2, etc.) or inclusion of N_2 to produce NO and the yellow-green afterglow caused by the reaction of oxygen atoms with nitric oxide.

References

1 Demetriades, S. T. and Farber, M., "A Theoretical Study of the Recombination Kinetics of Atomic Oxygen," AFOSR TN 58-18, ASTIA AD 148057, Nov. 8, 1957.

2 Demetriades, S. T., "Upper Atmosphere Atomic-Oxygen Power Plant," *J. Aero/Space Sci.*, vol. 25, Oct. 1958, pp. 653–654.

3 Kaufman, F., "Air Afterglow and Kinetics of Some Reactions of Atomic Oxygen," *J. Chem. Phys.*, vol. 28, Feb. 1958, pp. 352–353.

4 Kaufman, F., "Air Afterglow and Its Use in the Study of Some Reactions of Atomic Oxygen," Proc. Roy. Soc., London, to be published.

5 Garvin, D., "The Oxidation of Carbon Monoxide in the Presence of Ozone," *J. Amer. Chem. Soc.*, vol. 76, March 20, 1954, pp. 1523–1527.

6 Benson, S. W. and Axworthy, A. E., Jr., "Mechanism of the Gas Phase; Thermal Decomposition of Ozone," *J. Chem. Phys.*, vol. 26, June 1957, pp. 1718–1726.

7 Eyring, H., Gershinowitz, H. and Sun, C. E., "The Absolute Rate of Homogeneous Atomic Reactions," *J. Chem. Phys.*, vol. 3, Dec. 1935, pp. 786–796.

8 Linnett, J. W. and Marsden, D. G. H., "The Kinetics of the Recombination of Oxygen Atoms at a Glass Surface," Proc. Roy. Soc., London, vol. A 234, 1956, pp. 489–503.

9 Feldman, S., "The Chemical Kinetics of Air at High Temperatures; A Problem in Hypersonic Aerodynamics," Preprints of Papers, Heat Transfer and Fluid Mechanics Institute, California Institute of Technology, June 1957, pp. 173–192.

Estimation of Performance of Fuels With Hydrogen Peroxide Oxidizer

JOHN S. GORDON[1]

Thiokol Chemical Corp., Denville, N. J.

An empirical short method is described for determining rocket performance of fuels containing carbon, hydrogen, nitrogen and oxygen, with 90 per cent hydrogen peroxide oxidizer. The method is similar in approach to existing short methods for other oxidizers. The results in I_{sp} and C^* are uncertain by 0.3 per cent.

SHORT-CUT methods for estimating the performance parameters of various fuels containing carbon, hydrogen, nitrogen and oxygen with nitric acid, oxygen and ammonium nitrate oxidants were developed by Johnston.[2] Data for a variety of fuels with 90 per cent H_2O_2 have become available in the course of propellant investigations at Reaction Motors, Inc. These data are summarized in Table 1. Data from other sources are also included, but are older and believed less reliable. In general, the semi-empirical approach and nomenclature used by Johnston are retained in this analysis. Only the chemical formula and heat of formation of the fuel are required to make the performance calculation. Considerable time can be saved, compared to rigorous methods, and the short-method results can be used as a starting point for further rigorous calculations. Johnston describes an approximate method of developing a performance curve (at several O/F ratios) from a single peak I_{sp} value; this type of extrapolation was not believed useful enough to warrant inclusion in this study. NH_4ClO_4 oxidizer has been studied by the author.[3]

Received Jan. 2, 1959.

[1] Unit Supervisor, Propellants Liaison and Thermochemistry, Chemistry Department, Reaction Motors Div. Member ARS.

[2] Johnston, S. A., JPL Progress Report 20-202, 1953.

Derivation of Method

Analysis of the data in Table 1 shows that peak I_{sp} occurs at a mixture ratio corresponding to the undissociated exhaust products N_2, H_2O, $(x/3)$ CO_2 and $(2x/3)$ CO, from a fuel with the general formula $C_xH_yO_zN_w$. Ninety per cent H_2O_2 has the composition $H_2O_{1.8263}$ with a molecular weight of 31.237 and a standard heat of formation of −49.012 Kcal/mole, from gaseous O_2 and H_2 at 25 C. Development of an expression for heat release per unit mass of propellant follows.

Reaction Products

$$C_xH_yO_zN_w + a\ H_2O_{1.8263} \rightarrow \frac{2x}{3}\ CO + \frac{x}{3}\ CO_2 + \frac{2a+y}{2}\ H_2O + \frac{w}{2}\ N_2$$

Oxygen Balance

$$z + 1.8263a = \frac{4x}{3} + \frac{2a+y}{2}$$

$$0.8263a = \frac{4x}{3} + \frac{y}{2} - z$$

$$a = 1.613x + 0.605y - 1.21z$$

Generalized Reaction Products

$$C_xH_yO_zN_w + (1.613x + 0.605y - 1.21z)\ H_2O_{1.8263} \rightarrow \frac{2x}{3}\ CO + \frac{x}{3}\ CO_2 + (1.613x + 1.105y - 1.21z)\ H_2O + \frac{w}{2}\ N_2$$

Combustion Energy Release

$$Q_{av} = \frac{2x}{3}(26.42) + \frac{x}{3}(94.05) + (1.613x + 1.105y - 1.21z) \times (57.8) - (1.613x + 0.605y - 1.21z)(49.01) + Q_F$$

where Q_F is the heat of formation of fuel.

$$Q_{av} = 17.61x + 31.35x + 93.23x + 63.87y - 69.94z - 79.05x - 29.65y + 59.30z + Q_F$$

$$Q_{av} = 63.14x + 34.22y - 10.64z + Q_F$$

or

$$U = 63.14\,(C) + 34.22\,(H) - 10.64\,(O) + Q_F \quad [1]$$

Mass of Oxidizer Per Mole of Fuel

$$X = 31.237\,(1.613x + 0.605y - 1.21z)$$

$$= 18.90\,[(8/3)\,(C) + (H) - 2(O)] \quad [2]$$

Energy Per Gram of Propellant

$$Q = \frac{U}{M + X}(\text{Kcal/gm}) \quad [3]$$

where M is the molecular weight of fuel.

The reader will note the similarity of this algebraic development to that given by Johnston for HNO_3 oxidizer. Values of Q were calculated for the eighteen fuels. Rigorous I_{sp}

[3] Gordon, J. S., Bulletin of the 14th Meeting, JANAF Solid Propellant Group, vol. 4, 1958, p. 221.

Table 1 Calculated frozen performance with 90 per cent H_2O_2 (600/14.7 pressure ratio)

O/F (stoich)	Fuel	Q_F Kcal/mole	Optimum O/F	r_p/r_c	T_c, K	H/C	I_{sp}	C^*	$\bar{M}_{ch}$	k_{ch}	k_e	Source
3.33	NH_3	−17.17	3.2	...	2360	atom ratio	243.6	5159	18.97	1.203	1.250	RMI
5.03	$C_2H_8N_2$	−6.36	5.09[a]	...	2652	...	247	...	...	...	...	Rand
8.17	$C_8H_{16\text{-}82}$	−67.145	6.9	0.73	2586	2.1	244[a]	...	...	...	...	RMI
2.36	N_2H_4	12.05	1.6[a]	...	2560	...	256	...	...	...	...	GE
3.54	CH_3OH	−57.02	2.85	...	2555	...	243	...	...	...	...	Rand
3.97	$C_3H_8O_2$	−93.13	3.5	...	2668	...	242	...	...	...	...	JPL
...	CH_3NO_2	−21.28	0.50	...	2890	...	251	...	...	...	...	Rand
...	C_8H_{18}	−59.74	6.0	...	2545	...	249	...	...	...	...	Rand
...	$N_2H_4H_2O$	−57.95	1.6	...	2261	...	238.5	...	...	...	...	Rand
5.03	$C_2H_8N_2$	+12.72	4.0	0.80	2738	4	253.5	5372	20.20	1.197	1.222	RMI
5.52	C_4H_3N	+71.39	4.0	0.725	2956	0.75	251.1	5312	22.36	1.195	1.223	RMI
5.52	C_4H_3N	+88.95	4.0	0.725	3013	0.75	254.3	5388	22.08	1.198	1.225	RMI
3.98	C_4N_2	+147.14	2.3	0.58	3129	0	254	...	22.88	...	...	RMI
5.64	C_5H_3N	105.82	3.9	0.69	3000	0.6	253.1	5349	22.34	1.197	1.224	RMI
5.52	C_5H_6O	30.63	4.1	0.74	2920	1.2	252.3	5329	21.91	1.192	1.220	RMI
6.29	C_5H_7N	73.52	4.7	0.75	2915	1.4	254.6	5384	21.40	1.195	1.224	RMI
3.32	$C_5H_{12}N_2O_3$	−91.8	2.9	0.87	2770	2.4	244.9	5176	22.15	1.188	1.217	RMI
8.06	$C_{9\text{-}66}H_{19}$	−57.22	6.9	0.86	2770	1.97	247.5	5251	21.55	1.187	1.217	RMI

[a] Accuracy questioned.

values were plotted against Q as shown in Fig. 1, and a good straight-line relationship resulted with an average deviation of ±1.3 sec from the rigorous I_{sp}

$$I_{sp} = 179.5 + 54.6\,Q$$

The 4-sec deviation for C_4N_2 indicated that a correction factor for H/C ratio might improve the results. A good hyperbolic relation between correction factor (X) and (H/C) was found empirically for the RMI-calculated data only

$$(X) = -1.95\left(\frac{C}{H}\right) + 2.15$$

An arbitrary maximum value of 6.0 for X is dictated by the results for C_4N_2. The second approximation for I_{sp} is thus

$$I_{sp} = 171.6 + 54.6\,Q - 1.95\left(\frac{C}{H}\right) \qquad [4]$$

Here the average deviation has been reduced only 11 per cent, to ±1.16 sec, but the internal agreement for the RMI-calculated data is excellent, ±0.33 sec. Noting that most of the fuels from sources outside RMI have negative heats of formation, correction factors based on Q_F and on Q^2 were attempted. Plots of Δ (long I_{sp} − second approximation I_{sp}) as functions of Q_F and of Q^2 showed only a fair correlation with Q_F in the form

$$\Delta = -0.4 + 0.009\,Q_F$$

The third approximation for I_{sp} is thus

$$I_{sp} = 171.2 + 54.6Q - 1.95\,(C/H) + 0.009\,Q_F$$

The average deviation for all data points has been reduced another 11 per cent, to ±1.03 sec, but the internal consistency of the RMI-calculated data is poorer, with an average deviation of ±0.47 sec. The added complexity with the 0.009 Q_F correction term evidently is not justified, and this term has no physical significance anyway.

Chamber Temperature

T_c is proportional to the total energy release from a unit mass of propellants divided by the mean specific heat of the reaction products. The mean molar specific heats of the primary combustion products are taken as:

Species	$\left(\frac{H - E_0}{T}\right)_{3000\ deg}$
CO	8.143
CO_2	12.992
N_2	8.087
H_2O	10.856

The mean specific heat of products from one mole of fuel, at

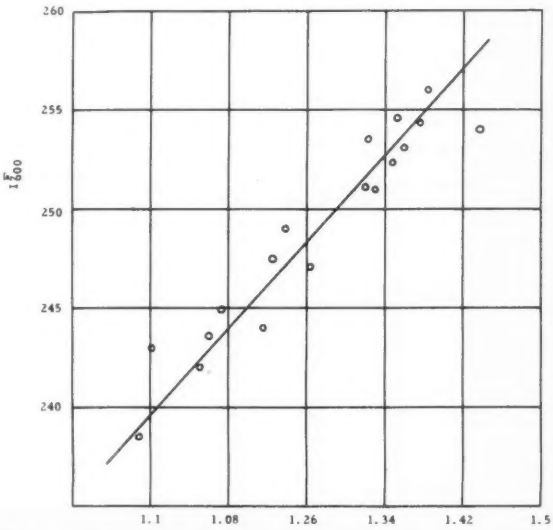

Fig. 1 Theoretical frozen I_{sp} vs. $Q = U/(M + X)$. First approximation: $I_{sp} = 179.5 + 54.6\,Q$

the mixture ratio for peak I_{sp}, is derived as follows

$$C_xH_yO_zN_w + (1.613x + 0.605y - 1.21z)\ H_2O_{1.826z} \rightarrow$$

$$\frac{2x}{3}\ CO + \frac{x}{3}\ CO_2 + (1.613x + 1.105y - 1.21z)\ H_2O + \frac{w}{2}\ N_2$$

$$P = 8.143\left(\frac{2x}{3}\right) + 12.922\left(\frac{x}{3}\right) + 10.856\ (1.613 + 1.105y - 1.21z) + \left(\frac{w}{2}\right) 8.087$$

$$= (5.429 + 4.307)\ (C) + 17.511 + 11.996\ (H) - 13.136\ (O) + 4.044\ (N)$$

$$P = 9.74\ (C) + 17.51 + 12\ (H) - 13.14\ (O) + 4.04\ (N) \quad [5]$$

Values of P were then calculated for each fuel. Rigorous values of T_c were plotted against the heat release/average heat capacity parameter, U/P. A straight-line fit was obtained

$$T_c = 199\ (U/P) + 2065\ (\text{deg K}) \quad [6]$$

with an average deviation of ±76 K for all 18 points and ±46 K for the RMI-calculated points. No improvement in accuracy could be obtained by attempting a correction factor based on C atom ratio, or the atom-ratio parameter 2·O/(4·C + H). A straight-line plot of T_c vs. Q fits the data with an accuracy of ±120 K and is not very useful. The poor accuracy of this method for estimating T_c is disappointing in view of the ±15 K agreement obtained by Johnston with HNO_3 systems.

Molecular Weight

The ten sets of RMI-calculated data in Table 1 lead to a linear correlation between $\bar{M}$ and the estimated flame temperature

$$\bar{M} = 6.45 + 0.00529\ T_c\ (\text{average deviation } \pm 0.43) \quad [7]$$

The available data do not justify a more complex relationship. The estimated flame temperature from Equation [6] correlates better than the T_c from exact calculation.

Chamber Specific Heat Ratio (Frozen Composition)

K_c is essentially constant at 1.195 over the range of RMI-calculated data (average deviation ±0.004). C_p/C_v at T_c (for 600/14.7 expansion) is about 0.029 greater than at T_c.

Stoichiometric Mixture Ratio

By inspection of Equation [2], this is seen to be

$$r_s = \frac{18.9\ [4(C) + (H) - 2(O)]}{M} \quad [8]$$

Mixture Ratio for Peak I_{sp}

This correlates roughly with the H/C atom ratio in the fuel

$$\frac{r_p}{r_s} = 0.67 + 0.04\left(\frac{H}{C}\right) \leq 0.92 \quad [9]$$

Characteristic Velocity

Within the accuracy of the rigorously calculated data in Table 1, C^* may be expressed as a linear function of the heat release per unit mass

$$C^* = 3952 + 1.046Q\ (\text{average deviation } \pm 16\ \text{fps}) \quad [10]$$

An expression in the form $C^* = a + bQ - cQ^2$ could have been developed from the limited data available, but this was not believed justified, since the best equation for I_{sp} has no term in Q^2. The long-method C^* values are based on k_c rather than the effective γ for frozen expansion ($T_c/T_e = (P_c/P_e)^{(\gamma-1)/\gamma}$, or the average k between chamber and exhaust $\bar{k} = 1/2\ (k_c + k_e)$.

Extrapolation to 100 Per Cent Hydrogen Peroxide Oxidizer

Only four fuels were found in the literature with which both 90 and 100 per cent H_2O_2 had been given theoretical treatment. In general, it seems reasonable to add 1 sec I_{sp} and 30 K flame temperature for each additional 1 per cent concentration. Optimum and stoichiometric mixture ratios are 10 per cent less than for 90 per cent peroxide.

Summary

$$U = 63.14\ (C) + 34.22\ (H) - 10.64\ (O) + Q_F$$

$$X = 18.9\ [(8/3)\ (C) + H - 2\ (O)]$$

$$Q = U/(M + X)$$

$$I_{sp} = 171.6 + 54.6\ Q - 1.95\ (C/H)\ \text{(frozen, 600/14.7 pressure ratio)}$$

$$P = 9.74\ (C) + 17.51 + 12\ (H) - 13.14\ (O) + 4.04\ (N)$$

$$T_c = 199\ U/P + 2065\ (\text{deg K})$$

$$\bar{M} = 6.45 + 0.00529\ T_c$$

$$r_p = \frac{18.9\ (4{\cdot}C + H - 2{\cdot}O)\ [0.67 + 0.04\ (H/C)]}{M}$$

$$C^* = 3952 + 1.046\ Q$$

The expected uncertainties are

$I_{sp} \pm 1$ sec

$T_c \pm 70$ K

$\bar{M} \pm 0.4$

$r_p \pm 0.2$

$C^* \pm 16$ fps

DEPENDABILITY

another outstanding attribute of

DIMAZINE®

unsym-Dimethylhydrazine, UDMH

THE STORABLE FUEL

Performance data on DIMAZINE-powered rocket engines in military missiles and satellite launching vehicles shows DIMAZINE to be a highly reliable rocket fuel.

DIMAZINE provides fast, dependable hypergolic starts followed by smooth, stable combustion and easier shutdowns. Dependable instant readiness is assured for years by its outstanding stability during storage in missiles. It also has high performance, high thermal stability, low freezing point, low shock sensitivity, minimum susceptibility to contamination and high compatibility with almost all metals and appropriate sealing materials.

These manifold advantages combine to make DIMAZINE *the outstanding storable fuel.* We will be pleased to work with you in evaluating DIMAZINE and to supply detailed data on its properties and handling.

Putting Ideas to Work

FOOD MACHINERY AND CHEMICAL CORPORATION

Westvaco Chlor-Alkali Division

General Sales Offices:
161 E. 42nd STREET, NEW YORK 17

Book Reviews

Ali Bulent Cambel, Northwestern University, *Associate Editor*

Combustion and Propulsion, Third AGARD Colloquium, edited by M. W. Thring, O. Lutz, J. Fabri and A. H. Lefebvre, Pergamon Press, New York, 1958, 610 pp. $20.00.

Reviewed by A. K. Oppenheim
University of California

This impressive volume contains the proceedings of the unforgettable Third Combustion Colloquium of the Advisory Group for Aeronautical Research and Development of the North Atlantic Treaty Organization, which was held at Palermo, Sicily, March 17–21, 1958, and some selected papers of the 12th Meeting of the AGARD Combustion and Propulsion Panel, which took place the preceding year at Washington, D. C. The predominating area in this worthy collection of papers is the gasdynamic and engineering aspects of the subject matter, while the purely chemical considerations are significantly de-emphasized.

The proceedings of the Palermo Colloquium consist of five parts. The first—concerned with general features of propulsion systems—consists of Levine's discussion of problems involved in the development of large liquid rocket engines, and of a comprehensive survey, given by Lombard, of the overall performance characteristics of propulsion by air-breathing engines, including some interesting remarks on the future of transport aircraft.

The second part deals with interaction processes and includes the paper of Childs on the effect on turbojet combustors and afterburners of other engine components; an interesting discourse of Grivzs on "ram-rockets," that is, ramjets incorporating rocket thrust chambers as the primary combustion system; the report by Napolitano, Libby and Ferri on their recent work in the field of jet mixing, and the paper of Rudinger on the interaction between shock waves and flames.

The third part considers the problem of noise—primarily, of course, in the interest of its suppression. It is made up of a description by Sanders and North of methods used for reducing noise of jet engines, some thoughts of Richards on the design of nozzles for similar purpose, and the elucidation of the financial and physiological aspects of the problem supplied by Ducrot, Riehn, Roumilhac and Souvras.

The fourth part is devoted to combustion problems. It contains a controversial paper by Spalding, a concise review by Gerstein summarizing the present knowledge of chemical processes in flames, a discussion by Fouré on the fundamental features of the development of combustion chambers for aircraft propulsion, and a report by Schultz, Green and Penner on the study of the decomposition mechanism and related aspects of solid composite propellants.

The fifth part is titled Aerophysical Chemistry; it contains two informative surveys: One by Meyerott on the radiation heat transfer to hypersonic vehicles, and the other by Lees on related problems involving convective heat transfer, mass addition and chemical reactions. This is supplemented by a discussion by Laporte on the subject of high temperature shock waves, some interesting remarks by Schlüter on magnetohydrodynamics demonstrating the advantages of splitting pressure forces into components parallel and perpendicular to the direction of the magnetic field, and the report by Liepmann, submitted in the discussion, on magnetic effects in high speed boundary layer flow.

Part VI is made up of four selected papers from the 12th AGARD Combustion Panel, namely, an excellent review of flame stabilization by means of gaseous jets presented by Cambel, a report on a successful application of the crossflow jet principle for flameholding by Bertin and Salmon, the discussion of flame stabilization in boundary layers by Tau-Yi Toong, and Lutz's presentation of a graphical method for the analysis of gasdynamic mixing.

Ali in all, the volume forms a worthy addition to the distinguished series of AGARD publications, forming a valuable reference in the field of combustion and jet propulsion.

Some Problems in Chemical Kinetics and Reactivity, Volume I, by N. N. Semenov (translated from the Russian by Michael Boudart), Princeton University Press, Princeton, N. J., 1958, xii + 239 pp. $4.50.

Reviewed by S. S. Penner
California Institute of Technology

Semenov prepared in 1954 an extensive survey on chemical kinetics in chain reactions as a prelude to a symposium held in Moscow in 1955. The present book comprises the first of an expanded two volume edition based on the 1954 document.

The distinguished scientist presents in this book a readable account of his interpretation of recent progress on chain reactions. To western readers, the discussion should be of interest not only as a significant contribution from one of the leading kineticists of our time, but also as a valuable source of reference to relevant Russian publications, many of which have not been studied widely by scientists working outside of the Soviet Union.

The five chapters in Volume I include treatments on the following topics: Reactivity of monoradicals (94 pp.), competition between monoradical reactions (50 pp.), reactions of diradicals (22 pp.), dissociation of molecules and recombination of radicals (27 pp.), initiation of chain reactions by ions of variable valence (14 pp.), and wall initiation and termination of chain reactions (29 pp.). The treatment follows the approach of the classical chemical kineticist and contains abundant information on the reaction rates of free radicals formed from hydrocarbons, as well as a brief compilation of kinetics data for reactions between simpler chemical species. For people who are primarily interested in propulsion applications, the most valuable part of Volume I may very well be an extensive discussion and tabulation of bond energies and of reaction rates given in chapter I. Particular mention should also be made of the treatment of heterogeneous reactions given in chapter VI, since this discussion covers a field in which Russian scientists have made recently some important basic contributions.

Among the principal attractions of the book are the clarity and simplicity of the physical descriptions, the insight which the author provides for the mechanism of reaction processes, and the panoramic coverage on the rates of different classes of chemical transformations. The scientific community owes a debt of gratitude to the translator Michael Boudart who has rendered a singularly readable account of Semenov's work.

Aircraft Engines of the World, 1958/59, by Paul H. Wilkinson, Paul H. Wilkinson Publications, Washington, D. C., 1958, 320 pp. $15.00.

Reviewed by P. Roy Choudhury
University of Southern California

"Aircraft Engines of the World" gives a good coverage of all the current gas turbine, ramjet and rocket engines. It also lists the major reciprocating engines currently being used. A section on nuclear aircraft engines acquaints the reader with the latest activities in this area of propulsion. Available accessories and equipment, and fuel and lubrication are also included in this volume.

The author first describes different engines and their characteristics, and then lists them in tabular form for easy reference. Russian engines, which are of major interest these days, are also listed.

In short, the book is an excellent compilation of figures, tables and engine characteristics of all the known aircraft propulsion systems of the world.

Books Received

Liquids and Gases, by Alexander Efron, John F. Rider, New York, 1958, 117 pp. $1.20.

Mechanics, by Alexander Efron, John F. Rider, New York, 1958, 112 pp. $1.50.

Nuclear Energy, by Alexander Efron, John F. Rider, New York, 1958, 72 pp. $1.25.

Basic Pulses, by I. Gottlieb, John F. Rider, New York, 1958, 176 pp. $3.50.

Fundamentals of Nuclear Energy and Power Reactors, by Henry Jacobowitz, John F. Rider, New York, 1959, 144 pp. $2.95.

Fundamentals of Transistors, by Leonard Krugman, John F. Rider, New York, 1958, 176 pp. $3.50.

Gas Tubes, edited by A. Schure, John F. Rider, New York, 1958, 80 pp. $1.50.

Impedance Matching, edited by A. Schure, John F. Rider, New York, 1958, 128 pp. $2.90.

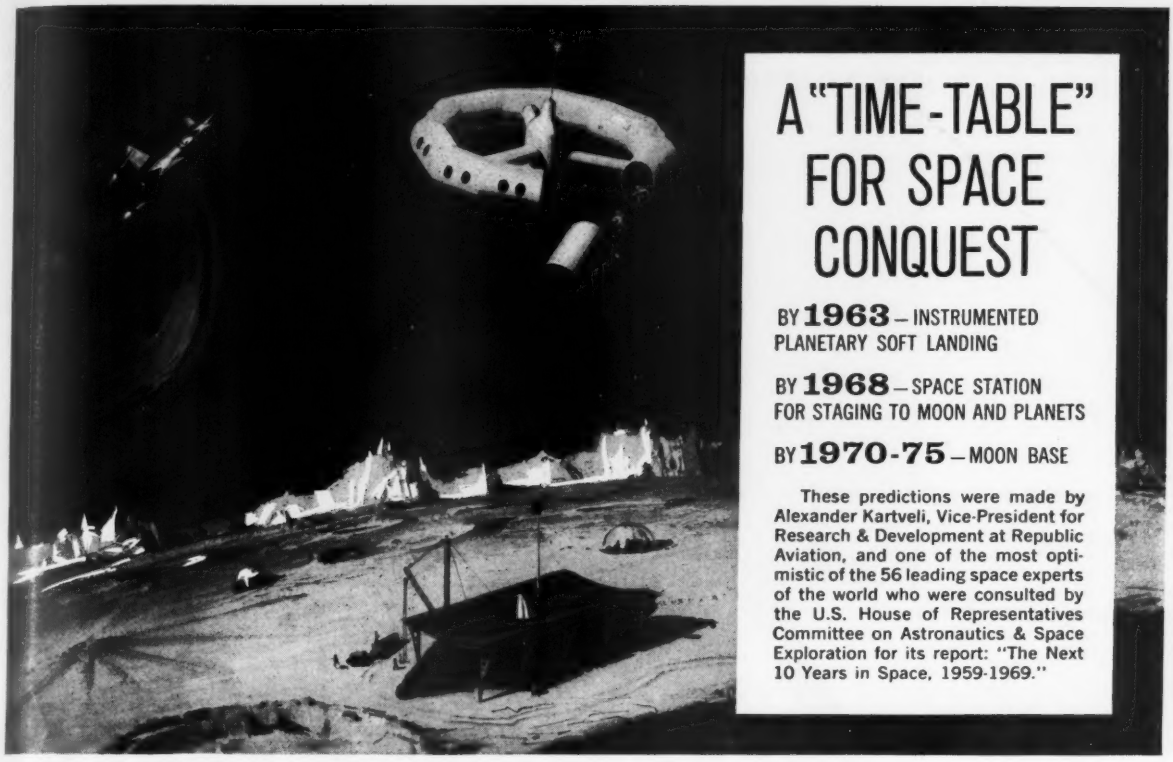

A "TIME-TABLE" FOR SPACE CONQUEST

BY **1963** – INSTRUMENTED PLANETARY SOFT LANDING

BY **1968** – SPACE STATION FOR STAGING TO MOON AND PLANETS

BY **1970-75** – MOON BASE

These predictions were made by Alexander Kartveli, Vice-President for Research & Development at Republic Aviation, and one of the most optimistic of the 56 leading space experts of the world who were consulted by the U.S. House of Representatives Committee on Astronautics & Space Exploration for its report: "The Next 10 Years in Space, 1959-1969."

JOIN REPUBLIC IN AN **INTEGRATED ATTACK** ON PROBLEM AREAS OF **SPACE EXPLORATION**

It's the fervent conviction of engineers and scientists at Republic Aviation that the courageous "Space Time-Table" above is entirely feasible – given a tradition-free, integrated approach to the problems. Such an approach is evident at Republic Aviation. Here, groups of specialists from many disciplines are working in close collaboration to solve problems across the entire spectrum of space technologies, which limit today's interplanetary and upper atmosphere flight capabilities.

Expanded by $35,000,000 last year, Republic's integrated Research and Development program has already produced signal advances in space guidance concepts; in new propulsion systems (plasma, nuclear); in radiation physics; in new materials and processing techniques; in unique hypersonic configurations; and in prototype development of hardware (as an example: hydraulic systems that operate reliably up to 1000°F).

Professional men—who can meet new challenges with enthusiasm and dedication – are urged to look into openings with our R&D groups, working in an atmosphere of exhilarating intellectual adventure.

Electronics
Inertial Guidance & Navigation
Digital Computer Development
Systems Engineering
Information Theory
Telemetry-SSB Technique
Doppler Radar • Countermeasures
Radome & Antenna Design
Microwave Circuitry & Components
Receiver & Transmitter Design
Airborne Navigational Systems
Jamming & Anti-Jamming
Miniaturization — Transistorization
Ranging Systems
Propagation Studies
Ground Support Equipment

Thermo, Aerodynamics
Theoretical Gasdynamics
Hyper-Velocity Studies
Astronautics Precision Trajectories
Airplane/Missile Performance
Air Load and Aeroelasticity
Stability and Controls
Flutter & Vibration
Vehicle Dynamics & System Designs
High Altitude Atmosphere Physics
Re-entry Heat Transfer
Hydromagnetics
Ground Support Equipment

Plasma Propulsion
Plasma Physics
Gaseous Electronics
Hypersonics and Shock Phenomena
Hydromagnetics
Physical Chemistry
Combustion and Detonation
Instrumentation
High Power Pulse Electronics

Nuclear Propulsion and Radiation Phenomena
Nuclear Weapons Effects
Radiation Environment in Space
Nuclear Power & Propulsion Applications
Nuclear Radiation Laboratories

Send resume in complete confidence to: Mr. George R. Hickman, Engineering Employment Manager, Dept. 10G

REPUBLIC AVIATION
Farmingdale, Long Island, New York

New Patents

George F. McLaughlin, *Contributor*

Radiant energy reflector (2,866,971). K. S. Kellher, Alexandria, Va.

A semispherical metallic reflector placed at one side of a dielectric sphere, having a variable index of refraction.

Mass deploying apparatus (2,869,426). W. J. Wilkie, Superior Township, Washtenaw County, Mich., assignor to Avco Mfg. Corp.

Apparatus for discharging a missile from an aircraft. Actuation of an explosive means within a chamber forcefully ejects the missile from spaced retaining hooks attached to the aircraft structure.

Temperature responsive rocket nozzle (2,870,599). T. M. Long, Somerville, N. J.

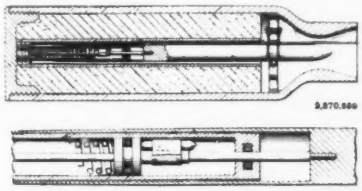

Rocket body with throat portion of variable area. Fluid in the chamber, having a pressure which is a function of temperature, adjusts the throat area. A collapsible tube surrounding the chamber actuated by combustible gases, seals the chamber against entry of the gases.

Variable ejector for iris nozzles (2,870,600). C. R. Brown, Mission, Kan., assignor to the U. S. Navy.

Sleeve mounted on a casing for longitudinal movement, and a movable closure overlying a variable area nozzle. A ring connected to a bar actuates the closure.

Afterburner exhaust nozzle variable area (2,870,602). R. G. Glenn, Merriam, Kan., assignor to the U. S. Navy.

Leaves forming an annular member, hinged to permit inward tilting. Rollers on tapered surfaces force the leaves to tilt toward the center of the nozzle to reduce its area.

Flow controlling mechanism for reaction-type motors (2,870,603). T. M. Long, Somerville, N. J.

Valve and body each provided with a bore serving as a passage for the flow of fluid oxidizer and fuel. Movement of one valve seat into and out of sealing engagement limits the flow, restricting movement of another valve seat.

Flame stabilizer for high velocity gas stream (2,870,604). E. W. Conrad, N. Royalton, Ohio, assignor to the U. S. Navy.

V-shaped gutter extending transversely of the gas stream and having coarse and fine screens upstream of the leading edge to reduce the local velocity of the stream laterally outward from the trailing edges.

Projectile launcher (2,870,678). P. H. Girouard, G. L. Schuyler and M. H. Baller, Washington, D. C., assignors to the U. S. Navy.

EDITOR'S NOTE: Patents listed above were selected from the Official Gazette of the U.S. Patent Office. Printed copies of patents may be obtained from the Commissioner of Patents, Washington 25, D. C., at a cost of 25 cents each; design patents, 10 cents.

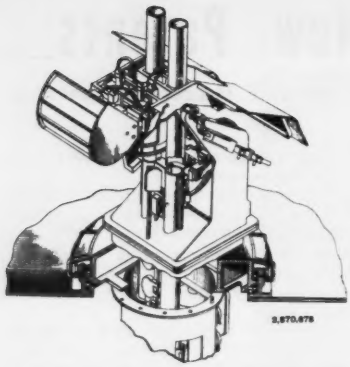

Missile guide tube and dummy gun mounted for independent movement in elevation. Means for bringing the guide tube into loading position when empty, and into firing position when loaded. Missiles are fired in the desired elevation angle by the position of the dummy gun.

Acceleration amplifier (2,870,675). W. W. Salisbury, Lafayette, Calif., assignor to Zenith Radio Corp.

Cylindrical coils placed end-to-end to form tubular bores. Phase-displaced currents and a motor armature comprise a conductive projectile movement within a motor stator. A localized field traversing the stator supports and moves the projectile at increasing acceleration.

Missile retaining device (2,870,677). F. Herrmann, W. Englewood, N. J., assignor to the U. S. Army.

Mechanism for releasably retaining a missile in launching position within a tube. A pair of plungers in the housing engage bores, urged radially outward by springs. A cap screw limits inward movement of the plungers.

Air intake control (2,870,956). H. B. C. Dhonau and S. E. Nelson, Indianapolis, Ind., assignors to General Motors Corp.

Blockage segmental flaps pivotally supported on links and movable from a position parallel to the wall of a gas compressor air intake to a position oblique to the wall when segments are moved axially.

Controls for aircraft (2,870,978). A. A. Griffith and A. W. Thorpe, Farnborough, England, assignors to Rolls-Royce Ltd., and the British Minister of Supply.

Pair of auxiliary jet nozzles from a gas turbine engine spaced apart on an aircraft wing to produce mutually opposed turning moments on the aircraft. The ratio in which the supply is divided between the nozzles is varied to alter the effective turning moment on the aircraft.

Method for transmitting intelligence (2,871,463). R. W. Beckwith, N. Syracuse, N. Y., assignor to General Electric Co.

Means responsive to signals of either of two frequencies to actuate a respective control device. Signals having a frequency varying regularly between the two actuating frequencies prevent actuation of the control.

Sustainer exhaust gas deflector (2,871,658). W. J. Keck, Sacramento, Calif., assignor to the U. S. Navy.

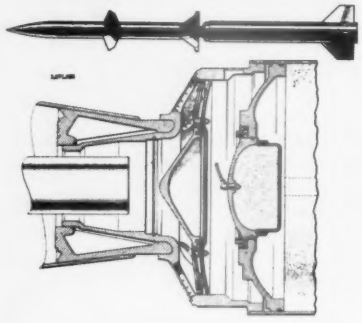

Safety device for preventing complete ignition of a pair of tandem rockets due to ignition of either rocket. A conical deflector deflects gases from the fore rocket to vent holes, sealing off the forward interior part to provide an isolating chamber for the fore rocket.

Jet diverting equipment (2,871,656). W. E. P. Johnson, Hempstead, London, England, assignor to Power Jets (Research & Development) Ltd.

Pair of pivotably mounted diversion members at the discharge end of the jet nozzle. A thermocouple is mounted with its hot junction in the air intake; another is mounted at a position where heating of the aircraft structure by the diverted jet can occur. Linkages control the movement of the members.

Explosively released nut (2,871,750). N. C. Parrish, Redondo Beach, Calif., assignor to Northrop Aircraft, Inc.

Breakaway attachment and fastening element. An explosive charge in a cavity may be detonated when desired by means of a pair of electrical leads terminating in the cavity.

Devices for measuring the temperature of a flame (2,871,759). A. G. L. Moutet, Villaine par Massy, France, assignor to ONERA Society.

Measurement of the radiant energy emitted by a given area of flame alone, and comparison with a source of radiation of known and constant energetic brightness.

Dropping mechanism (2,871,597). P. E. Yost, Hugo, Minn., assignor to General Mills, Inc.

Load releasing device for a balloon. Load units spaced around a circular member mounted on a support, and severing means for releasing individual load units.

Rocket (2,872,131). M. E. Lattmann, Zurich, Switzerland, assignor to Contraves AG.

Rocket guided by a high-frequency signal ray. Receiving and transforming devices for the signals produce two electrical voltages, the variable instantaneous values of which determine the distance of the CG of the rocket from the axis of the ray.

Device for decelerating the sinking speed of a dropped load (2,872,138). R. Vogt, Pacific Palisades, assignor to Aerophysics Development Corp.

Rocket secured to a support above a load, its exhaust directed downward. Plates deflect portions of the load laterally. Angles of plates may be varied to cause corresponding variation in the magnitude of the vertical thrust component.

Rocket and launching mechanism (2,871,762). E. Schmued, Los Angeles, Calif., assignor to Northrop Aircraft, Inc.

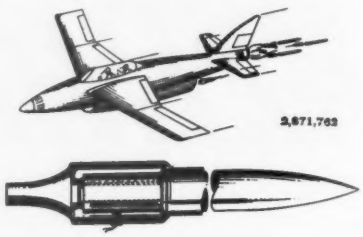

Means for controlling a finless rocket to have maximum stability as it leaves the launcher in a spinning condition without reducing the propulsive power, or causing loss of range. Spin is imparted in the launching tube by a source of power apart from the rocket.

Oxidized chromium-alumina metal ceramic protective tube (2,872,724.) L. A. Conant, Tonawanda, N. Y., assignor to Union Carbide Corp.

Sintered ceramic having a combined chromium and alumina content constituting 62.8 per cent (by weight). To increase resistance to penetration by molten metals, a metal oxide having an electrical resistance of 100 megohms is coated on the surfaces.

Pulse jet engine with acceleration chamber (2,872,780). P. Schmidt, Munich, Germany.

Chamber having an outlet end subdivided by walls aligned with the flow direction, and covered with material absorbing sound and shock waves. Air admitted at the front end passes solely through the combustion and acceleration chambers.

Liquid fuel control for jet engines (2,872,784). O. N. Laurence, Dorridge, England, assignor to Joseph Lucas (Industries) Ltd.

Means for preventing a temporary excess supply of fuel to an engine during acceleration. A liquid operated servomechanism controls the rate of fuel supply.

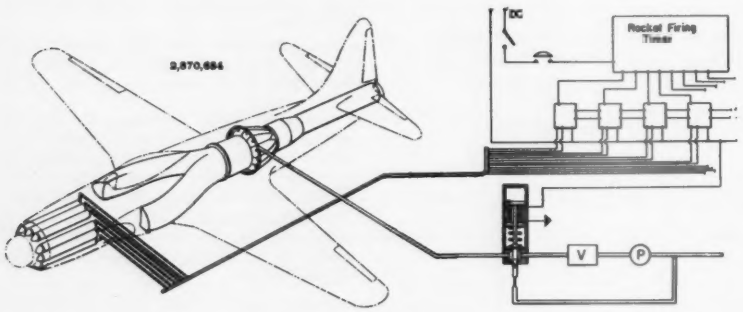

Turbine engine blow-out preventer (2,870,684). C. L. Johnson, Encino, Calif., assignor to Lockheed Aircraft Corp.

System to prevent interruption of turbine engine operation by the induction of high temperature gases released upon firing large caliber armament. Fuel flow is automatically reduced at the same rate as the air mass flow is reduced, thereby maintaining fuel-air ratio to assure stable combustion.

Technical Literature Digest——

M. H. Smith, *Associate Editor*, and **M. H. Fisher**, *Contributor*
The James Forrestal Research Center, Princeton University

Jet Propulsion Engines

Modified Tubular Combustors as High-temperature Gas Generators, by Robert Friedman and Eugene V. Zettle, *NACA Res. Mem.* E55H25, Oct. 1955, 17 pp. (Declassified from Confidential by authority of *NASA Pub. Announcement* 1, p. 15, 11/14/58.)

Experimental Determination of Gas Motion Accompanying Screeching Combustion in a 6-inch Simulated Afterburner, by Perry L. Blackshear, Warren D. Rayle and Leonard K. Tower, *NACA Res. Mem.* E53I28, Dec. 1953, 63 pp. (Declassified from Confidential by authority of *NASA Pub. Announcement* 1, p. 12, 11/14/58.)

Some Screeching-combustion Characteristics of a Transpiration-cooled Afterburner Having a Porous Wall of Wire Cloth, by William K. Koffel, James L. Harp Jr. and Lively Bryant, *NACA Res. Mem.* E54H27, Nov. 1954, 12 pp. (Declassified from Confidential by authority of *NASA Pub. Announcement* 1, p. 13, 11/14/58.)

Effects of Variations in Combustion-chamber Configuration on Ignition Delay in a 50-pound-thrust Rocket, by Dezso J. Ladanyi, *NACA Res. Mem.* E56F22, Oct. 1956, 53 pp. (Declassified from Confidential by authority of *NASA Pub. Announcement* 1, p. 16, 11/14/58.)

An Analysis of Ramjet Engines Using Supersonic Combustion, by Richard J. Weber and John S. MacKay, *NACA TN* 4386, Sept. 1958, 49 pp.

Application of Well Stirred Reactor Theory to the Prediction of Combustor Performance, by Allan Hardy Bonnell, *Proj. Squid, Tech. Rep.*, MIT-18-T (MIT, D.Sc. Thesis), 1958, 238 pp.

Atmosphere Breathing Engines in Astronautics, by S. W. Greenwood and D. S. Carton, *Cranfield Coll. of Aeron., Note* 88, Oct. 1958, 17 pp.

Hydrostatic Gas Bearings, by John H. Laub, *Calif. Inst. Techn., Jet Prop. Lab., Progr. Rep.* 20–353, Oct. 1958, 16 pp.

A Rapid Method for Calculating the "Off Design" Performance of Compressors and Turbines, by J. H. Horlock, *Aeron. Quart.*, vol. 9, Nov. 1958, pp. 346–360.

Measurements of Rocket Exhaust-gas Temperatures, by I. Warshawsky, *Instr. Soc. of America J.*, vol. 5, Nov. 1958, pp. 91–97.

Hydro-rockets for Underwater Propulsion, by G. Partel, *Fusées et Recherche Aéron*, vol. 3, no. 2, July 1958, pp. 59–64. (In French.)

Heat Transfer and Fluid Flow

Approximate Formula for the Thermal Conductivity of Gas Mixtures, by E. A. Mason and S. C. Saxena, *Phys. Fluids*, vol. 1, no. 5, Sept.-Oct. 1958, pp. 361–369.

Properties of Gases at Very High Temperatures, by I. Amdur and E. A. Mason, *Phys. Fluids*, vol. 1, no. 5, Sept.-Oct. 1958, pp. 370–383.

Criteria for Thermodynamic Equilibrium in Gas Flow, by Morton Rudin, *Phys. Fluids*, vol. 1, no. 5, Sept.-Oct. 1958, pp. 384–392.

Plasma Heating of Supersonic Airstreams, by Raymond L. Chuan, *Phys. Fluids*, vol. 1, no. 5, Sept.-Oct. 1958, pp. 452.

Some Examples of Turbulent Diffusion in Liquid Metals, by A. Paoletti and M. Vincentini, *Phys. Fluids*, vol. 1, no. 5, Sept.-Oct. 1958, pp. 453–454.

Energy Content and Ionization Level in an Argon Gas Jet Heated by a High Intensity Arc, by Gordon L. Cann and Adriano C. Ducati, *J. Fluid Mech.*, vol. 4, Sept. 1958, pp. 529–541.

Vaporization into a Hypersonic Laminar Boundary Layer, by Sinclaire M. Scala, *J. Aero/Space Sci.*, vol. 25, Oct. 1958, pp. 655–656.

Magnetogasdynamics of Hypersonic Couette Flow, by Z. O. Bleviss, *J. Aero/-Space Sci.*, vol. 25, Oct. 1958, pp. 601–615.

Transport Phenomena in Completely Ionized Gas Considering Electron-Electron Scattering, by M. S. Sodha and Y. P. Varshni, *Phys. Rev.*, vol. 111, no. 5, Sept. 1, 1958, pp. 1203–1205.

A Theory of the Cylindrical Ejector Supersonic Propelling Nozzle, by H. Pearson, J. B. Holliday and S. F. Smith, *J. Roy. Aeron. Soc.*, vol. 62, Oct. 1958, pp. 746–751.

Momentum and Mass Transfer by Eddy Diffusion in a Wetted-wall Channel, by A. M. Dhanak, *AIChE J.*, vol. 4, June 1958, pp. 190–196.

Flow Against a Vertical Plate with Large Suction, by J. R. Foote, *J. Aeron. Sci.*, vol. 25, July 1958, pp. 462–463.

Preliminary Experimental Investigation of Transpiration Cooling for an Afterburner with a Sintered, Porous Stainless Steel Combustion Chamber Wall, by W. K. Koffel, *NACA RM* no. E53D08, June 1953, 47 pp. (Declassified by authority of *NACA Res. Abstr.* no. 128, 5/2/58, p. 28.)

Analysis of a Transpiration-cooled Hemisphere-cylinder, by C. J. Scott, *J. Aeron. Sci.*, vol. 25, June 1958, p. 397.

Exploratory Tests of Transpiration Cooling of a Porous 8° Cone at M = 2.05 Using Nitrogen Gas, Helium Gas and Water as the Coolants, by L. T. Chauvin and H. S. Carter, *NACA RM* no. L55C29, June 1955, 22 pp. (Declassified by authority of *NACA Res. Abstr.* no. 126, 5/2/58, p. 35.)

Transition from Laminar to Turbulent Shear Flow—A Review of Some Recent Advances in its Understanding, by M. W. Morkovin, *Trans. ASME*, vol. 80, July 1958, pp. 1121–1128.

Mixing and Chemical Reaction in the Laminar Wake of a Flat Plate, by S. I. Cheng and A. A. Kovitz, *J. Fluid Mech.*, vol. 4, May 1958, pp. 64–70.

Partition of Energy in Hydromagnetic Turbulence, by S. Chandrasekhar, *Annals of Phys.*, vol. 2, Dec. 1957, pp. 615–626.

Measurements of Total Hemispherical Emissivity of Various Oxidized Metals at High Temperature, by W. R. Wade, *NACA TN* no. 4206, March 1958, 42 pp.

EDITOR'S NOTE: Contributions from Professors E. R. G. Eckert, J. P. Hartnett, T. F. Irvine Jr. and P. J. Schneider of the Heat Transfer Laboratory, University of Minnesota, are gratefully acknowledged.

Composition and Thermodynamic Properties of Air in Chemical Equilibrium, by W. E. Moeckel and K. C. Weston, *NACA TN* no. 4265, April 1958, 39 pp.

Approximations for the Thermodynamic and Transport Properties of High Temperature Air, by C. F. Hansen, *NACA TN* no. 4150, March 1958, 67 pp.

Boundary Layer Along Annular Walls in a Swirling Flow, by H. Yeb, *Trans. ASME*, vol. 80, May 1958, pp. 767–776.

Some Further Results on the Benard Problem, by W. H. Reid and D. L. Harris, *Phys. Fluids*, vol. 1, March-April 1958, pp. 102–110.

The Laminar Free-convection Heat Transfer from the Outer Surface of a Vertical Circular Cylinder, by K. Millsaps and K. Pohlhausen, *J. Aeron. Sci.*, vol. 25, June 1958, pp. 357–360.

Experimental Study of Thermal Convection in Rotating Liquid, by R. Hide, *Roy. Soc., London, Phil. Trans.* vol. A 250, July 31, 1958, pp. 441–478.

Flow of a Viscous Liquid on a Rotating Disk, by A. E. Emslie, T. F. Bonner and L. G. Peck, *J. Appl. Phys.*, vol. 29, May 1958, pp. 858–862.

A New Method for the Production of Plasma for Ion Sources, by A. Ziegler, *Zeit. Angew. Phys.*, vol. 10, April 1958, pp. 185–186. (In German.)

A Study of Temperature Measurement in a Solar Furnace, by B. B. Brenden, H. W. Newkirk Jr. and S. H. Woodcock, *Solar Energy*, vol. 2, Jan. 1958, pp. 13–17.

On Heat Transfer from the Condensation of Steam in the Presence of Inert Gases, by J. Madjeski, *Chemie-Ingenieur-Technik*, vol. 29, Dec. 1957, pp. 801–813. (In German.)

Heat Transfer in Film Condensation, by E. Baer and J. M. McKelvey, *AIChE J.*, vol. 4, June 1958, pp. 218–222.

Forced Convection for Gas Flow Normal to Circular Cylinder; Influence of Large Temperature Difference, by W. M. Kays, *Stanford Univ., Dept. Mech. Engng. TR* no. 35, June 1, 1958, 26 pp.

Transitional Correction to the Drag of a Sphere in Free Molecule Flow by R. M. L. Baker Jr. and A. F. Charwat, *Phys. Fluids*, vol. 1, March-April 1958, pp. 73–81.

Calculation of the Thermal Conductivity of Porous Media, by W. Woodside, *Canadian J. Phys.*, vol. 36, July 1958, pp. 815–823.

On One-dimensional Temperature Distribution in Two-layered Slabs with Contact Resistance at the Plane of Contact, by P. Seide, *J. Aeron. Sci.*, vol. 25, Aug. 1958, pp. 523–524.

Heat Transfer to Water in Turbulent Flow in Internally Heated Annuli, by R. P. Stein and W. Begell, *AIChE J.*, vol. 4, June 1958, pp. 27–31.

Steady Laminar Heat Transfer in Circular Tube with Prescribed Wall Heat Flux, by R. Siegel, E. M. Sparrow and T. M. Hallman, *Appl. Sci. Res.*, Section A, vol. 7, no. 5, 1958, pp. 386–392.

Heat Transfer in Swirling Laminar Pipe Flow, by R. Siegel and M. Perlmutter, *J. Appl. Mech.*, vol. 25, June 1958, pp. 295–297.

Correlation of Turbulent Heat Transfer in a Tube for the Dissociating System $N_2O_4 \rightleftarrows 2NO_2$, by R. S. Brokaw, *NACA RM* no. E57K19a, March 1958, 17 pp.

On Thermometer with Recovery Factor r Greater Than 1, by J. A. Rietdijk and A. Valstar, *Appl. Sci. Res.*, Section A, vol. 7, no. 4, 1958, pp. 251–355.

On Heat Transfer in Slip Flow, by S. H. Maslen, *J. Aeron. Sci.*, vol. 25, June 1958, pp. 400–401.

Note on the Stabilizing Effect of Centrifugal Forces on the Laminar Boundary Layer over Convex Surfaces, by L. Lees, *J. Aeron. Sci.*, vol. 25, June 1958, pp. 407–408.

On Hypersonic Stagnation-point Flow with a Magnetic Field, by N. H. Kemp, *J. Aeron. Sci.*, vol. 25, June 1958, pp. 405–407.

Prandtl-Meyer Expansion of Chemically Reacting Gases in Local Chemical and Thermodynamic Equilibrium, by S. P. Heims, *NACA TN* no. 4229, April 1958, 54 pp.

Evaporation, Heat Transfer, and Velocity Distribution in Two-dimensional and Rotationally Symmetrical Laminar Boundary Layer Flow, by N. Frössling, *NACA Tech. Mem.* no. 1432, Feb. 1958, 37 pp.

Periodic Boundary Layer Experiments in Liquid Helium, by R. J. Donnelly and A. C. H. Hallett, *Annals of Phys.*, vol. 3, March 1958, pp. 320–345.

Analysis of Turbulent Flow and Heat Transfer in a Flat Plate at High Mach Numbers with Variable Fluid Properties, by R. G. Diessler and A. I. Loeffler Jr., *NACA TN* no. 4262, April 1958, 61 pp.

Summary of Experimental Heat Transfer Measurements in Turbulent Flow for a Mach Number Range from 0.87 to 5.05, by M. J. Brevoort and B. D. Arabian, *NACA TN* no. 4248, May 1958, 43 pp.

Effect of Distributed Granular Type Roughness on Boundary Layer Transition at Supersonic Speeds with and without Surface Cooling, by A. L. Braslow *NACA RM* no. L58A17, March 10, 1958, 22 pp.

The Effect of Gas Properties on the Heat Transfer in Stagnation Flows, by I. E. Beckwith, *J. Aeron. Sci.*, vol. 25, Aug. 1958, pp. 533–534.

Fundamental Solutions for Heat Transfer from Nonisothermal Flat Plates, by Donald C. Baxter and W. C. Reynolds, *J. Aeron. Sci.*, vol. 25, June 1958, pp. 403–404.

New Method of Flow Visualization for Low-density Wind Tunnels, by R. A. Evans, *J. Appl. Phys.*, vol. 28, Sept. 1957, pp. 1005–1010.

An Approximate Analytical Method for Studying Entry into Planetary Atmospheres, by D. R. Chapman, *NACA TN* no. 4276, May 1958, 101 pp.

Two-dimensional Effects in Gaseous Detonation Waves, by James A. Fay and Gerhard Opel, *J. Chem. Phys.*, vol. 29, Oct. 1958, pp. 955–956.

Combustion, Fuels and Propellants

Effect of Pressure and Duct Geometry on Bluff-body Flame Stabilization, by Andrew E. Potter Jr. and Edgar L. Wong, *NACA TN* 4381, Sept. 1958, 31 pp.

Identification of Ions in Flame and Measurement of Their Concentration, by A. van Tiggelen, J. Deckers, J. Poncelet and R. Berendsen, *Univ. of Louvain, Lab. for Inorg. and Analyt. Chem., Tech. (Scientific) Note* 1, March 1958, 43 pp.

Preliminary Study of the Light Scattering Technique for Determination of Size Distributions in Burning Sprays, by D. A. Dobbins, *Princeton Univ., Dept. Aeron. Engng., Rep.* 430 (*AFOSR TN* 58–822; *ASTIA AD* 202906), July 1958, 54 pp.

Some Effects of High-energy Fuels on Aircraft Performance, by Abraham Hyatt, *Aero/Space Engng.*, vol. 17, Nov. 1958, pp. 45–50.

Thermal Conductivity of Liquid Ozone, by Thomas E. Waterman, Donald P. Kirsh and Robert I. Brabets, *J. Chem. Phys.*, vol. 29, Oct. 1958, pp. 905–908.

Present Status of Detonation Theory, by W. W. Wood and J. G. Kirkwood, *J. Chem. Phys.*, vol. 29, Oct. 1958, pp. 957–958.

Precision Flash X-Ray Determination of Density Ratio in Gaseous Detonations, by Russell E. Duff, Herbert T. Knight and John P. Rink, *Phys. Fluids*, vol. 1, no. 5, Sept.-Oct. 1958, pp. 393–398.

Transition from Slow Burning to Detonation in Gaseous Explosives, by Frederick J. Martin, *Phys. Fluids*, vol. 1, no. 5, Sept.-Oct. 1958, pp. 399–407.

Effect of Pressure on Ion Formation in Propane Air Flames, by I. R. King, *Proj. Squid, Tech. Rep.* EXP-7-P (*ASTIA AD* 159256), May 1958, 5 pp. (Available only on microcards.)

A Study of the Kinetics of the Hydrogen Oxygen Reaction in a New Flow Reactor, by Rudolph J. Swigart, *Princeton Univ., Dept. Aeron. Engng., Rep.* 432, Aug. 1958, 58 pp., 23 figs. (MSE Thesis.)

Carbon Disulfide Flames Influence on Moisture, by G. J. Gibbs, I. R. King, and H. F. Calcote, *Experiment Inc.*, CF 2264 (TM-642), May 1954, 27 pp.

Effect of Fuel Drop Size and Injector Configuration on Screaming in a 200-pound-thrust Rocket Engine Using Liquid Oxygen and Heptane, by Charles E. Feiler, *NACA Res. Mem.* E58A20a, June 1958, 27 pp. (Declassified from Confidential by authority of *NACA Res. Abstr.* 130, p. 25, 9/30/58.)

Effect of Fuels on Screaming in 200-pound-thrust Liquid-oxygen–fuel Rocket Engine, by Isaac Pass and Adelbert O. Tischler, *NACA Res. Mem.* E56C10, June 1956, 25 pp. (Declassified from Confidential by authority of *NACA Res. Abstr.* 130, p. 25, 9/30/58.)

Application of Well Stirred Reactor Theory to the Prediction of Combustor Performance, by Allen Hardy Bonnell, *Proj. Squid, Tech. Rep.* MIT-18-T (*ASTIA AD* 200821), Aug. 1958, 58 pp. (Available only on microcards.)

The Effects of Several Composition Factors on the Burning Rate of an Ammonium Perchlorate Solid Propellant, by Harold J. Taback, *Princeton Univ., Dept. Aeron. Engng., Rep.* 429, Sept. 1958, 68 pp., 34 figs. (MSE Thesis.)

Aluminum Borohydride-Hydrocarbon Mixtures as a Source of Ignition for a Turbojet Combustor, by Hampton H. Foter, Edward A. Fletcher and David M. Straight, *NACA Res. Mem.* E54K12, Feb. 1955, 24 pp. (Declassified from Confidential by authority of *NACA Res. Abstr.* 130, p. 24, 9/30/58.)

Introductory Study to Aerothermochemistry, by L. G. Napolitano, *L'Aerotecnica*, vol. 38, no. 2, April 1958, pp. 96–108. (In Italian.)

Kinetics of the Thermal Reactions of Ethylene, by George Dahlgren Jr. and John E. Douglas, *J. Amer. Chem. Soc.*, vol. 80, Oct. 5, 1958, pp. 5108–5110.

Numerical Calculation of the Temperature Rise in Ignition by Hot Wires, by H. L. Selberg and C. H. Johansson, *Arkiv für Fysik*, vol. 13, no. 5, 1958, pp. 423–427. (In English.)

Hydroxyl Concentrations in Rich Hydrogen-air Flames Held on Porous Burners, by W. E. Kaskan, *Combustion and*

Flame, vol. 2, Sept. 1958, pp. 229–243.

The Spontaneous Ignition of Alkyl Silanes, by S. T. Griffiths and R. R. Wilson, *Combustion and Flame*, vol. 2, Sept. 1958, pp. 244–252.

The Flashback of Laminar and Turbulent Burner Flames at Reduced Pressure, by B. Fine, *Combustion and Flame*, vol. 2, Sept. 1958, pp. 253–266.

Formation of Polycyclic Hydrocarbons in Diffusion Flames, by J. R. Arthur, B. T. Commins, J. A. S. Gilbert, A. J. Lindsey and D. H. Napier, *Combustion and Flame*, vol. 2, Sept. 1958, pp. 267–272.

Use of the Constant-volume Bomb Technique for Measuring Burning Velocity, by R. C. Eachenbach and J. T. Agnew, *Combustion and Flame*, vol. 2, Sept. 1958, pp. 273–285.

The Concentration of Hydroxyl and of Oxygen Atoms in Gases from Lean Hydrogen-air Flames, by W. E. Kaskan, *Combustion and Flame*, vol. 2, Sept. 1958, pp. 286–304.

A Note on Spalding's Centroid Formula, by J. Menkes, *Combustion and Flame*, vol. 2, Sept. 1958, pp. 328–330.

Note on Monocromatic Radiation Pyrometry for Measuring Flame and Exhaust Gas Temperatures, by R. H. Tourin and M. Grossman, *Combustion and Flame*, vol. 2, Sept. 1958, pp. 330–332.

Rocket Working Fluids. Hydrogen and Helium, by R. L. Potter, G. E. Guffner and T. F. Reinhardt, *Ind. & Engng. Chem.*, vol. 50, Oct. 1958, pp. 1557–1560.

Screw Extrusion Theory with Application to Double-base Propellant, by M. L. Jackson, F. J. Lavacot and H. R. Richards, *Ind. & Engng. Chem.*, vol. 50, Oct. 1958, pp. 1569–1576.

Ignition Limits of the Gaseous System Isopropyl Alcohol-Oxygen-Nitrogen, by Harry Sello, *Ind. & Engng. Chem.*, vol. 50, Oct. 1958, pp. 1561–1564.

Generalized Thermodynamic Properties of Diatomic and Triatomic Gases, by B. E. Saltzman, *Ind. & Engng. Chem.*, vol. 50, Oct. 1958, pp. 1593–1598.

Gaseous Detonations, XI, Double Waves, by Mark Cher and G. B. Kistiakowsky, *J. Chem. Phys.*, vol. 29, Sept. 1958, pp. 506–511.

The Development of a New Erosive Burning Law, by G. Robillard and J. M. Lenoir, *Calif. Inst. Tech., Jet. Prop. Lab., Publication* 91, April, 1957, 27 pp.

Screaming Tendency of the Gaseous-hydrogen-liquid-oxygen Propellant Combination, by Louis Baker Jr. and Fred W. Steffen, *NACA Res. Mem.* E58E09, Sept. 1958, 24 pp.

Phase Behavior in the Nitrogen Ammonia System, by H. H. Reamer and B. H. Sage, *Calif. Inst. Tech., Jet Prop. Lab., Progr. Rep.* 20–358, July 1958, 6 pp.

Temperature Gradient Tests of Inert Propellant Grains, by James F. Wiedman, *Redstone Arsenal, Ordn. Missile Labs., Rep.* 3M78N10, Aug. 1958, 4 pp, 23 figs.

Determination of Temperature Gradients in Solid Propellant Grains by Use of Scale Models, by Myron L. Cohen, *Redstone Arsenal, Ordn. Missile Labs., Rep.* 3R5F, July 1958, 67 pp.

The Thermal Decomposition of Liquid Nitric Acid, II, by H. F. Cordes, N. R. Fetter and J. A. Happe, *J. Amer. Chem. Soc.*, vol. 80, Sept. 20, 1958, pp. 4802–4805.

Free Radicals for High Energy Fuels, by D. E. Carr, H. M. Fox and E. D. Guth, *Aviation Age*, vol. 30, Oct. 1958, pp. 22–23, 191.

Homogeneous Catalysis for Homogeneous Reactors, Catalysis of the Reaction Between Hydrogen and Oxygen, by H. F. McDuffie, E. L. Compere, H. H. Stone, L. F. Woo and C. H. Secoy, *J. Phys. Chem.*, vol. 62, Sept. 1958, pp. 1030–1035.

An Analytical Study of Turbulent and Molecular Mixing in Rocket Combustion, by David A. Bittker, *NACA TN* 4321, Sept. 1958, 22 pp.

Mass Analysis of Flames and Flue Gases, by E. A. Bunt, *Univ. of Witwatersrand, Dept. Mech. Engng., Rep.* 2758, June 1958, 43 pp.

Propellant Vaporization as a Criterion for Rocket-engine Design; Calculations of Chamber Length to Vaporize Various Propellants, by Richard J. Priem, *NACA TN* 3883, Sept. 1958, 36 pp.

Study of Explosive Sensitivity of Cobalt Amine Complexes, by Taylor B. Joyner, *NAVORD Rep.* 5639, Oct. 1957, 13 pp.

Oxidation of 1,1-Dialkylhydrazines-chromatographic Separation and Ultraviolet Analysis of Some Tetraalkyltetrazenes, by Everett M. Bens and William R. McBridge, *NAVORD Rep.* 5879 (*NOTS* 2016), June 1958, 34 pp.

Molecular Structure and Infrared Spectrum of Nitrotrichloromethane, by Alexander H. Castelli, *Picatinny Arsenal, Feltman Res. and Engng. Labs., Tech. Rep.* 2537, Aug. 1958, 13 pp.

A High Rate Tension Tester, by Stephen Strella, Mitchel Chmura, Benjamin Holman and Harry Sigler, *Picatinny Arsenal, Feltman Res. and Engng. Labs., Tech. Rep.* 2487, Aug. 1958, 12 pp.

Rate of Reaction of Gaseous Fluorine with Water Vapor at 35°C, by Vernon A. Slabey and Edward A. Fletcher, *NACA TN* 4374, Sept. 1958, 16 pp.

Study of Combustion by Cinespectroscopy (Plenary Conference), by R. G. W. Norrish, *Inst. Francais du Petrole, Revue et Ann. Combustibles Liquides*, vol. 8, April 1958, pp. 313–332. (In French.)

Inhibition in the Gaseous Phase of Combustion of Carbon Oxides, I: The Phenomenon of Flames Long Retarded and Its Application to the Determination of the Kinetic Constants of Combustion Reactions, by H. James; **II: The Character of the Phenomenon of Inhibition by Ammonia,** by H. James and P. Lafitte, *Inst. Francais du Petrole, Revue et Ann. Combustibles Liquides*, vol. 8, April, pp. 338–358. (In French.)

A Method of Extracting Ions in Flames, by J. Deckers and A. Van Tiggden, *Inst. Francais du Petrole, Revue et Ann. Combustibles Liquides*, vol. 8, April 1958, pp. 349–358. (In French.)

Study of Oxidation of Hydrocarbons in Extremely Rigorous Experimental Conditions, by Z. G. Szabo and D. Gal, *Inst. Francais du Petrole, Revue et Ann. Combustibles Liquides*, vol. 8, April 1958, pp. 414–427. (In French.)

Thermal Aspects of the Combustion at Low Temperature of *n*-Pentane-Oxygen Mixtures, by R. Ben Aim and M. Lucquin, *Inst. Francais du Petrole, Revue et Ann. Combustibles Liquides*, vol. 8, April 1958, pp. 438–442. (In French.)

Flames of Mixtures of Hydrazine with Oxygen, Nitrous Oxide and Nitric Oxide, by P. Gray and J. C. Lee, *Inst. Francais du Petrole, Revue et Ann. Combustibles Liquides*, vol. 8, April 1958, pp. 443–450. (In French.)

Flame Propagation in Mixtures of Hydrazine, by S. deJaegere and A. Van Tiggelen, *Inst. Francais du Petrole, Revue et Ann. Combustibles Liquides*, vol. 8, April 1958, pp. 451–456.

Analysis of the Decomposition Products of Hydrazine, by G. Pannethier, H. Guenebaut and R. de Hartoulari, *Inst. Francais du Petrole, Revue et Ann. Combustibles Liquides*, vol. 8, April 1958, pp. 457–465. (In French.)

Burning of Gaseous Combustibles with Nitric Oxide, by G. K. Adams and G. W. Stocks, *Inst. Francais du Petrole, Revue et Ann. Combustibles Liquides*, vol. 8, April 1958, pp. 483–490. (In French.)

Burning-rate Studies, Part 7: Onset of Turbulent Combustion of Liquids Contained in Small Tubes, by A. Greenville Whittaker, T. M. Donovan and H. Williams, *J. Phys. Chem.*, vol. 62, no. 8, Aug. 1958, pp. 908–911.

The Theoretical Study of the Florine Molecule, by J. Eve, *Proc. Roy Soc.*, vol. 246A, no. 1247, Aug. 26, 1958, pp. 582–591.

Problems of Continuous Combustion in Aviation Engines, by A. Capetti, *L'Aerotecnica*, vol. 38, no. 1, Feb. 1958, pp. 3–7. (In Italian.)

Stabilization of Flames in Airbreathing Jet Engines, by F. Filippi, *L'Aerotecnica*, vol. 38, no. 1, Feb. 1958, p. 19–28. (In Italian.)

Liquid Propellants for Rockets, by L. Macioce, *L'Aerotecnica*, vol. 38, no. 1, Feb. 1958, p. 44–47. (In Italian.)

The Indication of the Specific Fuel Consumption of Turbojets, by P. Formentini, *L'Aerotecnica*, vol. 38, no. 1, Feb. 1958, pp. 39–43. (In Italian.)

Theoretical Investigation on the Fluid Dynamics of "Wave Engines" Operating according to the Principle of the "Comprex," by Dino Dini, *L'Aerotecnica*, vol. 38, no. 1, Feb. 1958, pp. 8–18. (In Italian.)

Aerodynamics of Jet Propelled Missiles

Drag Transformation and Reduction for Bodies of Revolution, by Roger P. Johnson, *Rand Corp., Res. Mem.* RM-2107 (*ASTIA AD* 156008), Aug. 1957, 73 pp.

Life of Slender Nose Shapes According to Newtonian Theory, by J. D. Cole, *Rand Corp., Paper* P-1270, Feb. 1958, 18 pp.

On the Problem of a Streamlined Profile in a Near Sonic Flow, by A. F. Kryuchin, *Rand Corp., Translation* T-74 (translation from *USSR Acad. Sci., Inst. Mech., Appl. Math. and Mech.*, vol. 18, 1954), Aug. 1957, 25 pp.

The High Speed Flow of Gas around Blunt Bodies, by Hyman Serbin, *Rand Corp., Paper* P-1172, Sept. 1957, 31 pp.

Materials of Construction

New Plasma Tools Handle Ultra-hard Metals, by Peer Fossen, *Missiles and Rockets*, vol. 4, Dec. 22, 1958, pp. 26–27.

Falcon Airframe Uses Die Casting, Magnesium Structure, by Irwin Stambler, *Space/Aeron.*, vol. 30, Dec. 1958, pp. 18–19.

Aeroelastic Problems Associated with High Speeds, and High Temperature, by E. G. Broadbent, *J. Roy. Aeron. Soc.*, vol. 62, Dec. 1958, pp. 867–883.

Methods of Protecting Reaction Motor Materials under Unstable Combustion Conditions, by B. Langenecker, *Fusées et Récherche Aéron.*, vol. 3, no. 2, July 1958, pp. 77–85. (In French.)

Thermal Stresses in Plates, by M. J. Forray, *J. Aero/Space Sci.*, vol. 25, Nov. 1958, pp. 716–717.

Behavior of Transparent Plastics under Thermal Shock, by Kh. Iablokoff and M. Hediard, *La Récherche Aéron.*, no. 66, Sept.-Oct. 1958, pp. 35–42. (In French.)

Instrumentation, Data Recording, Telemetering

The Constant Current Hot Wire Anemometer in Subsonic Compressible Flows, by D. I. Paddison, *Brown Univ., Div. Engng., Tech. Rep.* WT-29 (*AFOSR-TN-58-713; ASTIA AD* 162248), 1958, 37 pp.

Chronograph Error in Drag Measurements, by G. D. Kahl and F. D. Bennett, *Aberdeen Proving Ground, Ball Res. Labs., Mem. Rep.* 1161, Aug. 1958, 15 pp.

Static Calibration of Pressure and Force Gages (Joint Army Navy Air Force Solid Propellant Static Test Panel), *Solid Propellant Info. Agency,* Aug. 1958, 28 pp.

High Speed Framing Disc Camera, by C. H. Bagley, *Stanford Res. Inst., Poulter Labs., Tech. Rep.* 015-58, April 1958, 11 pp.

New Possibilities in the Design of Vibration Measuring Apparatus, by C. V. Basel, *Archiv für Tech. Messen,* no. 273, Oct. 1958, pp. 201–204. (In German.)

The Application of a Magnus Effect Flow Meter as a Laboratory Teaching Device, by Wesley J. Trathen, *Gen. Motors Engng. J.,* vol. 5, Oct.-Dec. 1958, pp. 12–15.

Manometric Pressure Measurement, by R. J. Cartier, *Instr. and Automation,* vol. 31, Dec. 1958, pp. 1980–1982.

Electronic Density Probe, by William G. Burt Jr., *Instr. and Automation,* vol. 31, Dec. 1958, pp. 1983–1984.

Proceedings, Conference on Radio Interference Reduction, 3d, Feb. 26–27, 1957, *Illinois Inst. Tech., Armour Res. Found.* (sponsored by Army Signal Engng. Labs.), Feb. 1957, 503 pp.

Pressure Probes Selected for Three Dimensional Flow Measurements, by D. W. Bryer, D. E. Walshe and H. C. Garner, *Gt. Brit., Aeron. Res. Council, Rep. and Mem.* 3037 (formerly *ARC Tech. Rep.* 3037), 1958, 26 pp.

A Survey of New Developments in Pressure Measuring Techniques in the NACA, by John Dimeff, *NATO, AGARD, Rep.* 166, March 1958, 25 pp.

Tests on Deflection of Flat Oval Bourdon Tubes, by G. Kardos, *ASME, Paper* 58-A-67, Nov. 1958, 6 pp.

Theory of High Pressure Bourdon Tubes, by W. Wuest, *ASME, Paper* 58-A-119, Nov. 1958, 12 pp. (*Ing. Arch.,* vol. 24, 1956, pp. 92–110.)

Pressure Pick Ups and Miniature Manometers Usable in Wind Tunnels and in Flight, by M. Bassière, *NATO, AGARD, Rep.* 173, March 1958, 18 pp. (In French.)

Electromagnetic Flowmeter Primary Elements, by V. P. Head, *ASME, Paper* 58-A-126, Nov. 1958, 7 pp.

Multi-variable Function Generator, by Thomas J. Kelley, *Instr. and Automation,* vol. 31, Nov. 1958, p. 1819.

Who Uses Medium-Size Computers, by Phyllis Huggins, *Instr. and Automation,* vol. 31, Nov. 1958, pp. 1827–1831.

Mathematical Elements for Analog Computers, by Charles Lax and Phillip I. Rafield, *Instr. and Automation,* vol. 31, Nov. 1958, pp. 1832–1833.

Pressure Transducers for Missile Test- and Control, by Yao Tzu Li, *ISA J.* (Instr. Soc. America), vol. 5, Nov. 1958, pp. 81–84.

Evolution of Test-range Instrumentation, by Dr. Joachim W. Muehlner, *ISA J.* (Instr. Soc. America), vol. 5, Nov. 1958, pp. 85–90.

Calibration of High-frequency-response Pressure Transducers, by Ralph Bowersox, *ISA J.* (Instr. Soc. America), vol. 5, Nov. 1958, pp. 98–103.

Magnetic Tape Storage of Telemetry Data, by Kenneth A. Hall, *ISA J.* (Instr. Soc. America), vol. 5, Nov. 1958, pp. 104–106.

Optical Instrumentation—Obsolescence or Revival, by Alexis B. Dember, *ISA J.* (Instr. Soc. America), vol. 5, Nov. 1958, pp. 107–113.

Review of High-temperature Immersion Thermal Sensing Devices for In-flight Engine Control, by Victor D. Sanders, *Rev. Sci. Instr.,* vol. 29, Nov. 1958, pp. 917–928.

High Speed Multiple-spark Light Source, by Merle R. Wilson and Richard J. Hiemenz, *Rev. Sci. Instr.,* vol. 29, Nov. 1958, pp. 949–950.

Microcomparator Illuminations System for Improved Resolution of Rayleigh Diffusionmeter Diagrams, by J. L. Oncley, M. Ludwig and T. E. Thompson, *Rev. Sci. Instr.,* vol. 29, Nov. 1958, pp. 985–987.

Convection Free Instrument for Measuring Infrared Radiation in the Atmosphere, by Robert L. Aagard, *Rev. Sci. Instr.,* vol. 29, Nov. 1958, pp. 1011–1015.

Temperature Error Associated with Imbedded Thermocouples, by A. R. Thomas, B. Schurin and J. C. Morris, *Rev. Sci. Instr.,* vol. 29, Nov. 1958, pp. 1045–1046.

Pressure Calibrator for Field Use, by Earl T. Pearson, *Rev. Sci. Instr.,* vol. 29, Nov. 1958, pp. 1052–1053.

Tube Diameter and Thickness Gauge for High Temperatures, by Ian Finnie, *Rev. Sci. Instr.,* vol. 29, Nov. 1958, p. 1054.

Guidance Systems and Components

Inertial Guidance for Hypersonic and Orbital Vehicles, by George W. Johnson and R. B. MacDonald, *Inst. Aeron. Sci., Rep.* 59-33, Jan. 1959, 23 pp.

Guidance Requirements of Ballistic Satellites, by Murray J. Stateman, *Inst. Aeron. Sci., Rep.* 59-30, Jan. 1959, 16 pp.

Servomechanisms and Controls

An Introduction to the Time Modulated Acceleration Switching Electrohydraulic Servomechanism, by Stephen A. Murtaugh Jr., *ASME, Paper* 58-A-159, Nov. 1958, 6 pp.

A Weight Comparison of Several Attitude Controls for Satellites, by James J. Adams and Robert G. Chilton, *NASA Memo* 12-30-58L, Feb. 1959, 19 pp.

Design of Automatic Flight Control Systems for Manned Space Vehicles, by Albert J. Kelly, *Inst. Aeron. Sci., Rep.* 59-32, Jan. 1959, 14 pp.

A High Resolution Servo, by W. A. Good, *Wissenschaftlichen Gesellschaft für Luftfahrt,* Jahrbuch, 1957, Braunschweig, Friedr. Vieweg & Sohn, 1958, pp. 368–370.

Space Flight

A Note on "A Nuclear Electric Pro-

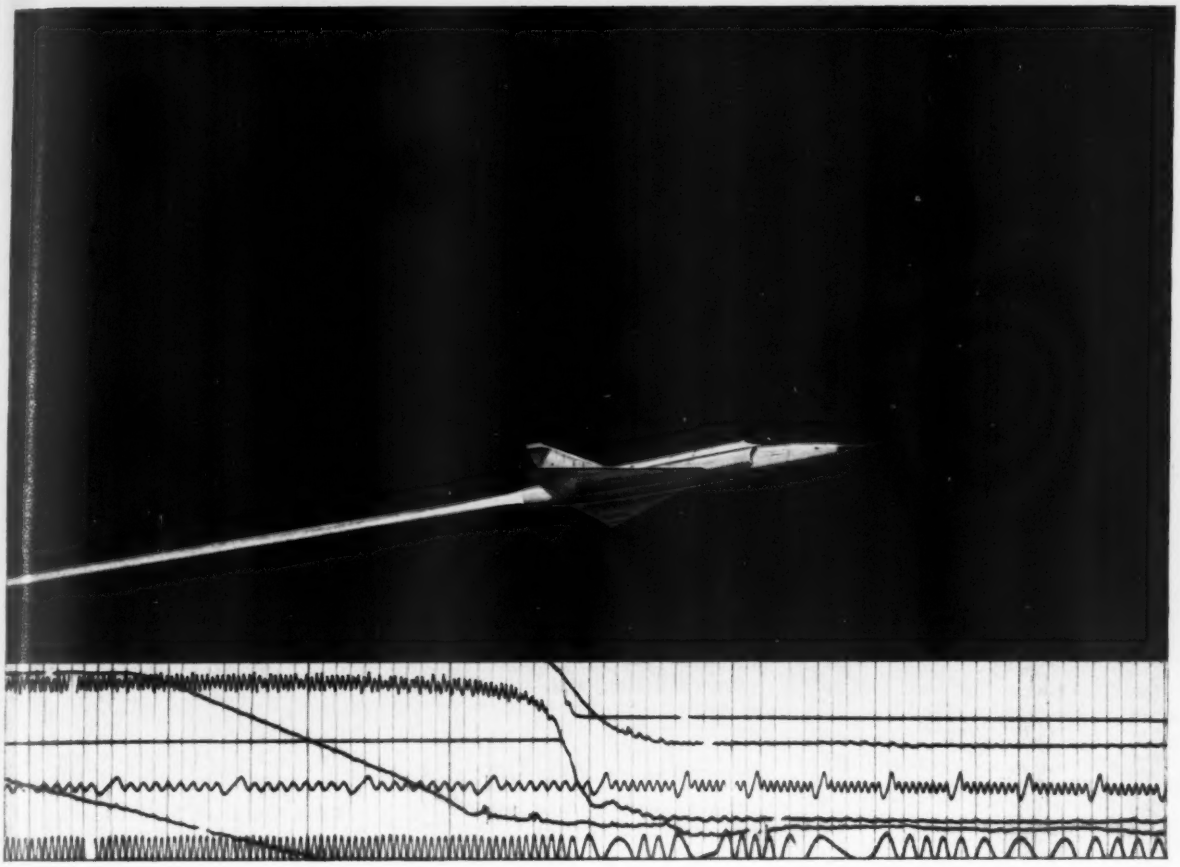

Now from Du Pont:

a complete line of photorecording papers and films

Du Pont now makes photorecording papers *and* films for your various recording needs. Here's what our complete photorecording line includes:

PHOTORECORDING PAPERS

Lino-Writ 1. Orthochromatic paper designed for average test requirements at lower writing speeds.

Lino-Writ 2. Moderately high-speed orthochromatic paper for use in intermediate speed recording requirements.

Lino-Writ 3. For high-frequency oscillographic traces without loss of detail.

These three papers are available in two types: Type B, standard-weight stock when greater opacity is required, and Type W, a thin, 100% all-rag stock.

Lino-Writ 4. It's the toughest, fastest, whitest paper you can use; 20% thinner than Type W, accommodates writing speeds as high as 5000 cps at maximum amplitude. Exceptional exposing and processing latitude. All-rag stock has unusual wet or dry strength.

PHOTORECORDING FILMS

CRONAR* Recording Film (High Speed)—relative speed (tungsten): 30.

Lino-Flex 1 (Regular Speed)—relative speed (tungsten): 10.

Both of these films are on Du Pont's exclusive CRONAR polyester photographic film base, which offers unexcelled strength, exceptional dimensional stability and flexibility. These fast-drying films have a fine matte surface which accepts pencil and ink markings.

PHOTORECORDING CHEMICALS

Lino-Writ Rapid Processing Chemicals Kit. Du Pont's high-speed, low-odor chemicals designed for rapid stabilization processing of papers *and* films.

For more information on our complete photorecording line, write: E. I. du Pont de Nemours & Co. (Inc.), Photo Products Department, Wilmington 98, Delaware. In Canada: Du Pont Company of Canada Limited, Toronto.

*CRONAR is Du Pont's trademark for its polyester photographic films

This advertisement was prepared exclusively by Phototypography

DU PONT
REG. U. S. PAT. OFF.

Better Things for Better Living . . . *through Chemistry*

pulsion System," by H. Preston-Thomas, *J. Brit. Interplanet. Soc.*, vol. 16, Sept.-Oct. 1958, pp. 508–516.

Multidirectional G-protection in Space Vehicles, by Harald J. vonBeckh, *J. Brit. Interplanet. Soc.*, vol. 16, Sept.-Oct. 1958, pp. 525–533.

Observations at the Mullard Radio Astronomy Observatory (on Satellites), *Cambridge, Proc. Roy. Soc.*, vol. 248A, Oct. 28, 1958, pp. 3–9.

Interferometer Measurements on the First Satellites, by A. N. Beresford, *Proc. Roy. Soc.*, vol. 248A, Oct. 28, 1958, pp. 10–15.

Observations on the USSR Earth Satellite Radio Signals, by H. V. Griffiths, *Proc. Roy. Soc.*, vol. 248A, Oct. 28, 1958, pp. 16–23.

Radar Observations of the Russian Earth Satellites and Carrier Rocket, by The Staff of the Jodrell Bank Exp. Sta., *Proc. Roy. Soc.*, vol. 248A, Oct. 28, 1958, pp. 23–33.

Flight Vehicle Design and Testing

Mathematical Theory of the Optimum Trajectories of a Rocket, by Angelo Miele, *Purdue Univ., School of Aeron. Engng., Rep.* A-58-10 (*AFOSR-TR*-58-154; *ASTIA AD* 206361), Nov. 1958, 35 pp.

Dynamic Stability of Re-entry Vehicles, by Norris F. Dow, ASTRONAUTICS, vol. 4, March 1959, pp. 32–33, 66.

Aerophysics, Astrophysics

New Research on Old Gravitation, by R. H. Dicke, *AEC*, NYO-8144, Oct. 1958, 11 pp.

Dirac's Cosmology and the Dating of Meteorites, by R. H. Dicke, *AEC*, NYO-8145, Nov. 1958, 4 pp.

Bakerian Lecture: The Nature of the Cosmic Radio Sources, by M. Ryle, *Proc. Roy. Soc., London* vol. A248, Nov. 25, 1958, pp. 289–301.

Discontinuities in Spherically Symmetric Gravitation Fields and Shells of Radiation, by W. Israel, *Proc. Roy. Soc., London*, vol. A248, Nov. 25, 1958, pp. 404–416.

On the Interplanetary Gas and Its Magnetic Field, by L. Block, *Arkiv f. Fysik*, vol. 14, no. 2, 1958, pp. 179–193.

Cosmic Ray Orbits in Interplanetary Magnetic Fields, by L. Block, *Arkiv f. Fysik*, vol. 14, no. 2, 1958, pp. 161–178

Interplanetary Magnetic Field and Its Control of Cosmic-ray Variations, by J. H. Piddington, *Phys. Rev.*, vol. 112, Oct. 15, 1958, pp. 589–596.

Structure of Particles of Linearized Gravitational Theory, by R. Sachs and P. G. Bergmann, *Phys. Rev.*, vol. 112, Oct. 15, 1958, pp. 674–677.

Project Prairie Grass, a Field Program in Diffusion, by Air Force Cambridge Research Center, Geophysics Res. Directorate, *Geophysical Res. Paper* 59 (*Air Force Cambridge Res. Center, Tech. Rep.* 58-235), vol. I, 280 pp. (*ASTIA AD* 152272); vol. II, 209 pp. (*ASTIA AD* 152573), July 1958.

Contributions to Stratospheric Meteorology, by Air Force Cambridge Res. Center, Geophysics Res. Directorate, *GRD Res. Note* 1 (*Air Force Cambridge Res. Center, TN* 58-450; *ASTIA AD* 152626), Aug. 1958, 134 pp.

Thomas-Fermi Equation of State for Dilute Gases, by Richard Latter, *Rand Corp., Res. Mem.* RM 1847-AEC (*ASTIA AD* 123511), Jan. 1957, 20 pp.

Spectroscopic Observations of Venus for Rotation Made at Mount Wilson in 1956, by Robert S. Richardson, *J. Brit. Interplanet. Soc.*, vol. 16, Sept.-Oct. 1958, pp. 517–524.

Ionizing Radiation Associated with Solar Radio Noise Storm, by K. A. Anderson, *Phys. Rev.*, vol. 112, no. 1, Oct. 1, 1958, pp. 333–334.

Atomic Energy

Cohesion in Plasma, by Melvin A. Cook and William S. McEwan, *J. Appl. Phys.*, vol. 29, Nov. 1958, pp. 1612–1613.

Observations on the Plasma Produced in a Magnetic Mirror Geometry, by W. B. Johnson, *Phys. Rev. Letters*, vol. 1, no. 9, Nov. 1, 1958, pp. 333–334.

The Diffusion of Magnetic Fields in a Cylindrical Conductor, by J. H. Adlam and R. J. Taylor, *Gt. Brit., Atom. Energy Res. Estab., AERE T/M* 160, 1958, 12 pp.

Tests of a Direct Cycle Nuclear Turbojet System, by D. R. Shoults, Cincinnati, *Interavia*, vol. 13, Dec. 1958, pp. 1316–1317.

Magnetically Confined Plasmas, by A. C. Kolb, *Phys. Rev.*, vol. 112, Oct. 15, 1958, pp. 291–295.

Vlasov Instability in Longitudinal Plasma Oscillations, by Peter L. Auer, *Phys. Rev. Letters*, vol. 1, no. 11, Dec. 1, 1958, pp. 411–412.

Our Stake in Thermonuclear Power, by John M. Carroll, *Electronics*, vol. 31, Dec. 19, 1958, pp. 75–77.

USSR May Have Tested Atom Rocket, by Alfred J. Zachringer, *Missiles and Rockets*, vol. 4, Dec. 22, 1958, pp. 13–14.

Studies of Neutron Production in Linear Deuterium Pinches, by P. Ohlin, K. Siegbahn, T. Sundrstrom and S. Svennerstedt, *Nuclear Instr.*, vol. 3, no. 4, Oct. 1958, pp. 237–244.

The Mechanism of Neutron Emission in High Energy Fission, by D. M. Skyrme and G. N. Harding, *Nuovo Cimento*, vol. 9, Sept. 16, 1958, pp. 1082–1092. (In English.)

The Runaway Effect in a Fully Ionized Plasma, by E. R. Harrison, *Phil. Mag.*, Ser. 8, vol. 3, Nov. 1958, pp. 1318–1327.

Safety Hazards of Nuclear Propulsion, II, by Leo Seren, *Space/Aeron.*, vol. 30, Dec. 1958, pp. 48–52.

Experiments on the Ohmic Heating and Confinement of Plasma in a Stellarator, by T. Coor, S. P. Cunningham, R. A. Ellis, M. A. Heald and A. Z. Kranz, *Phys. Fluids*, vol. 1, no. 5, Sept.-Oct. 1958, pp. 411–420.

"Runaway" Electrons and Cooperative Phenomena in B-1 Stellarator Discharges, by W. Bernstein, F. F. Chen, M. A. Heald and A. Z. Kranz, *Phys. Fluids*, vol. 1, no. 5, Sept.-Oct. 1958, pp. 430–437.

The Divertor, a Device for Reducing the Impurity Level in a Stellarator, by C. R. Burnett, D. J. Grove, R. W. Palladino, T. H. Stix and K. E. Wakefield, *Phys. Fluids*, vol. 1, no. 5, Sept.-Oct. 1958, pp. 438–445.

Interferometric Measurement of Electron Concentrations in Plasmas, by Ralph A. Alpher and Donald R. White, *Phys. Fluids*, vol. 1, no. 5, Sept.-Oct. 1958, pp. 452–453.

What Are the Safety Hazards of Nuclear Propulsion? by Leo Seren, *Space/Aeronautics* (formerly *Aviation Age*), vol. 30, Nov 1958, pp. 18–22.

Russian Technical Articles*

Interaction of a Shock Wave with a Boundary Layer by the Leading Edge of a Flat Plate at High Supersonic Speeds with Radiation, by G. A. Kulonen, *Leningrad Univer., Vestnik*, vol. 13, no. 7, 1958, pp. 172–188. (In Russian.)

The Behavior of a Completely Ionized Plasma in a Strong Magnetic Field, by S. I. Braginskii, *Soviet Phys.-JETP*, vol. 6, March 1958, pp. 494–498.

Stationary Convective Flow of an Elastically Conducting Liquid between Parallel Plates in a Magnetic Field, by G. E. Gershuni and E. M. Zhukhovitskii, *Soviet Phys.-JETP*, vol. 34 (7), no. 3, Sept. 1958, pp. 461–464.

Stability of the Stationary Convective Flow of an Electrically Conducting Liquid between Parallel Vertical Plates in a Magnetic Field, by G. E. Gershuni and E. M. Zhukhovitskii, *Soviet Phys.-JETP*, vol. 34 (7), no. 3, Sept. 1958, pp. 465–470.

Radiation of Plasma in a Magnetic Field, by B. A. Trubnikov, *Akad. Nauk SSSR, Doklady*, vol. 118, Feb. 11, 1958, pp. 913–916. (In Russian.)

Unsteady Flow with Heat Transfer in a Viscous Incompressible Fluid between Two Rotating Disks when There is Injection of the Fluid, by G. A. Tirskii, *Akad. Nauk SSSR, Doklady*, vol. 119, March 11, 1958, pp. 226–228. (In Russian.)

Stationary Convection in a Plane Liquid Layer Near the Critical Heat Transfer Point, by L. P. Gor'kov, *Soviet Phys.-JETP*, vol. 6, Feb. 1957, pp. 311–315.

Study of Heat Transfer in a Spiral Canal, by G. Fastovsky and A. E. Rovinsky, *Teploenergetica*, no. 1, Jan. 1957, pp. 39–42. (In Russian.)

Some Problems of Magnetogasdynamics with Account of Finite Conductivity, by G. S. Golitsyn and D. P. Staniukovich, *Soviet Phys.-JETP*, vol. 6, June 1958, pp. 1090–1093.

Investigations of the Burning of Homogeneous Mixtures in Turbulent Streams by Recording Fluctuating Temperatures, by I. V. Kokushkin, *Akad. Nauk SSSR, Izvestiia, Otdelenie Tekh. Nauk*, no. 8, Aug. 1958, pp. 1–11. (In Russian.)

On Drag Coefficients in the Motion of Burning Particles, by V. N. Basov and V. A. Popov, *Akad. Nauk SSSR, Izvestiia, Otdelenie Tekh. Nauk*, no. 8, Aug. 1958, pp. 12–14. (In Russian.)

The Phase Diagram of the Hydrogen-Deuterium System, by V. S. Kogan, B. G. Lazarev and R. F. Bulatova, *Soviet Phys.-JETP*, vol. 34 (7), no. 1, July 1958, pp. 165–166.

The Radiation from an Electron Moving in a Magnetoactive Plasma, by V. Ia. Eidman, *Soviet Phys.-JETP*, vol. 34 (7), no. 1, July 1958, pp. 91–95.

The Effect of Coulomb Correlations on the Spectrum of Electron-Plasma Oscillations, by P. S. Zyrianov, *Soviet Phys.-JETP*, vol. 34 (7), July 1958, pp. 160–161.

On the Theory of the Stability of Liquid Jets in an Electric Field, by G. A. Glonti, *Zhurnal Eksper. i Teoret. Fiziki*, vol. 34, no. 5, 1958, pp. 1329–1330. (In Russian.)

Distribution of Momentum in a Continuous Fluid Jet at a Supersonic Velocity, by A. A. Semerchan, L. F. Vereshchagin, F. M. Filler and N. N. Kuzik, *Zhurnal Tekhn. Fiziki*, vol. 28, Sept. 1958, pp. 2062–2071. (In Russian.)

Acceleration of Plasma in a Magnetic Field, by G. V. Gordeyev and A. L. Gubanov, *Zhurnal Tekhn. Fiziki*, vol. 28, Sept. 1958, pp. 2046–2054. (In Russian.)

Weak Waves in a Compressible Fluid With Account of Emission, by V. A. Prokof'yev, *Prikladnaya Matematika i Mekhanika*, vol. 21, Nov.-Dec. 1957, pp. 775–782. (In Russian.)

Ion Gun Operating at 20 to 30 Kilovolts, by L. N. Bukhovskaya, *Pribory i Tekhnika Eksperimenta*, no. 2, March-April 1958, pp. 49–51. (In Russian.)

Heat Transfer to Liquid Metals, by S. S. Kutateladze, E. N. Borishanskiy and I. Novikov, *Atomnaya Energiya*, vol. 4, May 1958, pp. 422–436. (In Russian.)

On Riemann Waves in Magnetohydrodynamics, by A. G. Kulikovskiy, *Doklady Akadamii Nauk SSSR*, vol. 121, Aug. 21, 1958, pp. 987–990. (In Russian.)

Investigation of the Kinetics of the Combustion of Hydrogen With Oxygen Above the Lower Limit of Self-ignition, by L. V. Karmilova, A. B. Nalbandyan and N. N. Semenov, *Zhurnal Fiz. Khimii*, vol. 32, June 1958, pp. 1193–1204. (In Russian.)

On the Stability of Flame Propagation, by Ya. B. Zel'dovich and G. I. Barenblatt, *Prikladnaya Matematika i Mekhanika*, vol. 21, no. 6, 1957, pp. 856–859. (In Russian.)

The Interaction Between Ozone and Methyl Hydroperoxide, by N. A. Kleymenov and A. B. Nalbandyan, *Doklady Akademii Nauk SSSR*, vol. 118, Jan. 1958, pp. 125–127. (In Russian.)

On the Combustion of and Heat Transfer by Dispersed Liquid Fuel in a Turbulent Air Flow, by G. N. Delyagin and B. V. Kantorovich, *Inzhenerno-Fizicheskiy Zhurnal*, no. 3, March 1958, pp. 24–39. (In Russian.)

The Reactions of Nitrogen in Explosions, by A. Ya. Apin, Yu. A. Lebedova and O. I. Nefedova. *Zhurnal Fiz. Khimii*, vol. 32, April 1958, pp. 819–823. (In Russian.)

The Glowing of Air During a Strong Explosion and the Minimum Brightness Effect of a Fireball, by Yu. P. Rayzer, *Zhurnal Eksper. i Teoret. Fiziki*, vol. 34, no. 2, 1958, pp. 483–493. (In Russian.)

Measurement of Ionization Intensity in (Acetylene) Flames, by V. S. Rossikhin and N. A. Nesterko, *Zhurnal Fiz. Khimii*, vol. 31, no. 12, 1957, pp. 2663–2667. (In Russian.)

Pressure Impact on the Lower Concentration Limit of the Flame Disruption in a Flow, by M. A. Peshkin, *Zhurnal Fiz. Khimii*, vol. 31, no. 12, 1957, pp. 2757–2758. (In Russian.)

Protective Coatings for High-Temperature Alloys, by V. A. Parfenov, *Metallovedeniye i Obrabotka Metallov*, no. 6, June 1958, pp. 33–37. (In Russian.)

Some Questions on the Motion of a Solid Body (Gyroscope) in a Newton Field of Forces, by V. V. Beletskiy, *Prikladnaya Matematika i Mekhanika*, vol. 21, no. 6, 1957, pp.749 –758. (In Russian.)

Proportional Navigation as a Problem in Cybernetics, by A. S. Kel'zon and O. V. Grigor'yev, *Doklady Akademii Nauk SSSR*, vol. 121, July 21, 1958, pp. 432–435. (In Russian.)

* The Editors of Technical Literature Digest are making a systematic search for pertinent Russian articles, both in the original Russian and in translated form. For the balance of 1959, these will appear in a separate section with this heading, mainly to draw the readers' attention to the new listing. After that, they will appear item by item under the proper subject headings.

Index to Advertisers